UNIVERSITY OF CALIFORNIA, SAN DIEGO

# Fluid Stress on the Surface of a Migrating Leukocyte in a Flow Field and the Involvement of Formyl Peptide Receptor in Its Mechanotransduction

A Dissertation submitted in partial satisfaction of the requirement for the degree

Doctor of Philosophy

in

Bioengineering

by

Susan Shan Su

Committee in charge:

Professor Geert W. Schmid-Schönbein, Chair
Professor Shu Chien
Professor Mark Ellisman
Professor Mark Ginsberg
Professor Constantine Pozrikidis

2007

The Dissertation of Susan Shan Su is approved and it is acceptable in quality and form for publications on microfilm:

---

---

---

---

---

Chair

University of California, San Diego

2007

DEDICATION

*to my father*

TABLE OF CONTENTS

# LIST OF ABBREVIATIONS

| | |
|---|---|
| ATP | Adenosine Triphosphate |
| BSA | Bovine Serum Albumin |
| CAM | Cell Adhesion Molecule |
| cdk | Cyclin-Dependent Kinase |
| cGMP | Cyclic Guanosine Monophosphate |
| DAG | Diacylglycerol |
| EPCR | Endothelial Cell Protein C Receptor |
| FBS | Fetal Bovine Serum |
| fMLP | N-Formyl-Methionyl-Leucyl-Phenylalanine |
| FPR | N-Formyl Peptide Receptor |
| GEF | Guanine Nucleotide Exchange Factor |
| GAP | GTPase-Activating Protein |
| GDP | Guanosine Diphosphate |
| GFP | Green Fluorescent Protein |
| GP | Glycoprotein |
| GPCR | G-Protein Coupled Receptor |
| GTP | Guanosine Triphosphate |
| HUVEC | Human Umbilical Venous Endothelial Cell |
| ICAM | Intercellular Adhesion Molecule |
| Ig | Immunoglobulin |
| $IP_3$ | Inositol Triphosphate |
| LFA-1 | Lymphocyte Function-Associated Antigen-1 |
| NO | Nitric Oxide |
| PAF | Platelet Activating Factor |
| PBS | Phosphate Buffered Solution |
| PI3K | Phosphatidylinositol 3-Kinase |
| $PIP_2$ | Phosphatidylinositol 4,5-Biphosphate |
| $PIP_3$ | Phosphatidylinositol 3,4,5-Triphosphate |
| PKC | Protein Kinase C |
| PLC | Phospholipase C |
| PMN | Polymorphonuclear Leukocyte (Neutrophil) |

| | |
|---|---|
| PSGL-1 | P-selectin Glycoprotein Ligand 1 |
| RBC | Red Blood Cell |
| SCD | Sickle Cell Disease |
| SHR | Spontaneous Hypertensive Rat |
| SOD | Superoxide Dismutase |
| vWF | von Willebrand Factor |
| VCAM | Vascular Cell Adhesion Molecule |

LIST OF FIGURES

ACKNOWLEDGEMENTS

First and foremost, I like to thank my advisor, Dr. Geert W. Schmid-Schönbein, for his brilliant ideas, guidance, and insurmountable patience. I would not have been able to do half of the work in this dissertation if it were not for the help of a few mentors over the past few years: Dr. Sheng Tong, Dr. Hainsworth Y. Shin, and Dr. Ayako Makino. Of course there is the helping hand here and there from the colleagues of Microcirculation Lab. Last but not least on my list of academic acknowledgements – my committee members, for their insightful suggestions and warm encouragements.

Getting a PhD is a tough six-year test of determination and endurance. I want to thank my mom for standing behind me with the greatest support every step of the way. She never questioned any of my decisions and actions, having complete trust that I would do the right thing. For the many times when I was down, she shared inspirational real-life stories to get my spirits back up. I am indebted to my older sister, literally and figuratively, for financing my multiple vacation trips and for letting me postpone my entry into the big scary real world. If it weren't for her, who shoulders all the family responsibilities like what is expected of the first child in a Chinese family, I would not have the leisure in spending time outside of research to pick up the many new hobbies and activities. I am grateful for the temporary home and weekend getaways that my Aunt Minsheng provided during holidays and birthdays. Her loving warmth and wonderful home-cooking gave me the shelter when I was most in need of family presence. I like to thank my roommate Ying-Ja Chen, for listening to my many

complaints and lending moral support during some of my most stressful months. Finally, a deep heart-felt “thank you” to the great friends from these long years: Nada Wasi, Anokhi Kapasi, John Mongan, Josh Pong, Anya Asanbaeva, Joy Nystrom Goor, Marzio Pedrali-Noy, Ondrej Libiger, and many many others from school and beyond.

# VITA

| | |
|---|---|
| 2001 | Bachelor of Science, Binghamton University – State University of New York |
| 2003 | Master of Science, University of California, San Diego |
| 2005 | Candidate of Doctor of Philosophy, University of California, San Diego |
| 2007 | Doctor of Philosophy, University of California, San Diego |

ABSTRACT OF THE DISSERTATION

Fluid Stress on the Surface of a Migrating Leukocyte in a Flow Field and the Involvement of Formyl Peptide Receptor in Its Mechanotransduction

by

Susan Shan Su

Doctor of Philosophy in Bioengineering

University of California, San Diego, 2007

Professor Geert W. Schmid-Schönbein, Chair

We recently demonstrated that migrating human leukocytes respond to small physiologic fluid stresses by active control in the projection and retraction of local cytoplasmic extensions (pseudopods). However, the regulatory mechanisms involved in this type of fluid shear response are currently unknown. Recent observations in our lab showed that the formyl peptide receptor, a G-protein coupled membrane receptor, is important for the pseudopod retraction

response of neutrophils under fluid shear. We hypothesized that the surface distributions of these membrane receptors determines how the cell responds in a laminar flow field. In the first part of this work I developed a method to compute the fluid stress distributions on the membrane of a single migrating leukocyte. We found that the shear stresses are highest at the top of an adherent cell and is lowest in the contact region with its substrate. However, the cell retracts its pseudopods more in the vicinity of the attachment sites close to the substrate adhesion region than at its top. Membrane protrusions, such as pseudopods, also experience enhanced shear stresses but tend to be lower than that at the top surface. This evidence shows a non-linear relation between the shear magnitude and degree of pseudopod retraction. The second part of the dissertation focuses on the location of FPR before and after flow application. Using FPR-GFP-transfected cells, we observed that there is an increased aggregation of receptors in a perinuclear compartment of the cell. There is a very small decrease in GFP-derived fluorescence intensity in the cell membrane and cell cytoplasm, suggesting that internalization of the receptor is not limited to a single region on the surface of the cell. The prolonged FPR detention in an intracellular compartment suggests that fluid shear stress may prevent receptors being recycled back to the membrane. This feature may serve as a desensitization mechanism of the cell to prevent activation on the cell surface. The observation is in line with previous observations suggesting that laminar fluid flow may deactivate the cell even in the presence of low concentrations (up to 10nM fMLP) of inflammatory mediators.

# INTRODUCTION

Inflammation serves as a repair process that fights off invasion of a host tissue by foreign materials or organisms, closes a wound, replaces damaged tissues, and even restores tissue function. Many diseases are accompanied by markers and manifestations of inflammation. While in diseases like infections the cause of inflammation is known, there are many diseases in which we do not understand the trigger mechanisms that lead to inflammation. Thus there is a need to study trigger mechanisms as well as the progression of inflammation, especially in cardiovascular complications in which tissue repair is never achieved (chronic inflammation).

Leukocytes have long been recognized for their essential roles in the inflammation process. They aggregate at sites of infection, release enzymes that degrade foreign pathogens, phagocytose damaged cells, prepare the host with molecular memories of the damaging microorganism, and finally facilitate the repair process. For reasons still unknown, leukocytes may accumulate in tissues even if there is no exogenous irritant present or after the removal of such microbes. Through their functions designed for elimination, such as oxidative burst, host tissues end up suffering injury or further damage.

Leukocytes are able to reach the first signs of infection within minutes through the circulatory system. Since leukocytes are constantly exposed to plasma fluid flow regardless of the size of the blood vessel, it is reasonable to hypothesize that cell membrane mechanisms have evolved to transmit mechanical signals into a cascade of events that control migration, adhesion,

chemotaxis, innate immune functions, and other cell functions. It has been documented in several studies that fluid shear stress can keep leukocytes in their round passive shape (Moazzam, DeLano et al. 1997; Fukuda and Schmid-Schonbein 2002; Makino, Glogauer et al. 2005). However, the mechanisms by which leukocytes sense mechanical stresses are still not completely understood.

This dissertation serves as a study to better characterize the behavior of leukocytes, especially neutrophils, in the microvasculature. Pseudopod formation requires an intact actin cytoskeleton with polymerization of F-actin which can be controlled by membrane receptors (Wymann, Kernen et al. 1990,Coates, 1992 #178; Coates, Watts et al. 1992). We hypothesize that since fluid shear stress can regulate the pseudopod extension/retraction process, there must be mechanisms on the cell surface that relay the mechanical signal to the intracellular domain. In the first part of this dissertation I compute the fluid stresses on the surface of a migrating cell in order to identify local membrane regions with high and low stresses acting on the membrane. In the second part, I focus on elucidating the role of the N-formyl peptide receptor in leukocyte fluid shear response by observing its distribution both on the membrane and inside the cell during exposure to flow.

## Background

### Microcirculation

The microcirculation refers to a network of arterioles, venules, and capillaries that serve as the regulators of peripheral blood flow. The structure of the microcirculation varies greatly from tissue to tissue and the vessel network is

much more dense than the typical tree structure of the macrocirculation (arteries and veins). Arterioles range from 100μm in diameter down to about 10μm in the terminal arterioles; capillaries can have a lumen smaller than a leukocyte; the venules range in 10-100μm in diameter and are the most important part of the microcirculation for the understanding of inflammation (Movat 1985) based on their early manifestation of increased vessel permeability and the attachment of leukocytes to the vessel walls.

At the microvascular level, when the diameter of the vessels are on the same order of magnitude as that of a red blood cell, blood can no longer be considered as a fluid of uniform viscosity. Instead, blood plasma and the two major groups of cells have to be treated separately. In most capillaries, cells can only pass through in a single-file manner. Plasma, though laden with ions, lipids, and proteins, is a Newtonian fluid, which means its viscosity does not change under physiological shear rates (Thurston 1972). Erythrocytes and leukocytes are viscoelastic solids (Schmid-Schonbein, Sung et al. 1981; Evans 1989). They will passively deform under a pressure drop and shear stresses to pass through capillaries of smaller diameters (Bagge and Branemark 1981; Doerschuk, Beyers et al. 1993).

Resistance to blood flow can be controlled by arterioles, venules, and even capillaries. Vessel constriction and dilation are adjusted by smooth muscle cells. These cells control organ perfusion under different physiologic conditions, e.g. enhanced flow to the digestive system after a meal. They are subjected to a variety of biochemical and mechanical factors and at the same time their

modulation of blood flow serves to regulate mechanical and biochemical stimuli on endothelial and blood cells. Since capillaries only allow cells to pass through one at a time, blockage of the vessel can occur easily due to either an activated leukocyte or a constricting smooth muscle sphincter in terminal arterioles. This occurrence may sometimes remedy itself, but if prolonged, tissue death can result.

## Inflammation in the Microcirculation

As early as 1893, Metchnikoff has observed in his experiments with tadpoles that stopping blood flow led to emigration of leukocytes that eventually cause the death of the organism. Microvascular inflammation is a most active field of research and its importance in the understanding of the progression of diseases cannot be over-emphasized.

Inflammation was traditionally characterized by four general cardinal signs: redness, swelling, pain, and heat. Today we define it as a series of molecular and cellular events that leads in many situations to repair of tissue infections or injuries. The exact sequence of events varies depending on the type of injury, be it a localized bacterial infection or a systemic shutdown as in the case of physiological shock.

At the microcirculatory level, typical signs of inflammation include increased vessel diameter and leakiness, capillary stasis, leukocyte extravasation into the surrounding tissues, release of proteolytic enzymes and oxygen free radicals, necrosis and apoptosis of tissues and phagocytes, and finally, regeneration of functional and connective tissues (Schmid-Schonbein 2006). In many instances, the causes for these processes are unknown and they lead to a

positive feedback loop of chronic inflammation, subsequently to organ failure and death.

Expressions of membrane molecules on both the endothelial cells and leukocytes are greatly enhanced during inflammation, leading to rolling and entrapment of leukocytes in peripheral venules and pulmonary capillaries (Doerschuk 2001). It has long been accepted that leukocytes migrate through the junctions between endothelial cells via homophilic binding of PECAM-1 and translocation of VE-cadherin, a process known as diapedesis (Carman and Springer 2004). However, there is also mounting evidence to suggest that endothelial cells form pockets after ICAM-1 expression enhancement, where neutrophils and lymphocytes are trapped, and eventually allowing these cells to reach the interstitial side of the vessel (Engelhardt and Wolburg 2004). In either case, the integrity of the endothelial layer, and subsequently, of the basement membrane are compromised. The increased vascular permeability allows plasma, protein, as well as red blood cells, to easily leak into nearby tissues (Engelhardt and Wolburg 2004).

Neutrophils are phagocytic and release proteases that help degrade cellular debris in the damaged tissue. As part of the process, they also release high concentrations of cytotoxic molecules such as superoxide and other free radicals that are potentially harmful to tissues. Macrophages, differentiated from monocytes, are recruited to the site of inflammation hours after neutrophil arrival. Their major contribution is the removal of cell debris, but they also release several anti-inflammatory cytokines, in particular interleukin 10 (IL-10) and transforming

growth factor beta (TNF-β), which serve to stop inflammation and initiate tissue repair (Fujiwara and Kobayashi 2005). The final stages in resolving inflammation is the regrowth of new tissues. This will involve formation of scar tissues and then generation of new cells and extracellular matrix, often accompanied by new blood and lymphatic vessels.

## Leukocyte Functions

Leukocytes are major players in the inflammatory cascade. Capture of circulating leukocytes in the microcirculation is a key step in inflammation, including a sequence of reactions to contain and destroy microorganisms and chemicals that cause irritation in tissues.

Polymorphonuclear cells (PMNs, also known as neutrophils) are the first leukocytes to accumulate at infection sites, followed by mononuclear cells, but even then PMNs make the predominant portion of exudates (Kopaniak, Issekutz et al. 1980). Neutrophils make up about 50% to 70% of all white blood cells.

Under normal physiological conditions, neutrophils maintain an overall passive spherical cell shape while passing through the circulation. Upon activation, they extend cytoplasmic projections that hinder their passage through small blood vessels and enhance transendothelial migration into the surrounding tissues. The sequence of events in leukocyte extravasation in the postcapillary venules first involves formation of tethers with the endothelium that permits rolling along the apical surface of the endothelial cells near an inflamed area. The leukocytes express adhesion molecules such as L-selectins and PSGL-1 at the tips of membrane microvilla to facilitate the initial capture on the endothelium (von

Andrian, Hasslen et al. 1995). They then activate integrins, most notably CD18, for firm adhesion to endothelial receptors such as ICAM-1 (Feng, Nagy et al. 1998). Subsequently, leukocytes migrate along the vessel until they finally disrupt the endothelial junctions (Del Maschio, Zanetti et al. 1996) or traverse directly through the endothelial cell (Feng, Nagy et al. 1998) to enter the extracellular domain. These steps – tethering, rolling, adhesion, and transmigration are carefully regulated by the interactions between specific leukocyte and endothelial cellular adhesion molecules (CAMs) (Springer 1994; Witko-Sarsat, Rieu et al. 2000; Harlan and Winn 2002; Simon and Green 2005). Selectins and selectin-ligands, heterophilic transmembrane glycoproteins, are heavily involved during the initial tethering step. Integrins, transmembrane dimers that consist of one α and one β subunit, are essential for leukocyte firm adhesion on the endothelium and migration within the inflamed tissues. Lastly, the immunoglobulin (Ig) superfamily signals directional diapedesis of leukocytes (Springer 1994; Witko-Sarsat, Rieu et al. 2000; Harlan and Winn 2002; Simon and Green 2005).

Mediated by stimulation of oxidants, proteases, bioactive lipids, and cytokines from endothelial cells and other leukocytes (Yonekawa and Harlan 2005), neutrophils in the tissue release enhanced amounts of superoxide through activation of an NADPH oxidase enzyme, xanthine oxidase. The antimicrobial products that are released, such as reactive oxygen species, are equally harmful to host tissues. The excessive accumulation of neutrophils in the tissues results from impaired cellular functions will lead to chronic inflammation and tissue injury. It is a fine balance between mechanical and chemical signals that determines the difference between normal leukocyte function and dysfunction.

It has long been observed in clinical settings that neutrophils are heterogeneous (Gallin 1984). It is still unclear if the differences observed in the cells reflect actual subpopulations of the phagocytes or simply due to the age of the cells. It has also been suggested that individual cells express different levels of various receptors, which can lead to dysfunction of the cells and therefore pathological conditions in the host. Interestingly, past experiments in this lab also led to the same observations, that under very similar *in vitro* conditions, cells respond in complete opposite fashions (Moazzam, DeLano et al. 1997; Coughlin and Schmid-Schonbein 2004).

## Diseases Associated with Leukocyte Dysfunction

Inflammation with dysfunction of leukocytes has been linked to a variety of serious diseases including cancer (Coussens and Werb 2002), autoimmune diseases (Frostegard 2005), obesity (Avogaro and de Kreutzenberg 2005), type 2 diabetes (Pradhan, Manson et al. 2001), age-related macular degeneration (Edwards, Ritter et al. 2005; Haines, Hauser et al. 2005; Klein, Zeiss et al. 2005), and a wide range of cardiovascular diseases (Wong, Rosamond et al. 2005) such as atherosclerosis (Ross 1999), hypertension (Li and Chen 2005), and thrombosis (Andrews and Berndt 2004). In this section I will list some selected examples.

A range of cardiovascular diseases are affected by leukocyte accumulation in the vasculature. Angiotensin II, a known vasoconstrictive peptide that leads to hypertension, is found to provoke mesenteric mononuclear leukocyte adhesion in arterioles and neutrophil infiltration in postcapillary venules (Piqueras, Kubes et al. 2000; Alvarez, Cerda-Nicolas et al. 2004). Ischemia-reperfusion injury, which can

result in stroke and shock, can be prevented in animal models by blockade of leukocyte adhesion molecules (Thiagarajan, Winn et al. 1997). In thrombosis, endothelial cell protein C receptor (EPCR) binds to activated neutrophils and decreases leukocyte extravasation through inhibition of activated protein C (Esmon 2004). In patients who suffer from sickle cell disease (SCD), unstimulated neutrophils express an elevated level of surface integrins (Lard, Mul et al. 1999; Lum, Wun et al. 2004). These adhesion molecules greatly increase neutrophil adhesion to inflamed endothelium, which in turn recruits sickle red blood cells and induces vascular occlusion. The findings suggest that SCD neutrophils are more sensitive to chemical signals and they increase the patients' susceptibility to vascular diseases.

It is now well recognized that atherosclerosis is an autoimmune disease with clear signs of leukocyte infiltration (Mach, Schonbeck et al. 1998; Wick, Knoflach et al. 2004; Frostegard 2005). Blocking the binding of CD40 and CD40L, a receptor-ligand pair that is important for T and B cell interactions, can improve atherosclerosis and autoimmune disease (Mach, Schonbeck et al. 1998). In rheumatoid arthritis the expression of adhesion molecules on lymphocytes is increased, which indicates enhanced leukocyte recruitment to attack autologous tissues (Sfikakis and Tsokos 1995). In type I and II diabetes, circulating platelets express activated adhesion molecules that enhance leukocyte binding in the vasculature, increasing complications in the circulation (Tschoepe, Rauch et al. 1997). An elevated level of interleukin-6, a proinflammatory cytokine released into plasma by injured endothelium and macrophages, is found to be an indicator of eventual onset of type 2 diabetes (Pradhan, Manson et al. 2001). Adipose

tissue-derived capillary endothelium exhibits up-regulated levels of adhesion molecules that have the ability to recruit monocytes, which in turn become resident macrophages (Curat, Miranville et al. 2004). The resulting prevalence of macrophages in adipose tissue (Robker, Collins et al. 2004) may be the cause of the heightened inflammation in obese patients. Cancerous cells may be generated by the inflammatory responses, a process that involves reactive oxygen species from leukocytes that can lead to carcinogenesis (Ohshima and Bartsch 1994; Kuper, Adami et al. 2000). In addition, macrophages release vascular endothelial growth factors that promote angiogenesis and lymphogenesis and potentiate the growth and spreading of a tumor (Coussens and Werb 2002).

In the aforementioned cases, dysregulated leukocyte functions may be a major contributor to the progression and/or pathogenesis of these diseases. Therefore it is of great interest to study the causes and mediators that control neutrophil behavior.

## Cellular Mechanotransduction in the Circulation

Vascular endothelial cells and all circulating blood cells types have been shown to respond to fluid shear stress (Johnson 1994; Kroll, Hellums et al. 1996; Moazzam, DeLano et al. 1997; Baskurt and Meiselman 2003; Ahn, Jun et al. 2005; Helmke 2005). In particular, endothelial cells and leukocytes, including monocytes, lymphocytes, and neutrophils, undergo morphological changes as part of the response to fluid shear stress (Langille and Adamson 1981; Davies,

Mundel et al. 1995; Moazzam, DeLano et al. 1997) in addition to functional changes.

### Fluid Shear Response in the Endothelium

Fluid shear stress is important in the regulation of many blood vessel functions. For instance, vascular endothelial cells that line the intraluminal surface of a blood vessel elongate in the direction of blood flow in relatively straight regions of arteries, and the cytoskeletal filaments in these cells are oriented parallel to the major axis of cell elongation (Levesque and Nerem 1985; Galbraith, Skalak et al. 1998). However, disturbed flow near arterial bifurcations or high curvature regions was shown to elicit atherogenic responses that promote the onset of pathological conditions in the vasculature. Endothelial cells in these areas have a more polygonal shape, and cytoskeletal filament organization is more random (Ross 1999). The endothelial cytoskeleton adapts to external fluid shear through reorganization (Helmke and Davies 2002; Noria, Xu et al. 2004).

A recent examination of the human carotid atherosclerotic plaques showed that apoptosis of endothelial cells preferentially occur in upstream region of the plaque, where flow is disturbed and fluid shear stress is higher, as compared to the downstream region (Tricot, Mallat et al. 2000). Kuchan *et al* showed that a step laminar flow field causes cultured endothelial cells to increase nitric oxide (NO) production with an initial burst and then at a sustained level (Kuchan and Frangos 1994). The rapid initial production of NO was invariant for shear stresses within the physiological range of 6-25dyn/cm$^2$ whereas the sustained release of NO was dependent on the level of shear stress. Furthermore, expression of

surface receptors (Tzima, del Pozo et al. 2001) are changed in the short-term and ion channels, G proteins, and transmembrane adhesion receptors are activated within seconds after onset of shear stress (Davies 1995), suggesting that they may be mechanotransducers. It is still unsettled whether these cellular responses are dependent on shear magnitude (Passerini, Milsted et al. 2003), spatial shear gradients (Tardy, Resnick et al. 1997; Nagel, Resnick et al. 1999), or temporal shear gradients (White, Haidekker et al. 2001).

Akimoto *et al* found that DNA synthesis of human umbilical venous endothelial cells (HUVECs) was arrested by steady laminar shear stress through inhibition of the activities of cyclin-dependent kinase (cdk) 2 and cdk4 (Akimoto, Mitsumata et al. 2000). It was suggested that once steady laminar shear stress is removed, endothelial cells will proliferate uncontrollably and contribute to atherosclerosis. In addition to regulating genes that control endothelial growth, shear stress modulates the expression of genes that are responsible for functions such as cell adhesion, vaso-regulation, and cell activation (see review (Li, Haga et al. 2005)).

**Fluid Shear Response in Erythrocytes**

The majority of studies on the red blood cell (RBC) response to fluid shear are focused on its effect on the viscosity of whole blood, i.e. the non-Newtonian properties of blood. The response of the red cells is caused directly by a viscoelastic deformation of individual red cells as well as an effect on red cell aggregation. RBC aggregate size is inversely proportional to the magnitude of shear stress, and therefore it changes viscosity of whole blood based on the flow

rate within the circulatory system (Baskurt and Meiselman 2003). Red blood cells deform proportionally to shear magnitude, both in steady state and oscillatory motions (Nakajima, Kon et al. 1990). Red cells can be fractionated into subpopulations, e.g. a high-density (which has been identified as a functionally older group and has a higher hemoglobin content that increased its intracellular viscosity) and a low-density group. Higher density cells deform proportionally to sinusoidal oscillatory stresses of up to 1.7Hz but low density cell can deform up to 2.7Hz. This has implications for the ability of erythrocytes to pass through microcirculation under varying physiological conditions. RBC deformability is also dependent on the viscosity of the suspension medium (Kon, Maeda et al. 1987). Increasing the viscosity of medium enhances the ellipsoidal deformation of red cells but when fixed cells are added, the intact cells do not show such a deformation pattern. The authors suggested that laminar flow field around the intact cells had been disrupted in the latter case (Kon, Maeda et al. 1987).

Membrane properties of red blood cells also alter under shear applied by a ektacytometer, resulting in increased permeability to cations (Johnson 1994). The flux of sodium and potassium increases slowly until a shear stress of about 800dyn/cm$^2$ is reached and thereafter the flux rises exponentially. The degree of deformation shows an opposite behavior in that the red cells become increasingly elliptical with added shear until they reach an ellipticity of about 0.7, at which point they require much higher stress to induce further elongation.

When red blood cells are exposed to continuous low shear stress (420 s$^{-1}$ shear rate), Mizuno and colleagues found that the band 3 protein (B3, a major

protein in RBC membrane skeleton) density increases while there is a decrease in cell deformability (Mizuno, Tsukiya et al. 2002). Interestingly, short exposure to high shear stresses ($10^4$ $s^{-1}$ shear rate) does not lead to changes in the membrane skeleton of cells that are not fragmented instantaneously. This suggests a different and slower hemolysis process when RBCs are exposed to prolonged low shear.

Membrane permeability of red blood cells is also directly affected by fluid shear, resulting in increased leakiness to potassium ions (Ney, Christopher et al. 1990). Red blood cells at 37$^{o}$C are elliptically deformed in a Couette viscometer by shear stresses of 110dyn/cm$^2$. A net passive dose-dependent potassium efflux is measured in the supernatant. When shear stress application is combined with a lipid peroxidant, the leak increases significantly, but the effect is reversible upon flow cessation. This suggests that RBCs in pathological conditions, such as sickle cells, have compromised membrane functions that are sensitive to shear.

**Fluid Shear Response in Platelets**

Fluid shear is shown to play a role in platelet adhesion in the vasculature as well as in the activation of platelet membrane receptors, which facilitate further platelet aggregation and leukocyte recruitment (see review (Nesbitt, Mangin et al. 2006)).

In the presence of von Willebrand factor (vWF), a large glycoprotein normally found in blood plasma, platelet aggregation increases with increasing shear stress (Alevriadou, Moake et al. 1993; Konstantopoulos, Wu et al. 1995; Sugimoto, Tsuji et al. 1999). Alevriadou *et al* showed that platelet adhesion to

type I collagen increased as shear rate was increased from 100 $s^{-1}$ to 1500 $s^{-1}$ only when vWF was present in the plasma. Sugimoto *et al* identified a platelet glycoprotein (GP Ib) to be essential in the subsequent thrombus growth after platelet aggregation occurs on the endothelium (Sugimoto, Tsuji et al. 1999). Blocking GP Ib and vWF interaction In low shear (< or = 340 $s^{-1}$) does not prevent initial platelet adhesion to a collagen-coated surface and subsequent secondary thrombus formation but at high shear rates (> or = 1210$s^{-1}$) thrombus growth is prevented. More recent experiments have also shown that along with expression of surface glycoprotein ligands on leukocytes and endothelial cells, shear rates activate different surface adhesion molecules on platelets in the initial process of thrombus formation mediated through vWF (Andrews, Shen et al. 2001).

Platelets also show preferential binding to monocytes over neutrophils in flow (Ahn, Jun et al. 2005). At all shear rates (from 100 to 800 $s^{-1}$ ), monocyte-platelet heterotypic binding was increased progressively with increasing shear times (from 15 to 120 s) in the absence of exogenous stimulants whereas the incidence of neutrophil-platelet aggregation was hardly changed. Interestingly, fMLP stimulation led to moderate increase in monocyte-platelet binding but not neutrophil-platelet interactions.

**Fluid Shear Response of Leukocytes**

There is increasing evidence to suggest that fluid shear stress (~1 dyn/$cm^2$) acting on the cell membrane regulates leukocyte functions and its cell shape. Initially round cells project pseudopods under laminar fluid shear (Coughlin and Schmid-Schonbein 2004) while actively migrating neutrophils retract pseudopods

upon exposure to shear (Moazzam, DeLano et al. 1997; Fukuda, Yasu et al. 2000). Human neutrophils exposed to centrifugation show attenuated pseudopod retraction during shear flow compared to control group (Fukuda and Schmid-Schonbein 2002). Interestingly, centrifugation alone affects the response of leukocytes to fluid shear stress and their behavior *in vivo* (Fukuda and Schmid-Schonbein 2002), but the molecular mechanisms for this behavior is not understood.

A recent study suggested that leukocyte response to fluid shear is dependent on membrane adhesion molecules (Marschel and Schmid-Schonbein 2002). By using antibodies against $\beta_1$ and $\beta_2$ integrins to block their functions, the authors found that neutrophils that are attached to glass coverslip via $\beta_2$ integrins respond to flow from a micropipette by retraction of pseudopods whereas neutrophils attached via $\beta_1$ integrins showed little change in diameter. These two populations of neutrophils can be distinguished by their initial morphology in that the responding group has an initial major axis length of 1.7 times a round cell but the non-responding group has a “pancake” shape and a major axis length of 2.1 times that of a round cell.

Physiological levels of shear (12-30dyn/cm$^2$) increases intracellular $Ca^{2+}$ levels and is followed by neutrophil homotypic aggregation (Okuyama, Kambayashi et al. 1996). This aggregation can be eliminated by blocking the calcium ion influx using $NiCl_2$ or through pretreatment of antibodies against lymphocyte function-associated antigen-1 (LFA-1) or intercellular adhesion molecule-3 (ICAM-3). These results suggested the importance of calcium ion

channels in controlling neutrophil homotypic adhesion through LFA-1 and ICAM-3 under fluid shear. Further experiments by the same group using viscometer-applied shear led to the observations of actin polymerization in neutrophil cell-cell contact regions that was accompanied by an increase of intracellular $Ca^{2+}$ levels (Okuyama, Ohta et al. 1996). This is different from the actin polymerization in pseudopod formations due to stimulation by fMLP and there was no increase in calcium ion levels. Blocking LFA-1 and ICAM-3 with antibodies also inhibited actin polymerization. They concluded that F-actin assembly, mediated by $Ca^{2+}$ influx and adhesion molecules, was necessary for homotypic aggregation of neutrophils during shear.

To investigate the importance of red blood cells in the fluid shear response of leukocytes, Komai *et al* used a cone-and-plate device to shear fMLP-activated leukocytes in the presence and absence of erythrocytes (Komai and Schmid-Schonbein 2005). Leukocytes retracted pseudopods after shear but only in the presence of red blood cells, and replacement of erythrocytes with microspheres of the same size did not elicit retraction. However, when superoxide dismutase (SOD, a superoxide scavenger) was added to the shearing buffer, neutrophils again de-activated, suggesting that erythrocytes are necessary for the shear response of leukocytes by reducing superoxide levels. It was also found that at constant hematocrit and increasing plasma viscosity scaled by macromolecules, neutrophils showed a shear-stress-dependent but not shear-rate-dependent retraction.

Expression of various Rho-family small GTPases, which are signaling molecules for cytoskeletal organization, changes in response to shear. Using differentiated HL-60 cells, Makino *et al* found that Rac1 and Rac2 activities were decreased by fluid shear in a time- and magnitude-dependent manner, Rho activity only increased transiently, and Cdc42 remained unchanged (Makino, Glogauer et al. 2005). Inhibition of Rac1 and Rac2 in these cells abolished the retraction behavior in shear. Moreover, leukocytes from Rac1-null and Rac2-null mice failed to retract pseudopods when exposed to fluid shear, a behavior opposite to leukocytes of wild-type mice.

Green *et al* showed that when neutrophils roll on a layer of HUVECs or on an L lymphocyte monolayer co-expressing E-selectin (expressed on endothelial cells) and ICAM-1, the binding of E-selectin to L-selectin (expressed on leukocytes) and P-selectin glycoprotein ligand 1 (PSGL-1, also expressed on PMNs) led to the co-localization of the latter two to the trailing edge of the leukocyte (Green, Pearson et al. 2004). Using recombinant E-selectins, they were able to activate, in addition to L-selectin and PSGL-1 colocalization, clustering of high-affinity $\beta_2$ integrins (CD18) for capturing of ligands in shear flow, which can be prevented by inhibiting p42/44 mitogen-activated protein kinase. In addition, Fukuda *et al* observed in single and population studies of fresh human neutrophils that CD18 translocates to cell-substrate contact regions under shear and that the exterior domains of these integrins are cleaved in sustained flow (Fukuda and Schmid-Schonbein 2003). They were not able to obtain evidence of CD18 internalization from the surface into the cytoplasm of the cells and instead found that the down-regulation of $\beta_2$ integrins is reduced by inhibiting cathepsin B

(a cysteine protease). They suggested that fluid shear releases cathepsin B, which cleaves the extracellular domain of CD18 to cause cell detachment from the substrate. In an earlier related study, inflammatory mediators like platelet-activating factor (PAF) led a subpopulation of neutrophils to spread instead of retract under flow (Fukuda, Yasu et al. 2000). When cyclic GMP and nitric oxide donors were added, the cells again responded to fluid shear. Through in vivo experiments on PAF-treated rat mesentery, adding cGMP analog reduced pseudopod projection. In knock-out mice where the blood level of nitric oxide is low compared to wild-type, leukocytes' pseudopod retraction response was suppressed. Following up to this study, Fukuda *et al* found the human neutrophils irreversibly lose their retraction response to fluid shear after centrifugation (Fukuda and Schmid-Schonbein 2002). While leukocytes subjected to low-speed centrifugation (100 x g or 600 x g) exhibit attenuated retraction in flow applied from a micropipette, cells subjected to longer (15min instead of 5min) and higher speed centrifugation project extensions in flow. When rat leukocytes were reintroduced into the circulation after centrifugation, enhanced leukocyte adhesion and migration was observed in the rat mesentery, indicating that centrifugation damaged leukocyte fluid shear response.

In an attempt to elucidate in more details leukocyte behavior in hypertension, Fukuda *et al* found that glucocorticoid, specifically dexamethasone, led to a significant intracellular $Ca^{2+}$ increase in human neutrophils along with pseudopod extensions during fluid flow (Fukuda, Mitsuoka et al. 2004). Rats that were treated intramuscularly with dexamethasone for 7 days had more non-adherent leukocytes with pseudopods circulating in the bloodstream, as noted

from femoral arterial blood sample, compared to the wild-type. This finding led to the hypothesis that spontaneous hypertensive rats (SHRs) suffer from higher blood flow resistance in the peripheral vasculature partly because of their abnormal production of glucocorticoids (Fukuda, Yasu et al. 2004). SHR had a large percentage of leukocytes with pseudopods after fluid shear, which increased the stiffness of the cells, and adrenalectomy lowered that number. Blood from an SHR was injected into a Wistar (normotensive) rat and caused blood pressure to increase, suggesting that the blood itself was enough to raise resistance. Using a microchannel array analyzer, Fukuda and colleagues showed that dexamethasone-treated human neutrophils pass through the channels at a much slower rate than untreated cells. These two studies together provide substantial evidence in identifying one major determinant of the elevated blood pressure in SHRs, and offering an insight into essential hypertension (hypertension of undetermined causes) in humans.

## Cellular Shear-Sensing Mechanisms in the Circulation

Of the many leukocyte membrane mechanisms that may be responsive to a laminar fluid flow field, few have been studied. There are, however, major families of membrane elements that leukocytes share with endothelial cells. These membrane molecules, specifically ion channels and integrins, have been well studied in their roles regarding mechanotransduction in the endothelium. The following is a general overview of some past findings in endothelial and leukocyte mechano-responsive surface mechanisms.

**Ion Channels**

Ion channels are potential mechanosensors because they are located in the membrane. In cell-attached patch-clamp experiments, a stretch-sensitive cation channel was identified (Lansman, Hallam et al. 1987). The opening of this channel leads to an influx of calcium ions, then depolarization and activation of calcium-dependent responses. Low levels of shear stress can activate potassium-selective ionic currents in individual arterial endothelial cells (Olesen, Clapham et al. 1988). This current depends on the magnitude and duration of the applied shear stress and it desensitizes slowly. Fluid shear stress also induces calcium transients in HUVECs (Schwarz, Callewaert et al. 1992). The inward current is only observed when extracellular calcium is present, suggesting that the detected calcium signals are induced from the influx instead of membrane depolarization.

Yasu and colleagues found that nicorandil, an ATP-dependent potassium ($K_{ATP}$) channel opener, can suppress pseudopod formation in neutrophils subjected to 5 dyn/cm$^2$ of shear, therefore inhibiting the cells' migration *in vivo* (Yasu, Ikeda et al. 2002). By inhibiting nicorandil, intracellular calcium ion level can be increased by fMLP stimulation and pseudopods do not retract in flow. These experiments showed that $K_{ATP}$ channels may regulate cell shape change of neutrophils via changes in intracellular $Ca^{2+}$ concentration. $K_{ATP}$ channels are not the only ion channels involved in mechanotransduction. Previous studies from our lab have shown that voltage-dependent $Ca^{2+}$ channel blocker, diltiazem, partially restores fluid shear response of leukocytes that had been centrifuged (Fukuda and Schmid-Schonbein 2002). Diltiazem served to close the $Ca^{2+}$

channels to prevent calcium ion influx during pseudopod extension. The same treatment also blocks pseudopod formation even in the presence of dexamethasone, which leads to increase of intracellular $Ca^{2+}$ levels and pseudopod extension in flow (Fukuda, Mitsuoka et al. 2004). It is undetermined at this point whether the opening and closing of the channel is directly controlled by fluid shear stress or by a downstream response to other sensory mechanisms.

**Integrins**

Integrins are transmembrane heterodimers (α- and β-chains) that regulate important cellular functions such as proliferation, migration, and cytoskeleton organization through intracellular signaling molecules, particularly the small GTPases.

Studies of integrin mechanotransduction in endothelial cells provided much evidence for integrin-dependent responses. Wang *et al* applied mechanical stresses to endothelial cell surface receptors with a magnetic twisting device and found that $\beta_1$ integrin induced focal adhesion formation and allowed force-dependent cytoskeletal stiffening (Wang, Butler et al. 1993). In confluent endothelial layers, the size of focal adhesions (macromolecules through which the cytoskeleton is linked to integrins) is increased while the number of focal adhesion sites decrease during shear (Davies, Robotewskyj et al. 1994). In subconfluent endothelial cells, new focal adhesions are formed under the lamellipodia in the direction of flow as existing ones transiently cluster and then disperse (Li, Butler et al. 2002). Shear stress also regulates the activities of small GTPases through integrins (Tzima, del Pozo et al. 2001). Rac and Cdc42, which stimulates

lamellipodia formations and formation of actin-rich filopodia, respectively, are activated through integrin activation while Rho (facilitating detachment at the trailing end of a cell) is de-activated.

Leukocyte-specific integrins are composed of an α-chain (CD11) and a β-chain. The cytoplasmic domain of the β subunits is linked to actin binding proteins such as α-actinin, talin, filamin, and myosin (Pfaff, Liu et al. 1998; Sampath, Gallagher et al. 1998). Integrins in neutrophils comprise of three different β subunits, $\beta_1$, $\beta_2$, and $\beta_3$, of which $\beta_2$ (CD18) is the most abundant (Zhelev and Alteraifi 2002). Integrins are essential for firm adhesion of leukocytes to the vascular endothelium and are important for the extravasation process by binding to ligands such as fibrinogen, collagen, ICAM (intercellular adhesion molecules), VCAM (vascular cell adhesion molecule), and fibronectin (Carlos and Harlan 1994; Werr, Xie et al. 1998). Since integrins are not constitutively active, they are activated either outside-in or inside-out for adhesion to take place. ICAMs can initiate the outside-in activation while ligands binding to other surface glycoproteins can transduce signals to the cytoplasm, which in turn activates the integrins from the inside. Fukuda *et al* had found that the overall CD18 in a neutrophil under shear was redistributed from front to back (Fukuda and Schmid-Schonbein 2003). In the same set of studies, fluorescently labeled CD18 on the cell-coverslip contact surface was also observed to translocate towards the downstream side of the cell where the shear stresses tend to be the lowest. It was proposed that CD18 expression was controlled by a local mechanotransduction phenomenon.

**G-Protein Coupled Receptors**

G protein-coupled receptors (GPCRs) are integral membrane proteins that possess seven transmembrane helices. The ligands of GPCRs usually bind within the transmembrane domain instead of the extracellular domain. The inactive G protein is bound to the receptor in its inactive state. Once a ligand is recognized, the receptor shifts conformation and activates the G protein, which detaches from the receptor. The receptor will then either activate another G protein, or switch back to its inactive state. When the receptor has been exposed to a ligand for an extended period of time, protein kinases can phosphorylate the cytoplasmic domain. This in turn leads to down-regulation of the receptor and then internalization so the receptor will be dephosphorylated before returning to the membrane. There is increasing evidence supporting the hypothesis that GPCRs form dimers and even oligomers (Milligan 2001; Park, Filipek et al. 2004; Ciarkowski, Witt et al. 2005), indicating that they may form clusters instead of uniformly distributed throughout the membrane. Currently there is no direct evidence showing that GPCRs respond to mechanical forces in the absence of ligands. Treatment of neutrophils with platelet-activating factor receptor (PAF) antagonists significantly reduced leukocyte rolling and adhesion on thrombin-activated endothelium in fluid flow，suggesting both an involvement of PAF and the conformation of the GPCR (Macconi, Foppolo et al. 1995). Recent findings in our lab provide more direct proof of GPCR's mechanotransducing abilities by demonstration that knocking-in the formyl peptide receptor in undifferentiated hematopoietic cells allows the cells to respond to fluid flow by retracting pseudopods (Makino, Prossnitz et al. 2005).

## N-Formyl Peptide Receptors

N-formyl peptide receptors (FPRs) are predominantly found in neutrophils and monocytes. They are one major family of GPCR and are heavily involved in immune functions of polymorphonuclear and mononuclear phagocytes, which include chemotaxis, release of proteolytic enzymes, and superoxide production. fMLP binds to FPR with high affinity and leads to cellular activation even in picomolar concentrations (Boulay, Tardif et al. 1990). Receptors homologous to FPR have been found in several human tissues, specifically astrocytes and hepatocytes, suggesting that FPR may be involved in processes other than inflammatory reactions (Lacy, Jones et al. 1995). Similarly, functional FPR expressions are located in human lung and skin fibroblasts, implicating that these cells are capable of participation in immune defense (VanCompernolle, Clark et al. 2003).

### FPR Signal Transduction

FPR is functionally coupled to $G_i$-proteins, which consist of an α-subunit and a βγ-complex. Activation of the receptor by an agonist leads a conformational change that enables GDP to dissociate from $G_{i\alpha}$. GTP then binds to the heterotrimeric G protein, promoting $G_{i\alpha\text{-}GTP}$ and βγ-complex to separate. The βγ-complex then goes on to activate phospholipase C (PLC) and phosphatidylinositol 3-kinase (PI3K) (see review (Seifert and Wenzel-Seifert 2003)). PI3K converts the membrane phosphatidylinositol 4,5-biphosphate ($PIP_2$) into phosphatidylinositol 3,4,5-triphosphate ($PIP_3$). PLC cleaves $PIP_3$ to form secondary messengers, inositol triphosphate ($IP_3$) and diacylglycerol (DAG).

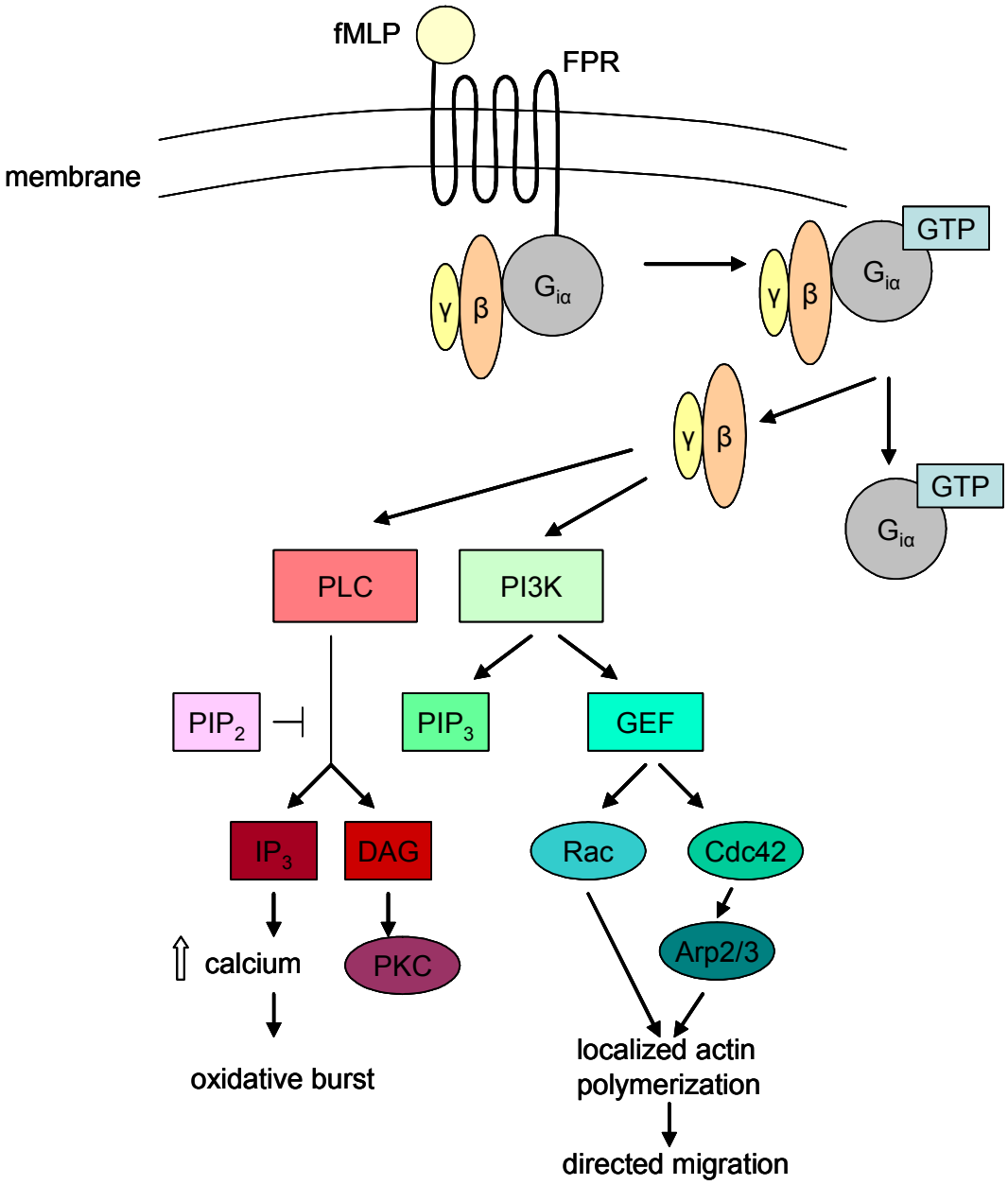


**Figure 2 FPR to actin assembly pathway.**

A schematic overview on the directed migration signaling cascade activated in neutrophils by fMLP binding to FPR (adapted from (Niggli 2003; Seifert and Wenzel-Seifert 2003; Panaro, Acquafredda et al. 2006)).

DAG activates a calcium-dependent protein kinase C (PKC), whereas $IP_3$ releases calcium from intracellular stores. An increase in calcium ion concentration is one of the earliest events of neutrophil response to formyl peptides. The activation of human neutrophils by chemotactic peptides evokes a rapid change in membrane potential and an increase in cytoplasmic $Ca^{2+}$ levels. These events are followed up to a minute later by the release of detectable levels of microbicidal agents formed by the oxidative burst. In addition, downstream of heterotrimeric G proteins, small GTP binding proteins of the Rho family, specifically Rac and Cdc42, are activated through guanosine exchange factors (GEFs), which then lead to actin assembly and localized membrane protrusions (see review (Panaro, Acquafredda et al. 2006)).

**Agonists and Antagonists of FPR**

A number of agonists have been synthesized based on peptide library to be used as tools in studying the leukocyte FPR. A hexapeptide, Trp-Lys-Tyr-Val-D-Met (WKYMVm) was synthesized from peptide library and found to activate several human leukocytic cell lines, by inducing migration and calcium ion influx, with just nanomolar concentrations (Le, Gong et al. 1999). Another group synthesized a derivative of fMLP, fMLP-OMe, and found that it caused the same activities in leukocyte as fMLP, which made it an ideal reference for characterizing other analogues by means of the induced activities in the leukocyte (Fabbri, Spisani et al. 2000). Yet another analogue, for-Met-Leu-Cys(OMe)-Cys(OMe)-Leu-Met-for, was synthesized to provide insight to the structure-activity relationship of FPR (Cavicchioni, Turchetti et al. 2003). This disulfur-bonded

peptide binds with good affinity to FPR and it takes little to cause chemotaxis in neutrophils. However, it does not solicit the same superoxide production that other peptides do, even at high concentrations.

What is interesting is that FPR can be activated by molecules that are not N-formylated. The synthetic T20/DP178 peptide can inhibit HIV-1 infection by preventing the viral envelop protein gp41 from changing its conformation that allows for fusion with human host cells (Su, Gong et al. 1999). The original peptide T20/DP178 is found naturally on the gp41 and is crucial in facilitating the fusogenic transformation. This synthetic peptide is a chemoattractant of peripheral blood phagocytes and acts through FPR.

Endogenous sources of FPR ligands have also been identified (Ernst, Lange et al. 2004). A synthetic peptide from the N-terminal of annexin-1 initiates directional migration responses in human monocytes in a dose-dependent manner. The activation was characterized by cell polarization, actin polymerization, and $Ca^{2+}$ mobilization. This peptide also desensitizes the cells from further activation by other agonists of bacterial origins, indicating that it competitively binds to FPR. Sun *et al* reported that cathepsin G, a proinflammatory serine protease found in neutrophil granules, can act as a chemoattractant for human phagocytes (Sun, Iribarren et al. 2004). When cathepsin G was added in the presence of FPR-specific antibodies and a known FPR antagonist, the cellular migration was inhibited. In addition to internalization of FPR after cathepsin G binding, calcium ion influx was attenuated compared to activation induced by fMLP.

Antagonists of FPR were studied mainly for their functions as potential diagnostic and therapeutic drugs. Dalpiaz *et al* synthesized several analogues of Phe-D-Leu-Phe-D-Leu-Phe derivatives with tert-butyloxycarbonyl at the N-terminal (BocPLPLP) and set off to analyze its effects on human neutrophils through *in vitro* assays chemotaxis (Dalpiaz, Ferretti et al. 1999). These derivatives were able to revoke neutrophil responses to fMLP as seen in reduction of $Ca^{2+}$ increase, superoxide anion production, and granule enzyme release. Chen et al examined the inhibitive effects of a bile acid (chenodeoxycholic acid) on leukocyte migration (Dalpiaz, Ferretti et al. 1999). It was found that this molecule competitively prevented fMLP and FPR-antibody binding to monocytes and thus inhibited leukocyte chemotaxis and calcium ion flux. Another endogenous source of antagonist possibly serving to keeping inflammation in check is spinorphin (a heptapeptide). Adding this peptide to normal mouse neutrophils led to calcium flux but did not bring about changes in FPR-knockout mice. Even though it was an agonist in terms of calcium ion mobilization, it was also effective at blocking fMLP-induced chemotaxis. While fMLP also activates FPR2 (low affinity subtype of FPR family of receptors), spinorphin fails to inhibit activation by levels of fMLP specific for FPR2, suggesting that it only acts through FPR. The use of agonists and antagonists is important for gaining insight into the functions and the processes through which such events occur.

**FPR in Immune Response**

When phagocytes are subjected to a uniform field of fMLP, they cluster to the tail end of fresh human neutrophils and become internalized (Loitto,

Rasmusson et al. 2001). They undergo a rapid phosphorylation and are transported to a Rab11-positive perinuclear recycling compartment (Boulay and Rabiet 2005). In the case of arrestin-deficient cells, N-formyl peptide receptors are trapped in the perinuclear compartment and do not get recycled back to the plasma membrane unless arrestin-2 or arrestin-3 has been restored (Vines, Revankar et al. 2003). Since arrestins are scaffolding proteins, it has been hypothesized that they regulate FPR dephosphorylation through targeting phosphatases to the endocytic vesicles that contain the receptors.

Migration of neutrophils is made possible by the cytoskeleton network assembly and disassembly. It has long been shown that integrins are linked to the cortical actin cytoskeleton (Wiesner, Lange et al. 2006). Upon leukocyte activation and binding with the endothelium, integrins form clusters to enhance adhesion even in the presence of shear stress. Experiments show that in order to rapidly mediate leukocyte adhesion in the bloodstream, multiple signaling proteins and their ligands are pre-assembled into complexes within the cell called signalosomes. These pre-existing complexes are thought to be different based on the type of leukocyte and contain different molecules (Laudanna and Alon 2006). Recent evidence shows integrin-mediated arrest of rolling leukocytes is triggered by chemoattractant binding to GPCRs on the leukocyte surface. It is still not known if the GPCRs make direct contact with the actin network although transient association fMLP-FPR complex with the cytoskeleton was induced by pulse-chase experiments and a half life of 30 seconds to 4 minutes was observed (Jesaitis, Naemura et al. 1984).

## Objectives and Specific Aims

The focus of my study is on fluid shear regulation of leukocyte pseudopod projection and retraction, a process important for cell circulation, spreading, and transendothelial migration. The distinctive and complex cell shapes of leukocytes cause a non-uniform fluid stress distribution over their membrane which in turn elicits involvement of different membrane mechanisms and downstream signaling molecules. The exact role played by fluid stress cannot be pinpointed until a more exact picture of the membrane fluid stress distribution is available. Therefore it is my objective to investigate the relationship between fluid stress distribution and neutrophil morphology and to identify a correlation between fluid stress distribution, candidate mechano-receptor distribution, and neutrophil morphology.

My Specific Aims are:

1) to compute the fluid stress distribution on the surface of a human neutrophil at various time points and to correlate the stress values with cell pseudopod activity;

2) and to determine formyl peptide receptor distribution before and after shear stress application and to correlate the spatial distribution of the two.

## MEMBRANE FLUID STRESS ANALYSIS

### Background

Various studies had been performed to compute the fluid stress distribution over cells adhered to a flat surface. Olivier and colleagues used 2D finite element analysis to determine the force and torque on a single endothelial cell at its various stages of spreading on the glass slide (Olivier and Truskey 1993). Representative images are taken of a bovine aortic endothelial cell when it just touches a coverslip in suspension with spherical shape, when it spreads for 15min, and when it is completely spread-out. By assuming that the volume of the cell does not change, the projected area of the cell varies at the different stages of spreading. The numerical computations showed that a spread out cell gains more than 7 times in projected area compared to a spherical cell but the drag force on the cell is reduced by 45% and the torque is reduced by 95%. In addition to reducing the drag force and torque, spreading allows cells to increase contact area and density of adhesion molecules, thereby minimizing the force exerted on each bond for attachment to the substrate.

Barbee *et al* carried out the first fluid stress computation using realistic cell shapes. The investigators obtained the topography of confluent endothelial cell layer with atomic force microscopy. They used spectral element analysis to compute the fluid stresses on the cell surface and found that peak stresses on the cell membrane are reduced by alignment to flow (Barbee, Mundel et al. 1995). Over a 24-hour exposure to 12dyn/cm$^2$ shear, the confluent endothelial layer mildly reduced the extent of undulations on the surface (from 1.22±0.07SD μm to

1.06±0.06 μm), which leads to a major reduction of peak shear gradient (from 0.39±0.19 $\mu m^{-1}$ to 0.25±0.11 $\mu m^{-1}$) on each cell.

Moazzam performed 3D finite element analysis on single adherent neutrophil by approximating the cell as a flat disk (Moazzam 1996). Flow was applied at a $30^{o}$ angle from a micropipette placed at 15μm from the centroid of the adherent cell with a maximum exit velocity of 1.46cm/sec. The maximum shear stress was calculated to be 0.46dyn/$cm^2$ and it was found in the front surface of the cell most near the pipette flow. A maximum pressure (normal stress due to the flow) was estimated to be 0.097dyn/$cm^2$ at the point close to the center of the neutrophil surface that is in line with the maximum velocity of the flow.

Pozrikidis used boundary element method to consider the case where a portion of a sphere projects from a smooth surface for the application of estimating the drag force and torque exerted on a cell by laminar flow (Pozrikidis 1997). The extent of protuberance is defined by the angle formed by the top of the sphere, the center of the sphere, and the contact point with the wall. There is a non-linear increase of the drag force and the torque on the projection relative to the angle. When the angle is at $135^{o}$, the shear stress at the top of the sphere is about 5.4 times that of the applied wall shear. In the case when the sphere just touches the wall, the maximum shear stress is found to be 6 times that of the wall shear. These numbers are close to the 2D case presented by Olivier *et al*, in which the maximum shear stress on a cell that has settled for 15min on the coverslip is almost 5 times that of the applied wall shear (Olivier and Truskey 1993). The slightly smaller shear in Olivier's computations may be due to the fact

that the spherical part of the geometry is attached to the wall by a foot and neck region that provides a non-angular transition from wall to the sphere.

Currently there are no published studies on the detailed membrane fluid stress distribution based on realistic 3-dimensional geometries of leukocytes. The stress distribution is quite non-uniform and highly dependent on the fine features of the geometry. My study is designed to provide an analysis of the location where a neutrophil responds locally to fluid shear on its membrane. The ability to locate specific regions on the cell where pseudopod extension or retraction can be seen is a key step in identifying the membrane transducers responsible for the fluid shear response. It gives us a better understanding of whether sites of high or low shear stress are associated with pseudopod projection.

## Materials and Methods

### Cell Culture

Acute human leukemic promyelocytic cells (HL60, ATCC) between 6 and 12 weeks old are cultured in RPMI 1640 medium (GIBCO, Invitrogen) supplemented with 10% fetal bovine serum (FBS) and 1% penicillin/streptomycin. They exhibit neutrophil-like functions (Gallagher, Collins et al. 1979) and express many of the same proteins as mature human neutrophils (Hauert, Martinelli et al. 2002) after a 5-day differentiation in media with 1.5% DMSO.

### *In vitro* Flow Chamber Experiments

Differentiated HL60 cells are stained with a red fluorescent membrane stain (PKH26, Sigma-Aldrich, $5x10^{-6}$ M final concentration) one day prior to experiments. $10^7$ cells are suspended in ½ mL of Diluent C (diluting solution for

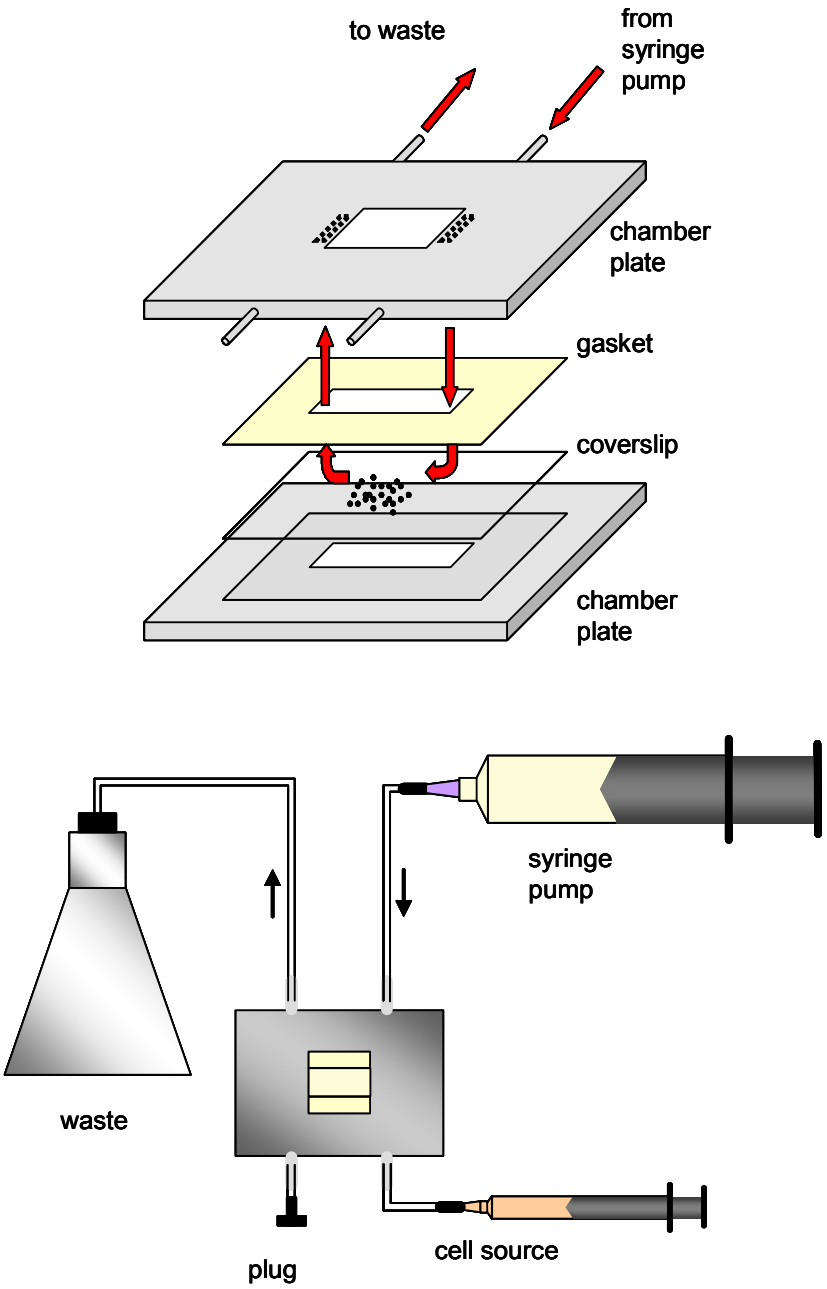


**Figure 3 Parallel-plate flow chamber set-up.**

Top: An exploded view of the flow chamber. Fluid flow is generated by a syringe pump, enters the chamber through an inlet, across the glass coverslip where the cells are free to migrate, and exit to waste flask through an outlet. A silastic gasket (250μm thick) sets the height of the flow channel. Bottom: A schematic drawing of the flow loop. Cells may be injected through one of the four ports prior to flow application or may be allowed to adhere on coverslip before chamber assembly. The last of the four ports is sealed with a plug in this experiment.

PKH26, Sigma-Aldrich) when 5 µL of PKH26 already diluted in another ½ mL of Diluent C is added and mixed well by repeated pipetting. The cells are incubated for 3 minutes at room temperature in PKH26 and 1mL of 10% FBS RPMI40 culture media is added to stop the staining action. Another 2mL of the same media is added after another minute. The cells are spun down at 150g for 3 minutes and washed twice with media. Just prior to the experiment, the cells (approximately $5x10^6$ cells/mL) are incubated with fMLP ($1x10^{-8}$ M final concentration) for 5 minutes. After injecting the cells into the parallel-plate flow chamber, they are allowed to settle and migrate freely on the glass coverslip (35x50mm #2 coverslips, Fisherbrand) for ~15min. A laminar flow of pH-adjusted and calcium-fortified PlasmaLyte at 2.2dyn/$cm^2$ is applied by a syringe pump (Harvard Apparatus) for 3 minutes.

## Image Acquisition

Confocal images (Biorad, OS2 Acquisition, 60x oil objective, 8x digital zoom, 128x128 pixels) of a migrating leukocyte are recorded along the z-direction (i.e., height) in 1µm intervals before, during, and after flow application. The measurements with the confocal microscope are verified at the beginning of each experiment by scanning a fixed fluorescent bead of fixed known diameter while adjusting the focus and checking the displacement read-out from the acquisition program. The strength of the laser (Krypton/Argon, 4-7mW before entering the confocal, 568nm excitation wavelength), level of gain, and iris size is adjusted for each cell in order to obtain optimal images. This is achieved by first putting the cell into focus under bright field, then scan with 10% laser power quickly while

adjusting the aperture size and gain magnitude. Then the strength of the laser is increased to 30% to check the change in image quality. If the contrast in pixel intensity between the cell and its surrounding is sharply increased, the laser strength is kept at 30%; otherwise it will be decreased back down to 10%. To determine the positions at the bottom and at the top of the cell, the focus is changed quickly in an upward direction while keeping the laser on. The upper and lower bounds of the scanning distance are estimated based on visually determining where cellular features can first be distinguished (in fluorescence) while altering the focal planes through the cell quickly.

## Reconstruction of 3D cell morphology

The 3D morphology of the cell is recreated numerically on the digitized images (Matlab R14 and FEMLAB 3.0a). The images are first processed digitally to generate enhanced contrast and then passed through a median filter which smoothes the cell edges with minimal loss of cell edge details (ImagePro). The perimeter of the cell is traced by hand on the computer. The 2D contour of the cell is then approximated by a 36-sided polygon (Matlab). Each segment is marked by two endpoints which will be used to match to a corresponding segment of each of the neighboring cell section images in the third dimension. The spacing between each section is determined from a length calibration (each pixel in the image represents a length of 0.263μm). To provide a better representation of the cell shape, the top-most section is represented by a 24-sided polygon instead of 36 sides. The 24 points are linked to the 36 points of the section below by manually creating solid tetrahedrons. To create a more realistic approximation

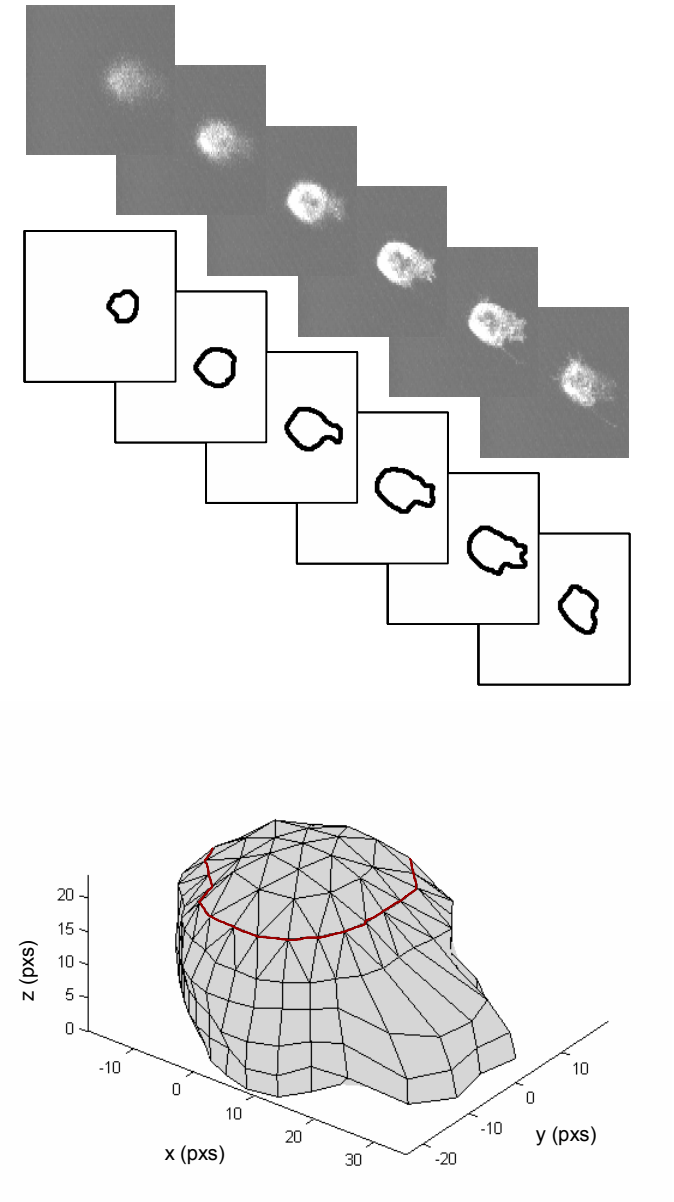


**Figure 4 Cell shape reconstruction.**

Top: Original confocal images and corresponding manually-traced cell outlines (each 128 x 128 pixels) of transverse sections of a migrating neutrophil. Bottom: The cell geometry used in the FEM model is reconstructed from stacking the 2D cell outlines. The top (above the red line) is extrapolated from points that define the rest of the cell. Each pixel corresponds to 0.263μm.

for the top of the cell, 19 points are extrapolated from the top 3 contours of the cell. The xyz positions of these points are used to generate solid tetrahedrons that form a cap, which sits on top of the cell geometry formed from confocal images. This complete 3D cell shape is then imported into a numerical finite element program (FEMLAB 3.0a) that uses basic Navier-Stokes equation to determine the fluid stress on the cell membrane.

## Fluid Flow Analysis

We assume plasma to be a Newtonian fluid. Based on the flow rate, the applied laminar flow in the parallel-plate flow chamber has a calculated maximum velocity of 1.41cm/s and a wall shear stress of 2.2dyn/cm$^2$ for a channel thickness of 250μm and width of 10.8mm. The flow is assumed to be at steady state and the flow around the cell is laminar and uniform because of low Reynolds number. The laminar flow is fully developed at a distance of 0.75μm from the flow chamber entry, as calculated from the expression (Fox and McDonald 1998)

$$\frac{L}{h} \approx 0.06\,\mathrm{Re} = 0.06\frac{\rho \bar{V} h}{\mu} \qquad (1)$$

where $L$ is the entrance length, $h$ is the chamber height, $\bar{V}$ is the average velocity (computed as flow rate divided by the cross-sectional area of the flow chamber), and $\mu$ is the dynamic viscosity. This indicates that all cells observed in the flow chamber are under fully developed steady state laminar flow.

The cell is assumed to be a solid viscoelastic body and gravity acting on the cell is negligible. The applied fluid stresses are not sufficient to induce an elastic deformation of the cell (Schmid-Schonbein, Sung et al. 1981). Newtonian

flow is governed by the continuity equation and the momentum equation (the Navier-Stokes equation).

$$\nabla \cdot \vec{v} = 0 \tag{2}$$

$$\rho \frac{\partial \vec{v}}{\partial t} + (\vec{v} \cdot \nabla)\vec{v} = -\nabla p + \mu \nabla^2 \vec{v} + \vec{F} \tag{3}$$

where $\vec{v}$ is the velocity vector, $p$ is pressure, and $\vec{F}$ is the total body force. Under the above assumptions, the momentum equation can be simplified to

$$\nabla p = \mu \nabla^2 \vec{v} \tag{4}$$

The equations are non-dimensionalized with the following values: the characteristic length is set to 5μm and the characteristic velocity at 1 cm/s, which gives a Reynolds number of 0.05. The dimensionless variables are defined as:

$$v_i^* = \frac{v_i}{1\,{}^{cm}\!/_{s^2}} \tag{5}$$

$$x_i^* = \frac{x_i}{5\mu m} \tag{6}$$

$$\mathrm{Re} = \frac{\rho\left(1\,{}^{cm}\!/_{s^2}\right)(5\mu m)}{\mu} \tag{7}$$

where $v_i$ is the dimensional velocity in the $i$ th direction. Plasma-Lyte, the shearing fluid, is incompressible and its dynamic viscosity is measured with a viscometer to be 0.98 centipoise (1 centipoise = 0.001 Pa/sec).

For the finite element model, the total modeling volume is set to have a height of 25 characteristic length units, which is at exactly half the height of the

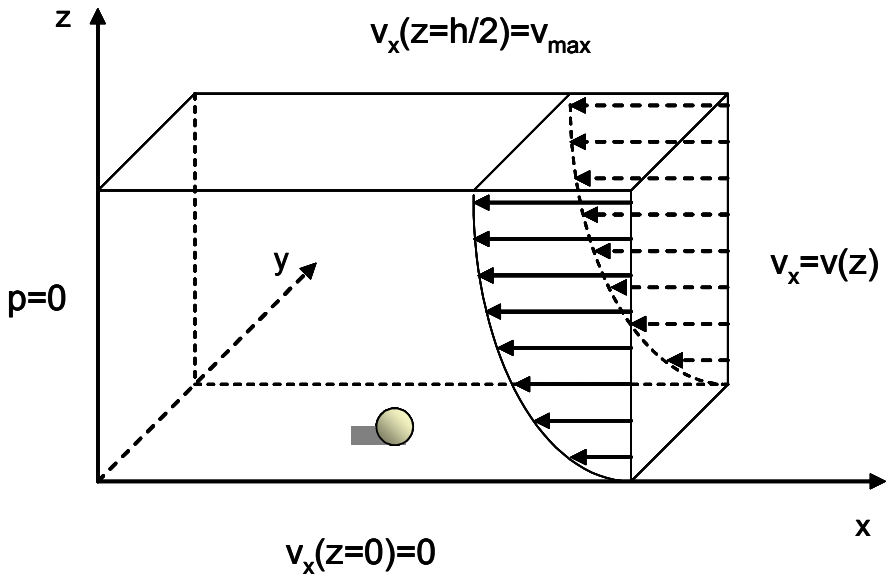


**Figure 5 Boundary conditions for finite element modeling.**

The cell surface and the glass coverslip are under no-slip conditions, whereas the top of the modeling volume experiences maximum flow velocity in the tangential direction. The flow profile is parabolic where $v_x$ = 0.0022*z*(50-z) with the de-dimensionalized cell diameter at approximate 2 units. The exit pressure is zero and the velocity is set to be normal to the exit boundary. The two boundaries normal to the y-axis experiences tangential velocity (in the x-direction).

flow chamber. The entrance length and the exit length are both about 14 units so the flow can develop fully and the exiting face will not see flow disturbance from the cell. The depth of the flow chamber is similar to the entrance and exit lengths at approximately 14 units on each side of the cell. The coverslip and the surface of the cell satisfy the no-slip condition. On all other boundary surfaces I assume zero normal stresses because the flow is unidirectional. A parabolic velocity profile is assumed at the entry to the modeling volume based on Poiseuille's equation.

A finite element mesh is generated (FEMLAB) with the highest density of elements on the cell surface and the cell contact areas. The size of the elements depends on the complexity of the surface details. The number of elements is 14000-22000 for each of the geometries modeled. The results are verified by checking the wall shear stress values away from the cell and comparing the shear distribution to that of a semicircle in the exact same flow field.

The numerical computation (FEMLAB) is based on the complete Navier-Stokes equation. A linear steady state solver is used in solving equation (3). Since the reconstructed 3D cell geometries were defined by tetrahedrons and have edges, the computation by FEMLAB produced some large stress values at the top and at a few isolated locations along the edges of some of the solid tetrahedrons. It is therefore necessary to evaluate the effects of such extreme stress values, i.e. how frequently these values occur on the geometry and what value would be reasonable if the geometry were smooth. Several smooth and well-defined geometries were created to provide an estimate for the range of

stress values. The computation by using the same finite element volume and same boundary conditions is first carried out for several semi-spherical geometries attached to a plane wall. For ease of creating such geometries, the four protruding semi-spheres had heights of 1, 1.25, 1.5, and 1.75 units (each unit is equivalent to 5μm) from the plane wall (see Figure 6), where a height of 1 is a hemisphere. To get a better understanding of the effect of a pseudopod projection from the cell body, a combination of a truncated ellipsoid and semi-sphere was used to find out how the maximum shear stresses change. A truncated ellipsoid with x-radius of 1.5 characteristic length units (parallel to direction of flow), y-radius of 1.5 units (perpendicular to direction of flow but in the plane of the wall), and z-radius of 0.5 units (perpendicular to direction of flow and wall) was added to the semi-spherical protrusions of 1.25, 1.5, and 1.75 (Figure 7).

Upon computing the fluid stress distribution for various smooth shapes of the same range of heights as the cell geometries, it is shown that at least 99% of cell surface has calculated stress values in the same range as that of a smooth geometry. The 1% large stress values are considered to be artifact of the current 3D geometry reconstruction method. The relationship between maximum stress value on a smooth protrusion from the wall and the height of the protrusion can be approximated by a linear regression function. This function is used to determine the maximum (based on the smooth geometries) fluid stress values versus artifact values. These large values occur on less than 1% of the finite elements and are therefore changed to the highest value within the cut-off range in order to provide an optimal view of the stress distribution on the cell surface. This also allows for a

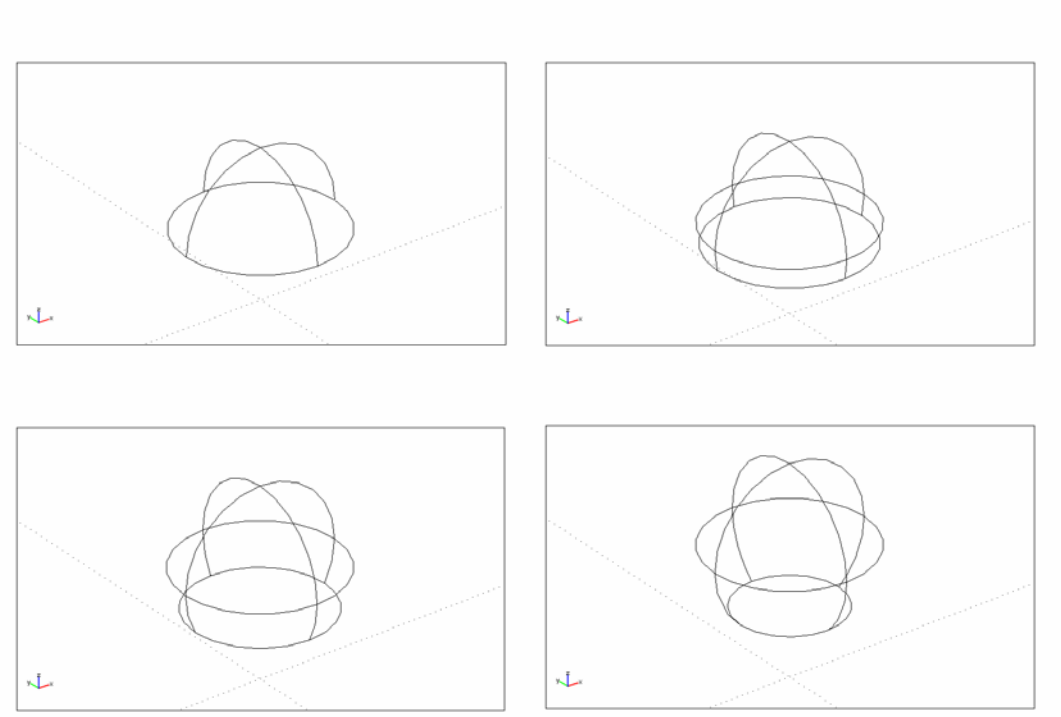

**Figure 6 Semi-spherical protrusions on a plane wall.**

Shown here are the four cases of semi-spherical protrusions on a plane wall where the radius of the sphere is 1 unit (each unit represents 5μm). The height of the top of the protrusions are 1 (top left), 1.25 (top right), 1.5 (bottom left), and 1.75 (bottom right).

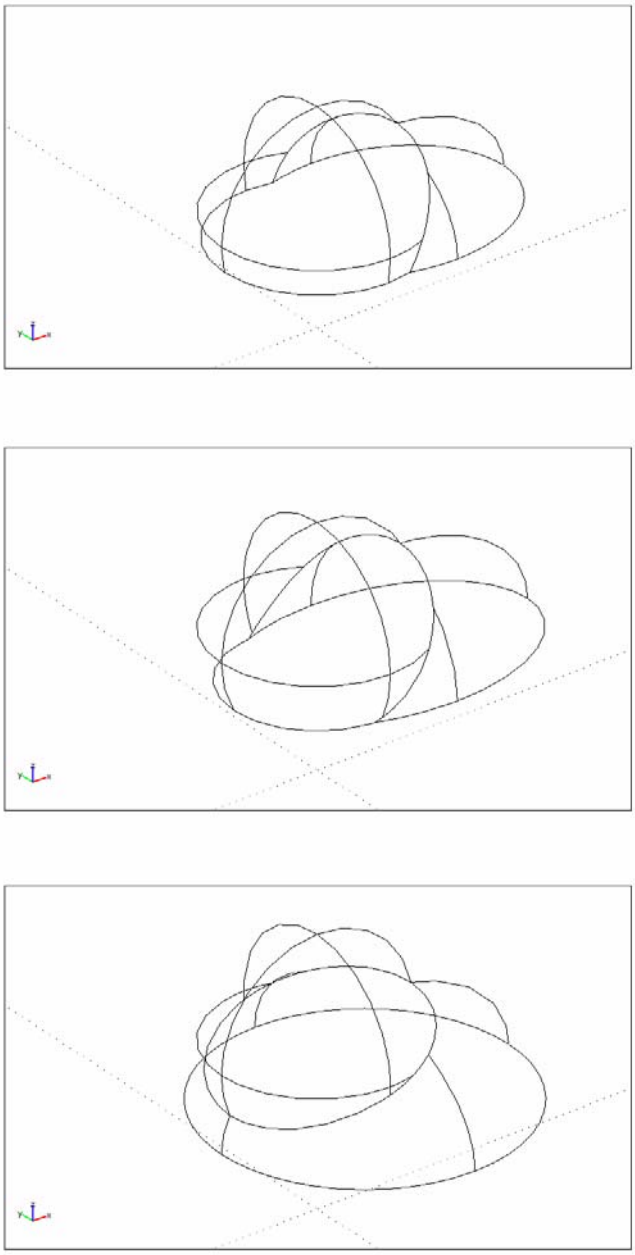

**Figure 7 Simulated cell geometry with truncated sphere and ellipsoid.**

Top: Semi-sphere of 1.25 units in height with ellipsoid (x-axis = 1, y-axis = z-axis = 0.5), whose center is shifted to x = 0.5. Middle: Semi-sphere of 1.5 units in height with ellipsoid of same dimensions but whose center is shifted to x = 0.5 and z = 0.25. Bottom: Semi-sphere of 1.75 units in height with ellipsoid (x-axis = 1.5, y-axis = 1.5, z-axis = 0.5), whose center is shifted to x = 0.5.

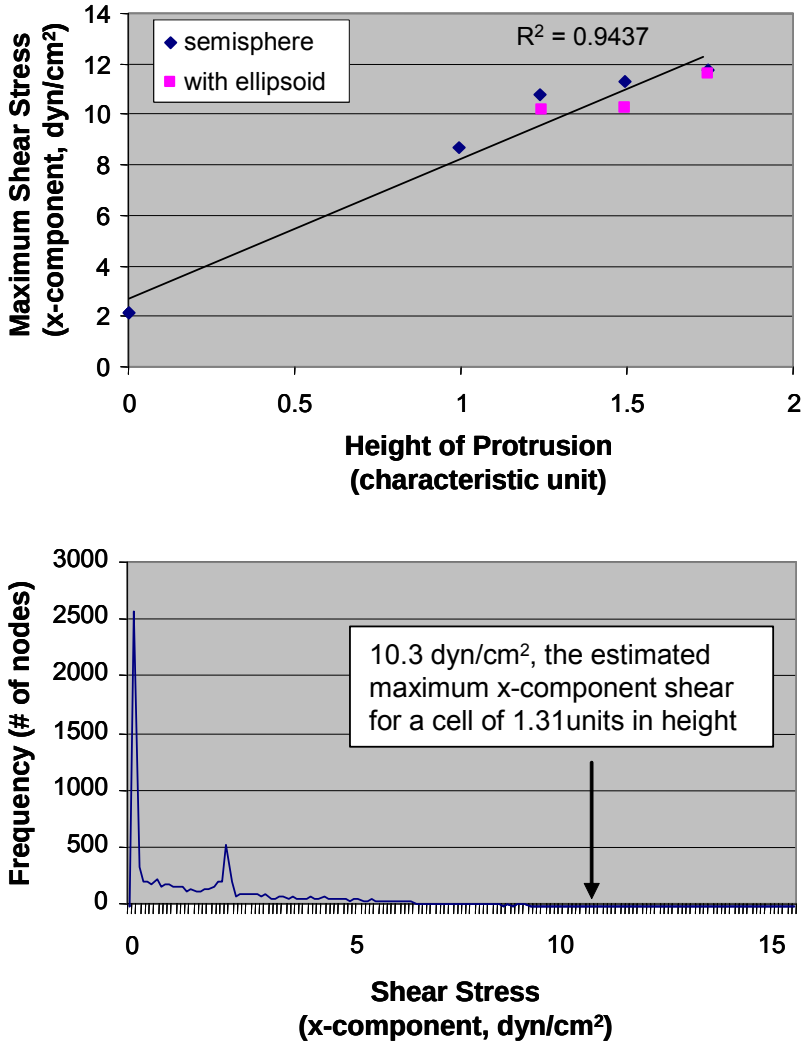


**Figure 8 Method of determining the maximum shear stress at top of cell.**

Top: The maximum shear stress for a semi-spherical and the spheroid-ellipsoid protrusions of various heights under the same flow conditions as the cell model exhibits a linear dependence on the height of the geometry. Bottom: The number of FEM nodes exhibiting shear stress values beyond the maximum value (found from the linear regression) composes less than 1% of the total number of nodes that define the modeling volume.

more precise analysis of the correlation between stress values and distribution with instantaneous cell surface radii.

## Stress Distribution and Pseudopod Length Estimate

The 2D geometric centroid of the cell on each image section is calculated from the outlines as follows:

The x- and y-coordinates of each pixel that defines the outline are averaged over the entire length of the outline and the resulting x- and y-values indicate the coordinates for the centroid of that section. The process is repeated for each of the 2D sections for the cell and the x-y position of the overall centroid is the average of the individual sections. The height of the centroid from the bottom image is determined to be exactly half of the maximum height of the cell at the initial time point (onset of flow). The computed centroids for the cell at subsequent time points are shifted in all three directions to match the centroid of the same cell at the onset of flow. This is done by manually changing the xyz coordinates of the centroid to those of the initial time point. Each cell surface is divided into 5 regions (Figure 9): right proximal (region 1), left proximal (region 2), left distal (region 3), right distal (region 4), and top (region 5). The left and right directions are determined by looking in the direction of flow. The average values for shear stresses, normal stresses, resultant stresses, and distance of the cell membrane from the centroid (radius, which serves as a measure for the pseudopod length) are computed separately for each membrane region.

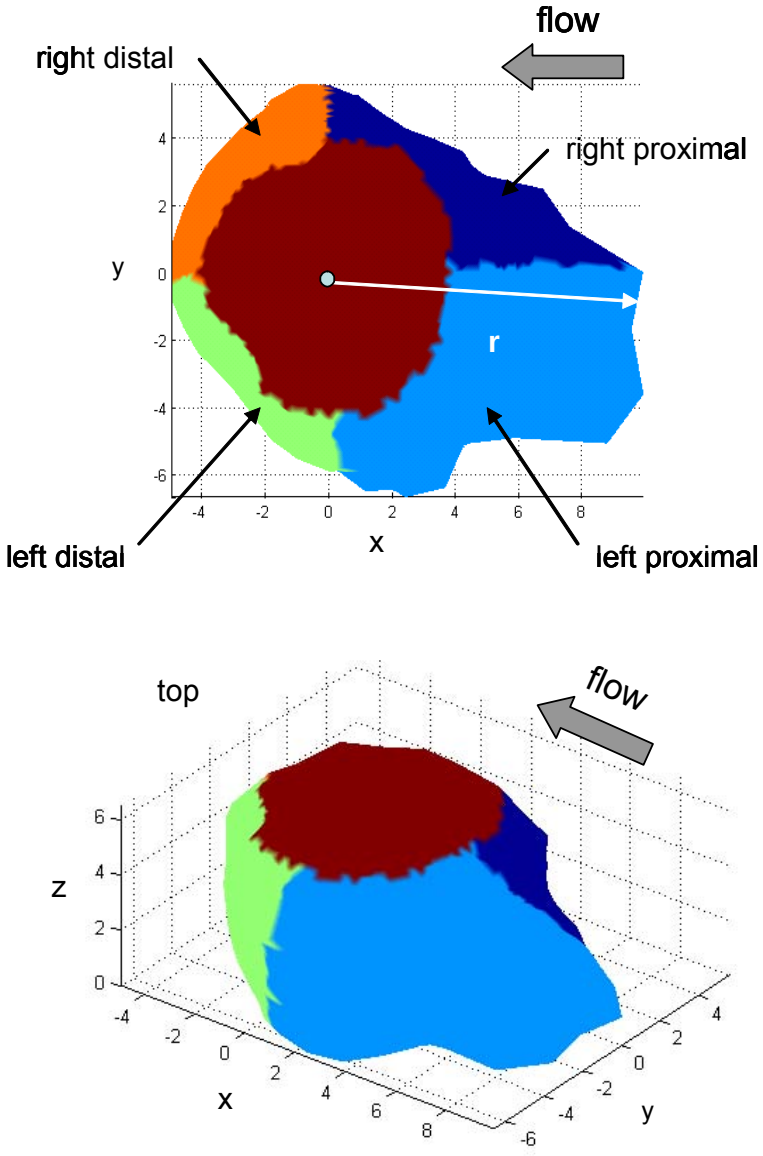


**Figure 9 Cell surface region definition.**

The cell geometry from each time point is divided into 5 surface domains, as indicated by the different colors. They are identified on a 2D projection (top) and 3D representation (bottom) by their relative location with respect to the source of flow. The extent of surface protrusion is defined by the distance from the calculated centroid of the cell to the surface (denoted by r).

## FEM Modeling of Membrane Folds

### Scanning Electron Microscopy (SEM)

Unpublished SEM images from a previous experiment (Schmid-Schonbein, Shih et al. 1980) were used for the shape and size approximation of membrane folds in the FEM model. The methods were outlined in the literature (Schmid-Schonbein, Shih et al. 1980). Fresh human venous blood samples were suspended with EDTA as an anticoagulant and allowed to sediment at room temperature for 25-40 minutes. The supernatant plasma layer containing mostly leukocytes was collected and suspended in 50ml NaCl solution of pH 7.4. The cells were fixed in 1% final concentration of glutaraldehyde solution and then fixed again at 2% glutaraldehyde solution for one hour. The cells were washed in cocadylate buffer (0.1M cocadylate, Fisher Scientific Co, Springfield, NJ, adjusted to pH 7.4 and filtered) and then in distilled water. The cells were rinsed in ethanol (80%, 90%, 95%, and 3 times in 100%) and air dried on microcover glasses. The cover glass was then glued to aluminum stubs with silver paint, coated with gold palladium using a Hummer I sputterer, and imaged in a JSM-25 scanning electron microscope (JEOL Corp., Peabody, MA) at 15kV. The length calibration was obtained from a standard grid for each image.

### Model of Membrane Folds

Smooth submicron cylindrical protrusions (see Figures 24-27) are used to model membrane folds on human leukocytes based on scanning electron micrographs. The height of each protrusion is 0.04 units (equivalent to 0.2μm) and the widest part of the base is 0.06 units (0.3μm) in diameter. In the model for

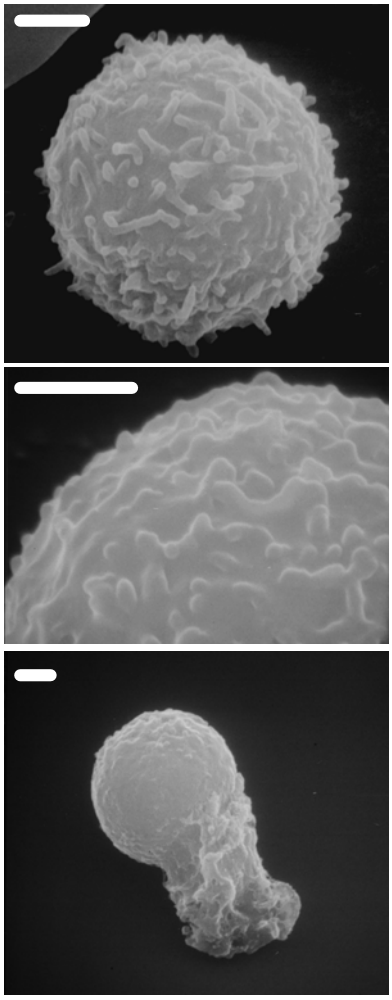

**Figure 10 Scanning electron micrographs of human neutrophils.**

SEM images allows for a better look at the size and shape of surface membrane folds on human neutrophils. Top: a quiescent neutrophil: middle: an enlarged view; bottom: an activated neutrophil with pseudopod extension. Bars: 1μm.

closely-clustered membrane folds, protrusions are spaced in a hexagonal pattern where the edge of the base just touches the neighboring protrusion. For the model of sparsely-spaced membrane folds, each protrusion is 0.75μm (center to center) from each other. The modeling volume is set at 1unit by 1unit by 0.5unit (equivalent to 5μm by 5μm by 2.5μm) so that the flow disturbance caused by the membrane folds is negligible at the boundaries of the volume. The inflow velocity profile is parabolic and with maximum velocity of 1.41cm/s at a height of 125μm from the glass coverslip (therefore an applied wall shear stress of 2.2dyn/cm$^2$).

Similar to the methods described under previous section “Fluid Flow Analysis,” a finite element mesh of ~15000 elements is generated (FEMLAB) with the highest density of elements on the membrane protrusions. The results are verified by checking the wall shear stress values away from the cell. A linear steady state solver is used for the numerical computation of the complete Navier-Stokes equation. The computation produced some large stress values at a few isolated locations at different regions of separate protrusions (side, top, and upstream regions). It is found that by eliminating the top 5% and the bottom 5% of the stress values (shear, normal, and resultant) the stress distributions become smoother and elimination of a higher percentage of stress values led to a marked change in the distribution profile. The remaining few (~20 isolated nodes out of ~4500) of enhanced stress values (>3 fold difference with a neighboring node) were manually changed to the stress value of a node of close proximity, and this gave a smooth stress distribution on each membrane fold.

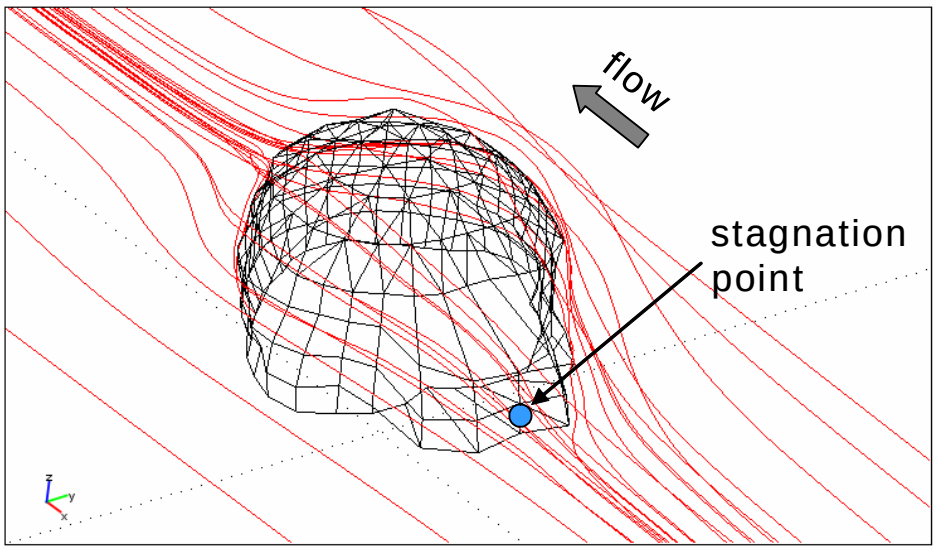


**Figure 11 Lack of recirculation zones in the flow field.**

The streamlines around a cell geometry stays continuous and smooth. The stagnation point occurs at the front (blue dot) and back (not shown) of the geometry where the velocity is equal to zero.

## Results

There exist stagnation points in the front and back of the cell, where the magnitudes of velocity and shear stresses are zero (Figure 11). At the low Reynolds number in this problem, recirculation zones do not occur and fluid particles do not get trapped in eddies upon passing over the cell surface. They pass around the cell in streamlines that run parallel to the base.

### Fluid Stress Distribution on the Cell Membrane

The validity of the FE model was verified by comparing the wall shear stress away from the cell to the same as analytical solution for Poiseuille's flow in a parallel-plate flow chamber. After computing the surface stresses for the semi-spherical protrusions, it was found that, interestingly, the maximum values for the x-component of shear stresses are linearly dependent on the height of the shape that protrudes from a flat surface. By adding a truncated ellipsoid to the spherical protrusion, the maximum x-component of the shear stress (always found at the top region of the geometry) was decreased but the x-component of the resultant stress was both decreased and increased. It is noted that in the two cases where the resultant stress decreased, the height of the truncated ellipsoid is 0.5 units (non-dimensionalized) for both and the heights of the semi-spheres are 1.25 and 1.5 units. The reductions are 11% and 6%, respectively. In the one case where the semi-sphere is 1.75 units high and the ellipsoid height remains at 0.5 units, the shear stress increases by nearly 7%. It is possible that the disparity in height between the ellipsoid and the semi-sphere determines how the maximum shear stresses are changed, but no further study was conducted since this issue is outside the goal of this research project.

From these computations with simulated geometries, it was found that the existence of a pseudopod can change the maximum shear stresses on the top of the cell, based on its size relative to the rest of the cell body. More importantly, an approximate range of surface stress values was obtained with these cases.

The fluid stress distribution on the plasma membrane depends on the instantaneous cell shape. Our results show that the maximum resultant stresses are located at the top of the cell. Sites of high stresses also occur at membrane protrusions, such as on top of a pseudopod. However, the magnitudes of these stresses are less than those at the top of the cell. The lowest stresses (~0dyn/cm$^2$) are located around the contact areas of the cell with the glass coverslip and at small regions of membrane indentations. The shear stress distribution shows a similar profile as that of the resultant stress. The lowest shear is found in the contact regions with the substrate and the highest on surface protrusions and near the top of the cell body. Due to the compressive fluid pressure, the normal stresses are highest at the front part of the cell. However, on the upper back region of the cell, there exist enhanced tensile normal stresses.

The normalized x-component of shear stress on the cell was compared to published results for shear flow over a protuberance of similar shape and height (Pozrikidis 1997). The comparison was made for the 3-min flow time point for the cell shown because it was most representative of a truncated sphere protruding from a plane wall, for which the normalized shear stress values had been calculated before. It was found that the normalized shear stress in the direction of flow at the top of the cell is approximately 6 times that of the wall

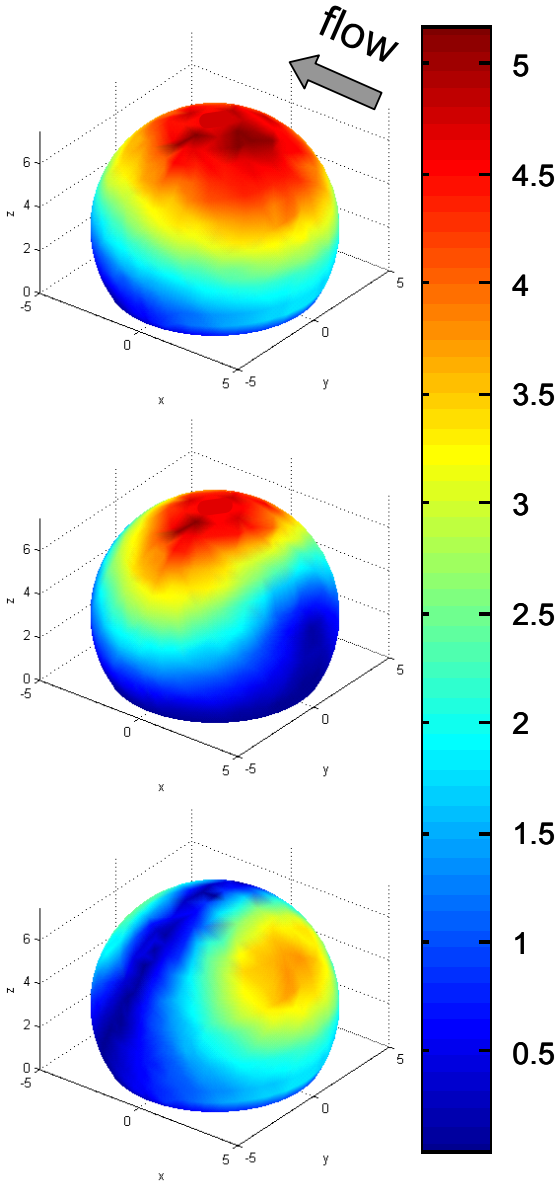


**Figure 12 Normalized stress distributions on the surface of a spherical geometry on a plane wall.**

Resultant stress (top), shear stress (middle), and normal stress (bottom) distributions on the surface of a combined geometry (truncated sphere similar to the size of a real cell) are normalized with respect to the applied wall shear stress of 2.2dyn/cm$^2$ in the negative x-direction. The color bar is unitless and the axes are in μm.

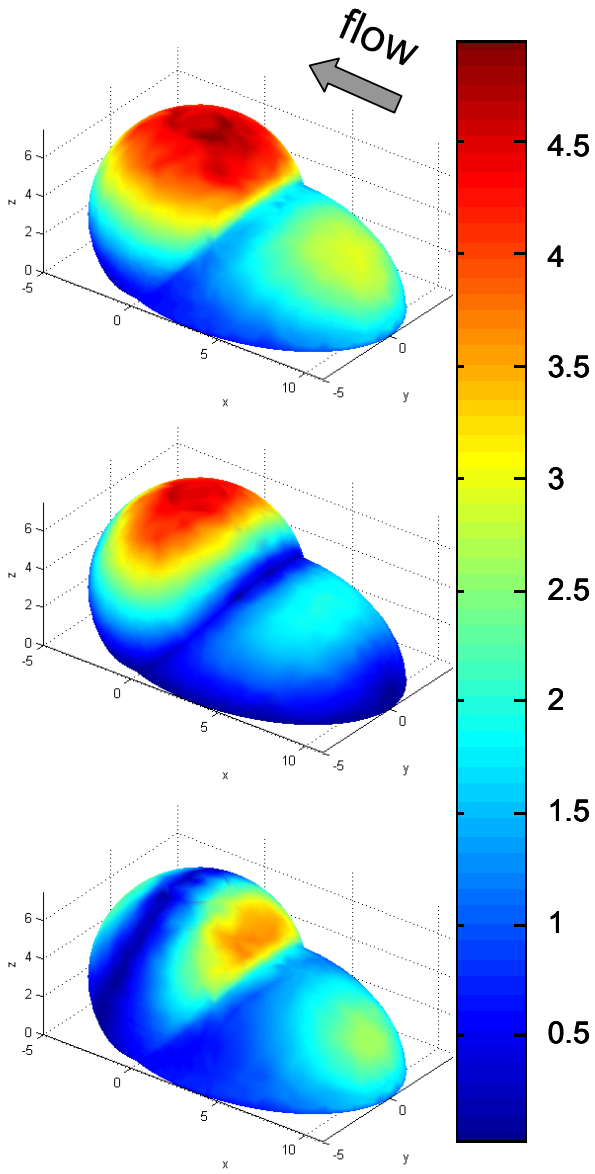


**Figure 13 Normalized stress distributions on the surface of a spherical-ellipsoidal geometry on a plane wall.**

Resultant stress (top), shear stress (middle), and normal stress (bottom) distributions on the surface of a combined geometry (truncated sphere and ellipsoid similar to the size of a real cell) are normalized with respect to the applied wall shear stress of 2.2dyn/cm$^2$ in the negative x-direction. The color bar is unitless and the axes are in μm.

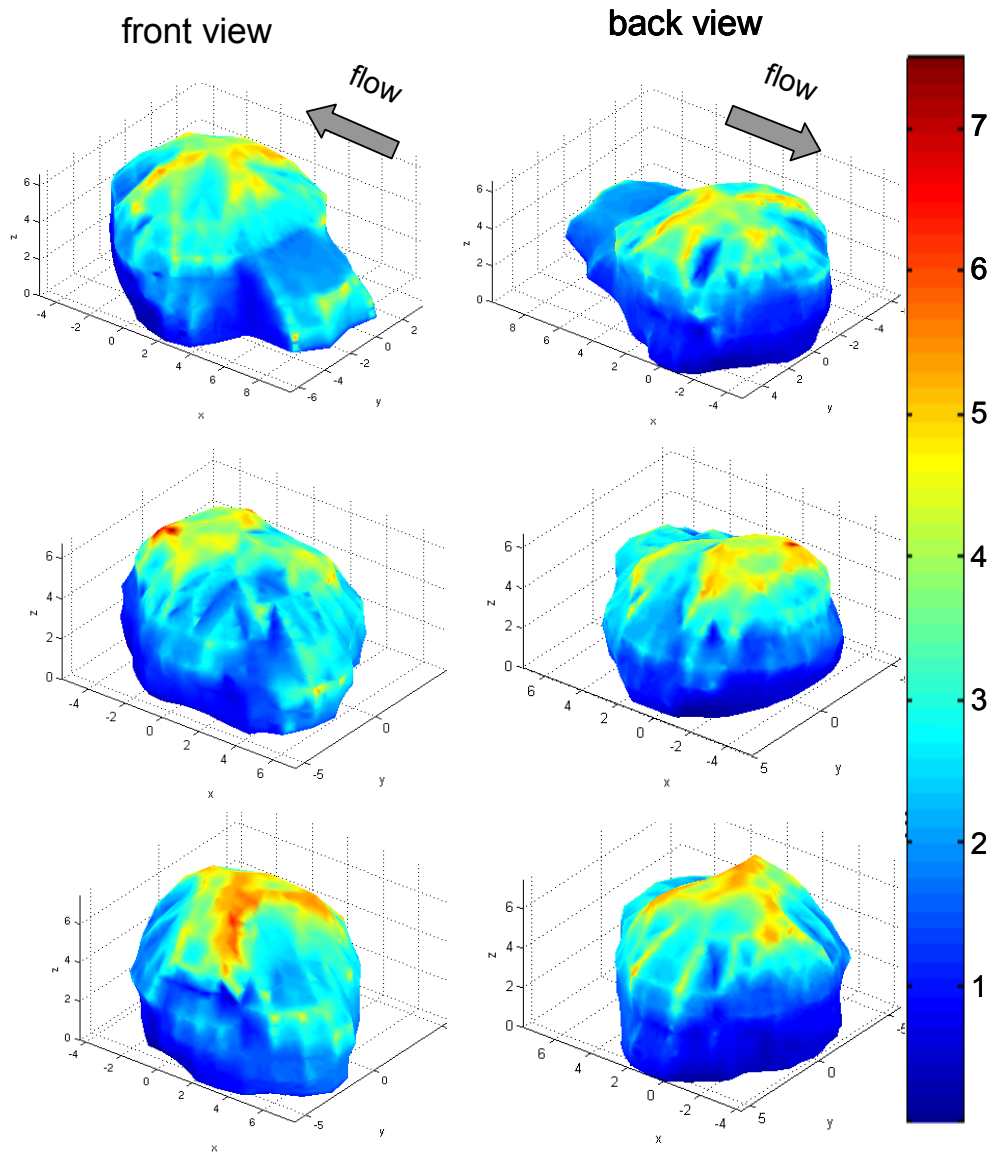


**Figure 14 Normalized resultant stress distributions on the surface of an adherent leukocyte.**

Resultant stress distributions (left: front view, right: back view) on the surface of one neutrophil are normalized with respect to the applied wall shear stress of 2.2dyn/cm$^2$ in the negative x-direction at the onset of flow (top), 1 minute into the flow (middle), and the end of a 3-min laminar flow application (bottom). The color bar is unitless and the axes are in μm.

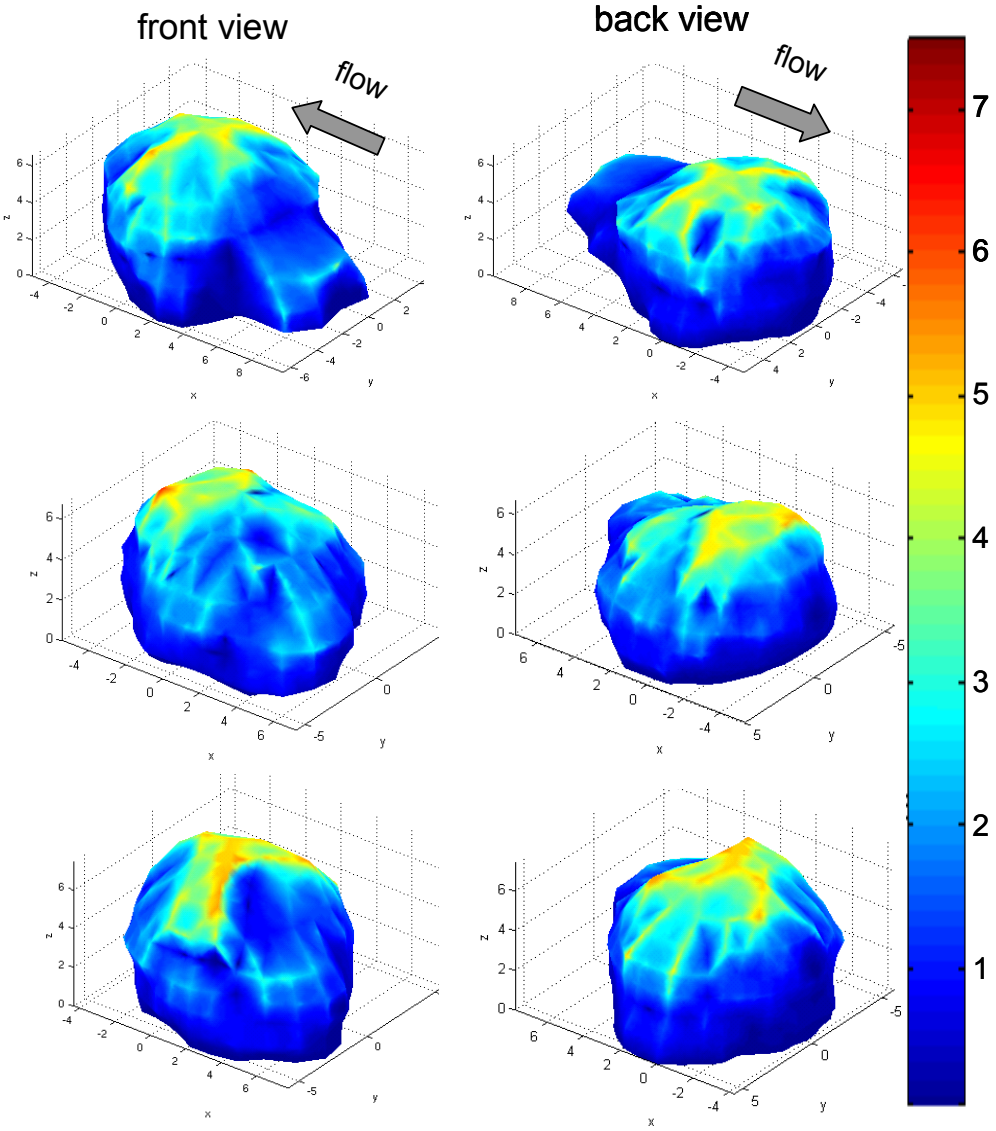


**Figure 15 Normalized shear stress distributions on the surface of an adherent leukocyte.**

Shear stress distributions (left: front view, right: back view) on the surface of one neutrophil are normalized with respect to the applied wall shear stress of 2.2dyn/cm$^2$ in the negative x-direction at the onset of flow (top), 1 minute into the flow (middle), and the end of a 3-min laminar flow application (bottom). The color bar is unitless and the axes are in μm.

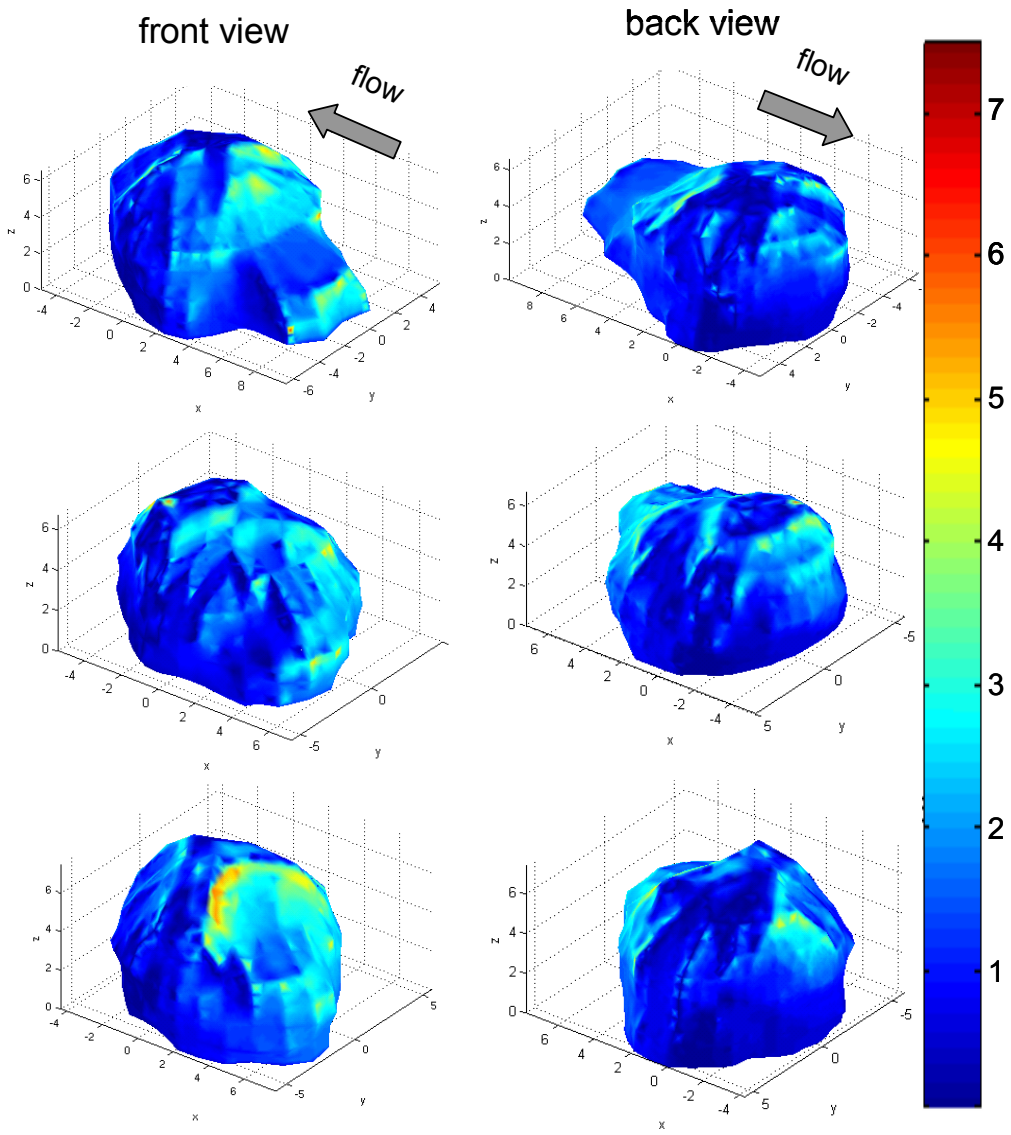


**Figure 16 Normalized normal stress distributions on the surface of an adherent leukocyte.**

Normal stress distributions (left: front view, right: back view) on the surface of one neutrophil are normalized with respect to the applied wall shear stress of 2.2dyn/cm$^2$ in the negative x-direction at the onset of flow (top), 1 minute into the flow (middle), and the end of a 3-min laminar flow application (bottom). The color bar is unitless and the axes are in μm.

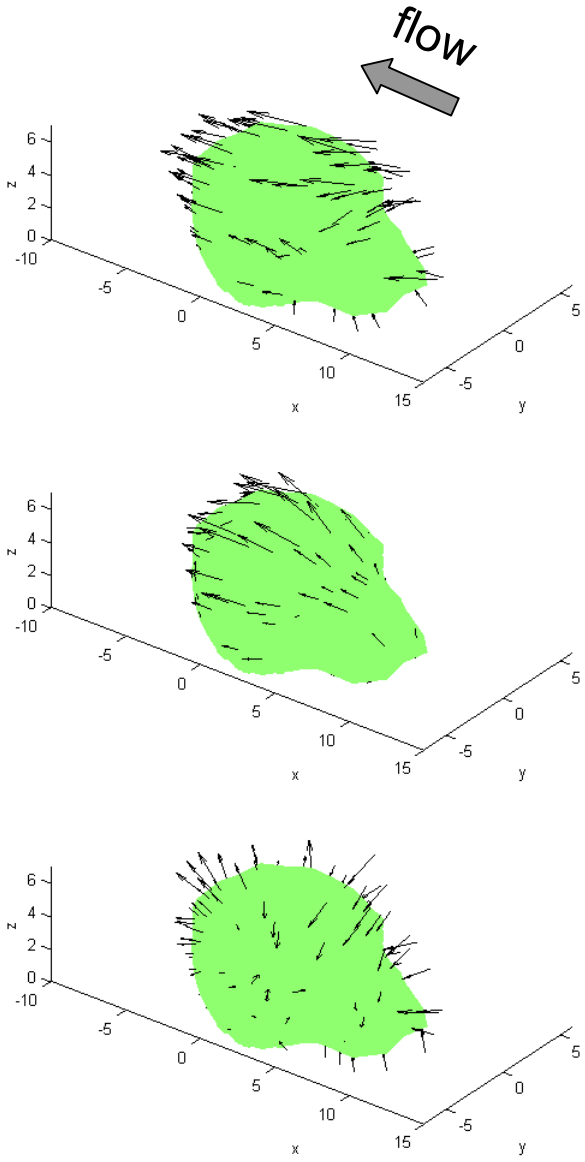


**Figure 17 Directions of normalized fluid stresses on the surface of an adherent leukocyte.**

Top: Resultant stresses act predominantly in the same direction as flow. Middle: Shear stresses always act tangential to the cell surface. Bottom: Normal stresses always act perpendicular to the cell surface, but towards the downstream portion of the geometry, these stresses are tensile instead of compressive as in the upstream side.

shear stress, which is very close to the aforementioned published results (Pozrikidis 1997). Away from the top, the extraneous features on the cell membrane do not contribute significantly to the maximum shear stress. Using this information, the extreme high shear stress values of reconstructed cell shapes are replaced by the maximum shear stress value approximated from the linear regression function (as shown in Materials and Methods section).

It should be noted that the exact direction of the stresses shown in Figures 12-16 are not depicted within the same figures. The resultant stresses act almost entirely in the directly of flow, shear stresses are always tangential to the surface of the protrusion, and normal stresses are always acting perpendicular to the surface of the protrusion. However, in the case of normal stresses, the back of the protrusion experiences a tensile stress (pulling on the surface) whereas the front of the protrusion sees a compressive stress (pushing on the surface). This fact cannot be clearly illustrated by the color figures which show only the magnitudes of stresses. For all cell geometries (as well as the semi-spherical protrusions) the normal stresses anywhere on the surface always have a component that acts in the direction of flow because there are no recirculation zones in any of the flow profiles. A representative case showing the directions and relative magnitudes of resultant, shear, and normal stresses for one cell geometry is presented (Figure 17).

## Membrane Fluid Stress Distribution and Cell Morphological Changes

Even though the stress values on the 5 cells are different, the shift in resultant stress on each cell is insignificant over the shear period from the

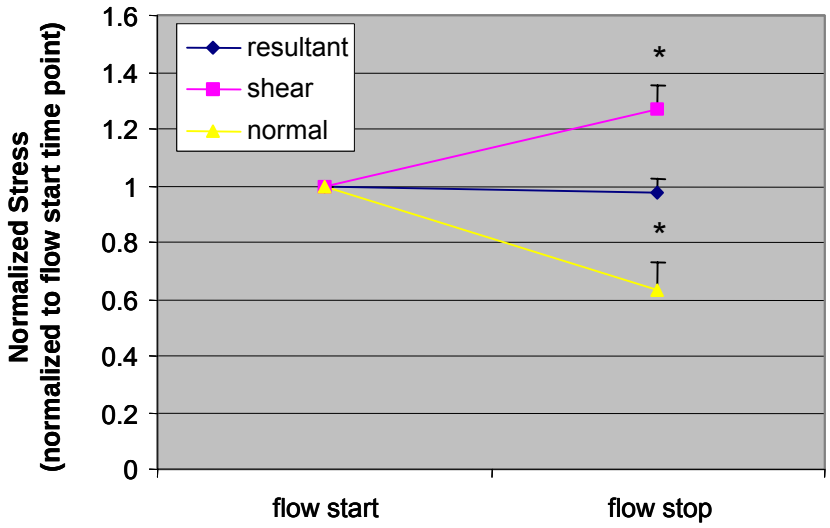


**Figure 18 Changes in average fluid stresses on the entire cell surface as a function of time.**

The cell-average resultant stress does not change between when flow was just started and immediately after flow has stopped. The cell-average shear stress increases by closet o 30% between the same two timepoints while the cell-average normal stress decreases by close to 40%. All stresses have been normalized to their values at the first timepoint. n=5 cells. Error bars: SE. *P<0.05.

beginning to its end at 3 minutes. It is interesting to note that the average resultant stress on the surface of the cell is relatively invariant with respect to the exact shape of the cell while the stress components changed significantly. Shear stresses increased significantly by about 25% and the normal stresses decreased by close to 40% (Figure 18). These opposing changes in the two stress vector components serve to keep the resultant stress on the cell surface at a constant.

The cell surface was then divided into 5 domains (as outlined in the Materials and Methods section of this chapter) to examine if the above changes are also evident in specific regions of the cell, in particular the front where normal stresses are highest and the top where shear stresses dominate. The amount of cytoplasmic extension or retraction of each surface region (relative to the cell centroid) is shown next to the change in average stresses within the same region. We find no linear or even monotonically increasing correlation between the magnitude or the direction of retraction and the magnitude of fluid stresses on the cell surface, i.e. surface regions experiencing the highest fluid stresses (resultant, shear, or normal) do not retract the most (Figures 19-21).

Looking at the fluid stresses on 5 cells, we found that the average stress values for each region did not change in the course of the 3min flow application (Figures 22). The average stresses (resultant, shear, and normal) for each region stayed constant within that region regardless of where that region is with respect to flow direction. The proximal regions experience higher normal stresses compared to the rest of the cell, but the level of that normal stress did not increase or decrease even after 3min of flow. The top region of the cell has

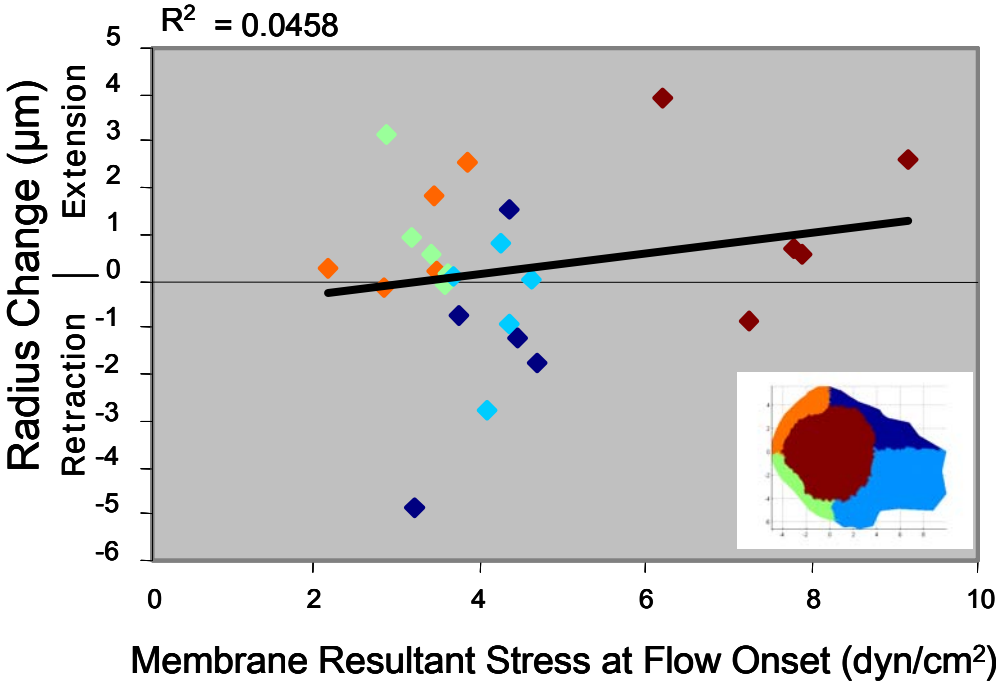


**Figure 19 Lack of simple correlation between resultant stress and pseudopod retraction.**

The extent of regional membrane retraction is not linearly dependent on the magnitude of the average membrane resultant stress within that region (each dot in the plot is color-coded by region)

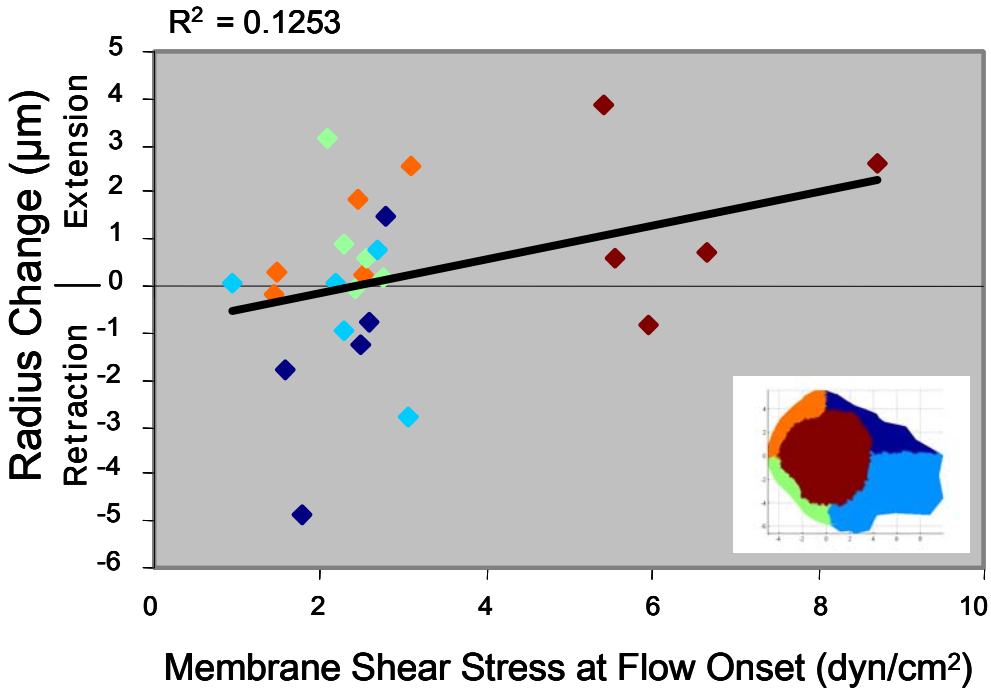


**Figure 20 Lack of simple correlation between shear stress and pseudopod retraction.**

The extent of regional membrane retraction is not linearly dependent on the magnitude of the average membrane shear stress within that region (each dot in the plot is color-coded by region)

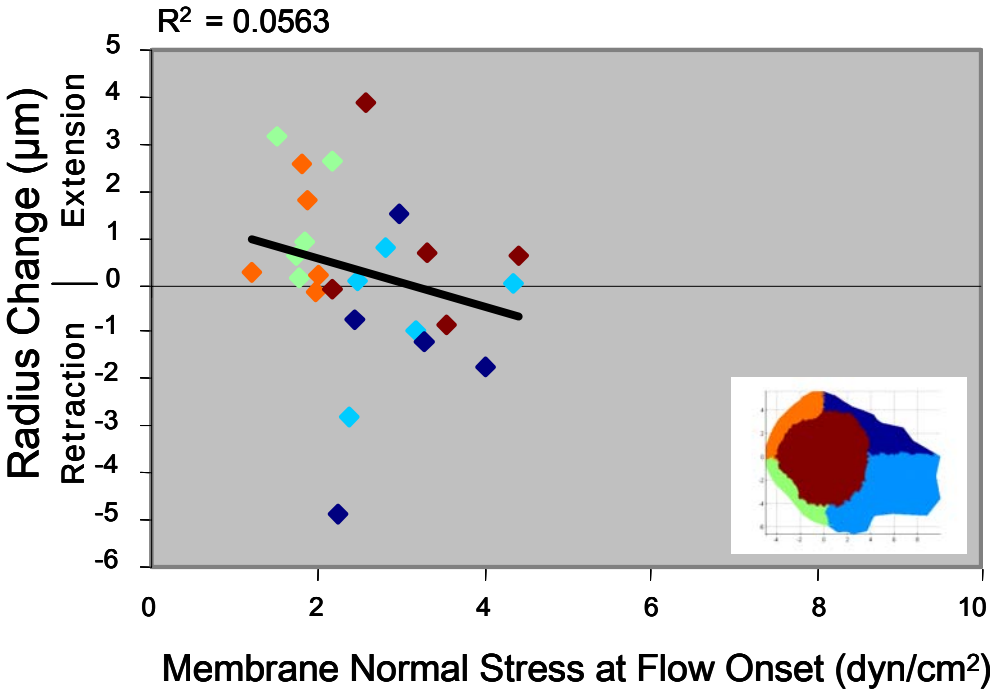


**Figure 21 Lack of simple correlation between normal stress and pseudopod retraction.**

The extent of regional membrane retraction is not linearly dependent on the magnitude of the average membrane normal stress within that region (each dot in the plot is color-coded by region)

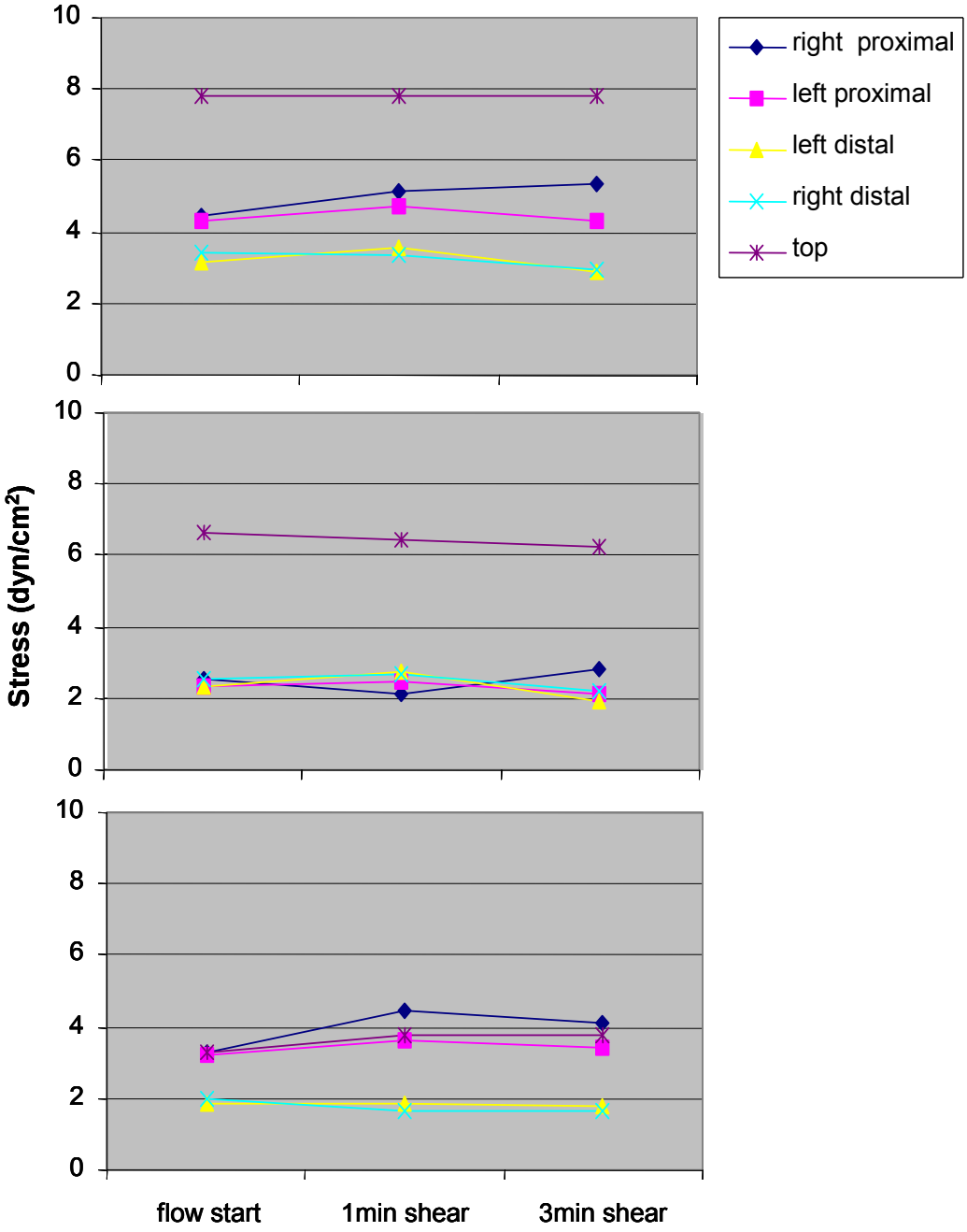


**Figure 22 Average regional cell surface fluid stress over time.**

The average resultant stress (top), shear stress (middle), normal stress (bottom) are computed for each region and plotted for the 3 time points (onset of flow, 1 minute into flow, and at the end of a 3-min flow). The change in average stress within each surface domain is very small compared to the magnitude of the stress.

significantly higher shear stresses relative to the other regions, but similarly, the level of that shear did not increase or decrease.

In addition, it is worth noting that even though the cell experiences a wide distribution of fluid shear stresses on its surface, most of the cell membrane is subjected to a minimum of 0.5dyn/cm$^2$ of shear stress (Figure 23), a level that was shown to induce cell retraction (Moazzam 1996). If the cell response to flow is regulated by a threshold mechanism, then there is an overwhelming surface area of the cell where the mechanism can be switched "on." The areas with less than the aforementioned threshold value form a ring very close to the glass coverslip.

## Stress Distribution on Membrane Folds

The presence of membrane folds on the surface of leukocytes leads us to investigate how they may change the stress distribution on the cell membrane. When membrane folds are closely clustered together, the middle protrusion is partially shielded from the flow pressure. As seen in Figure 24, even though the shear stress at the tip of the middle protrusion is the same as the other surrounding protrusions, the area exposed to enhanced shear stress (in light blue) is reduced along the sides of the membrane fold. The troughs formed both downstream and upstream of a protrusion experience ~0 dyn/cm$^2$ of shear stress. The normal stresses reach as much as twice the highest shear stresses and are concentrated on the upstream region of the protrusions directly exposed to flow. The area of the membrane folds exposed to enhanced normal stress progressively decreases for the downstream folds and this area had shifted

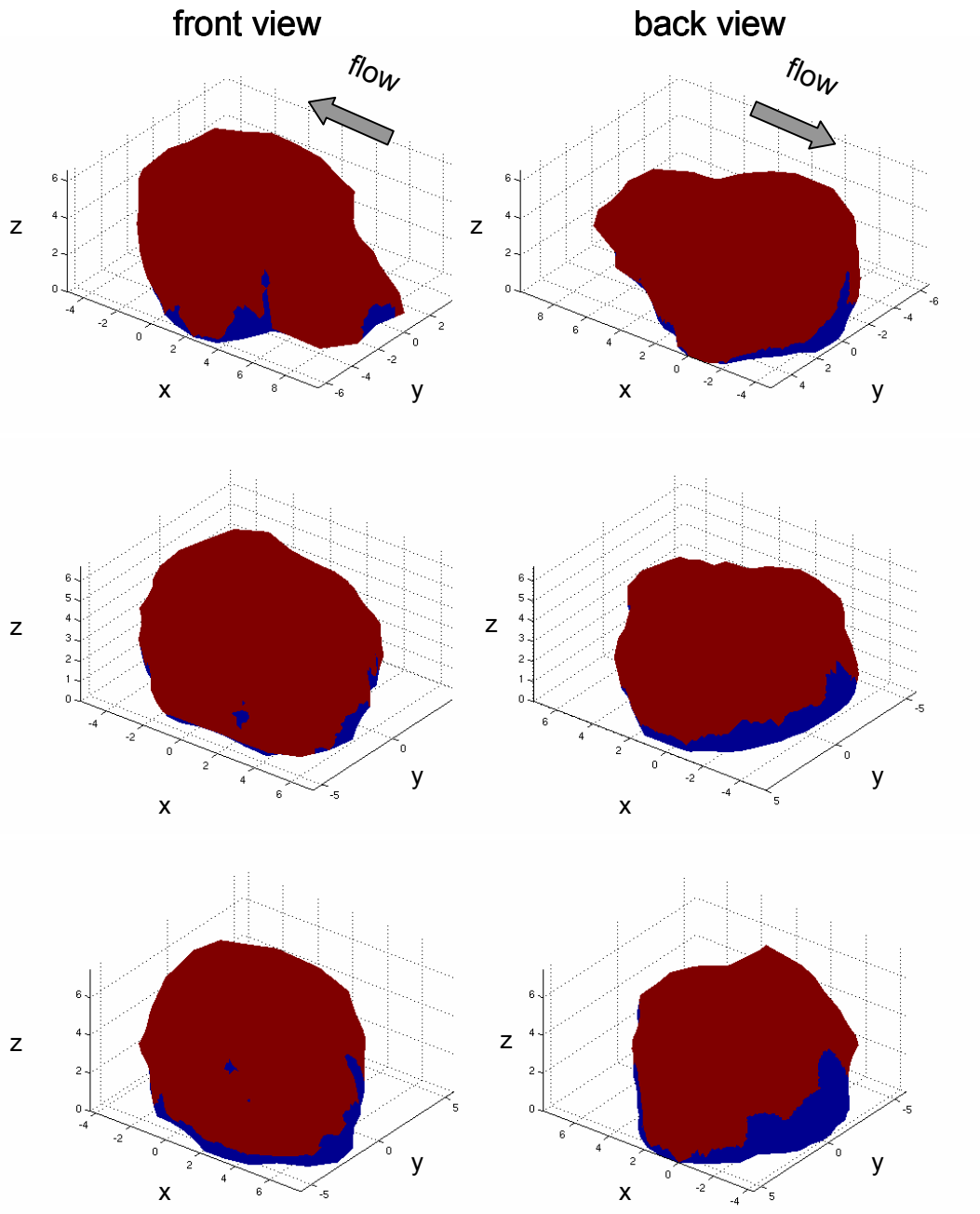


**Figure 23 Threshold plot of distribution of surface shear stress.**

Regions of the cell surface where shear stress magnitudes are equal to or greater than 0.5dyn/cm$^2$ are colored in red whereas regions experiencing shear stresses less than the threshold are colored in blue. Left: front view; right: back view; top: onset of flow; middle: 1min into flow; bottom: at the end of 3min-flow. The axes are in units of μm.

towards the tip of the fold as the magnitude of the maximum normal stress increased. The backside of each protrusion experiences zero (near top) to low magnitude (around the base, ~2 times of the applied wall shear) normal stress while the front side of the downstream folds is also exposed to similar magnitude of normal stress near the base. It is only evident from the stress direction plots (Figure 25) that the normal stresses on the downstream region are compressive. This is different from the downstream normal stresses observed from semi-spherical protrusions and the cell geometries examined earlier, which are tensile. This change of direction is an indication that due to the close proximity of the membrane folds, the unidirectional flow pattern is disturbed and recirculation zones form near the base on the downstream side of the membrane fold. Based on the resultant stress distribution, a protrusion in the center of a cluster of membrane folds is protected from both shear and normal stress components. The 3 upstream protrusions have a larger area exposed to enhanced fluid stresses (resultant) whereas the 3 downstream protrusions experience higher magnitude of fluid stresses in a smaller surface area closer to the tip.

For the sparsely spaced membrane folds (Figures 26 & 27), the stress distributions look different. The maximum shear and normal stresses are both higher, leading to a higher resultant stress as well. The areas exposed to fluid stresses are larger than that of clustered membrane folds. The fluid stress distributions on each protrusion are nearly identical because the flow is not disturbed by neighboring folds. From the stress vector plots (Figure 27), it can be seen that a lack of recirculation zones resulted in tensile normal stresses acting

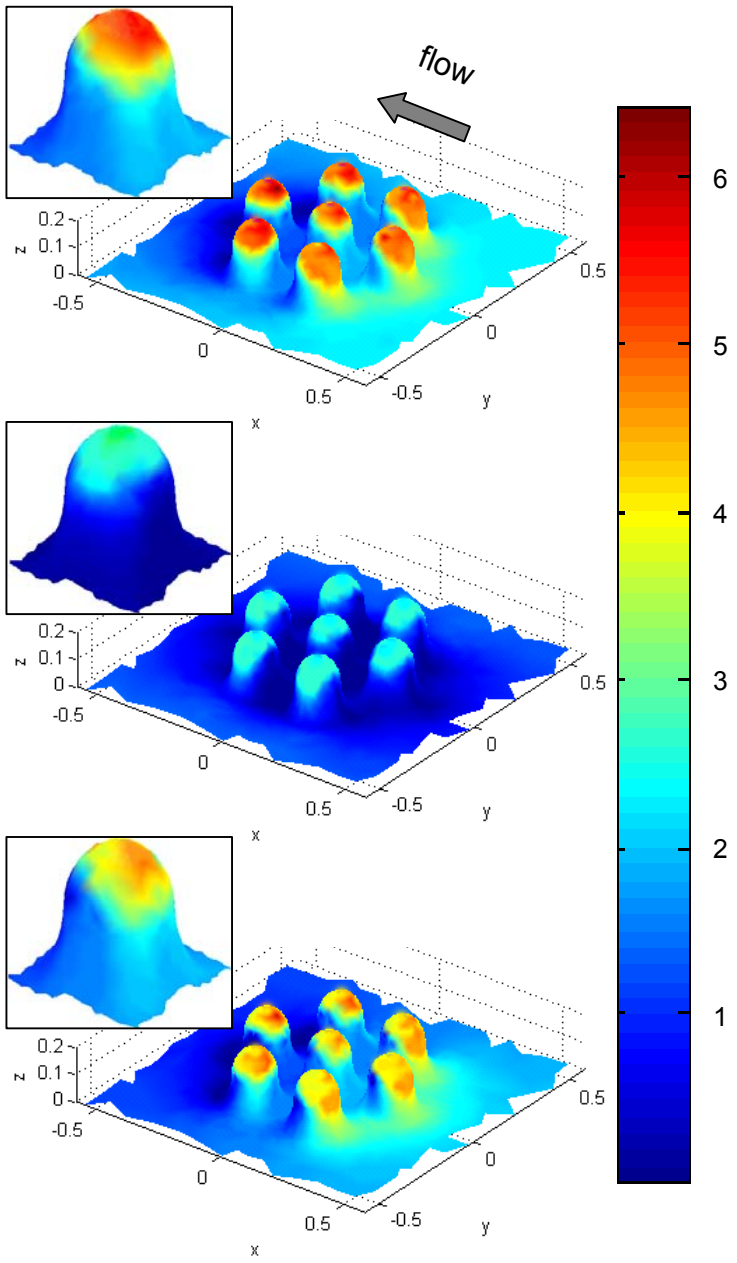


**Figure 24 Normalized surface stress distributions on closely clustered membrane folds.**

The tips of closely-cluster membrane folds experience higher stresses in both shear (middle) and normal (bottom) components (top: resultant stress). The troughs between each fold are shielded from shear stresses and the downstream region of each fold is protected from the normal stresses of the flow. Insets show a magnified view of the stress distributions on the fold in the center of the cluster. The surface stresses are normalized with respect to applied wall shear (2.2dyn/cm$^2$) and are therefore unitless. The axes are are in units of μm.

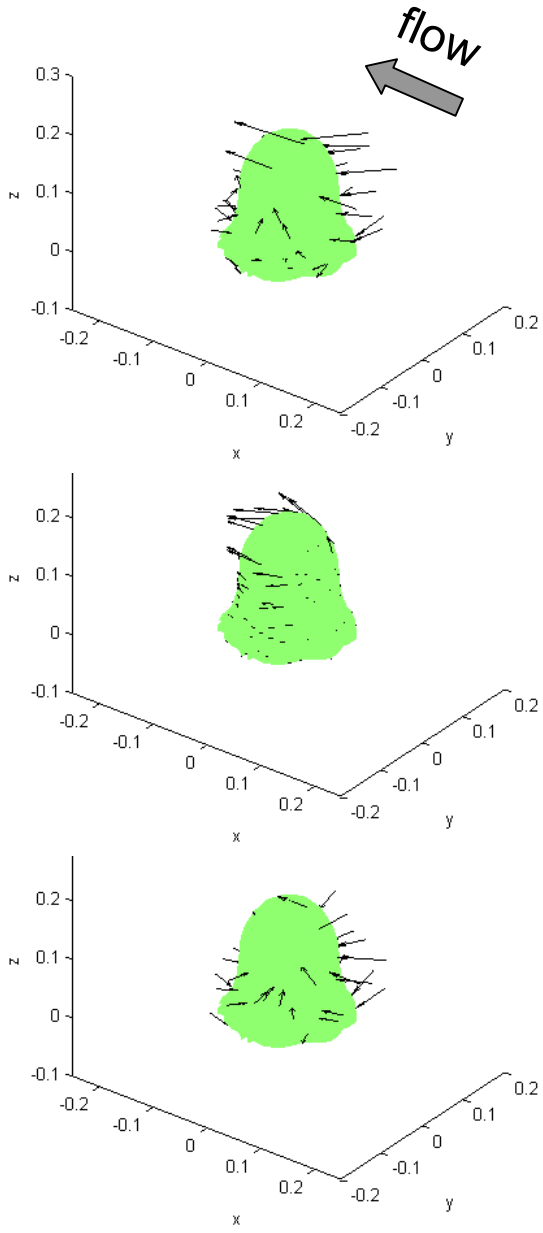


**Figure 25 Directions of normalized fluid stresses on the surface of the middle protrusion in a group of closely clustered membrane folds.**

Top: Resultant stresses act predominantly in the same direction as flow. Middle: Shear stresses always act tangential to the cell surface. Bottom: Normal stresses always act perpendicular to the cell surface. Due to the close proximity of other protrusions, there is a small reversal of flow behind the protrusion, close to the base, hence leading to a compressive normal stress even in the downstream region. This is dissimilar to the case for sparsely spaced membrane protrusions. Arrow length is proportional to the magnitude of stress.

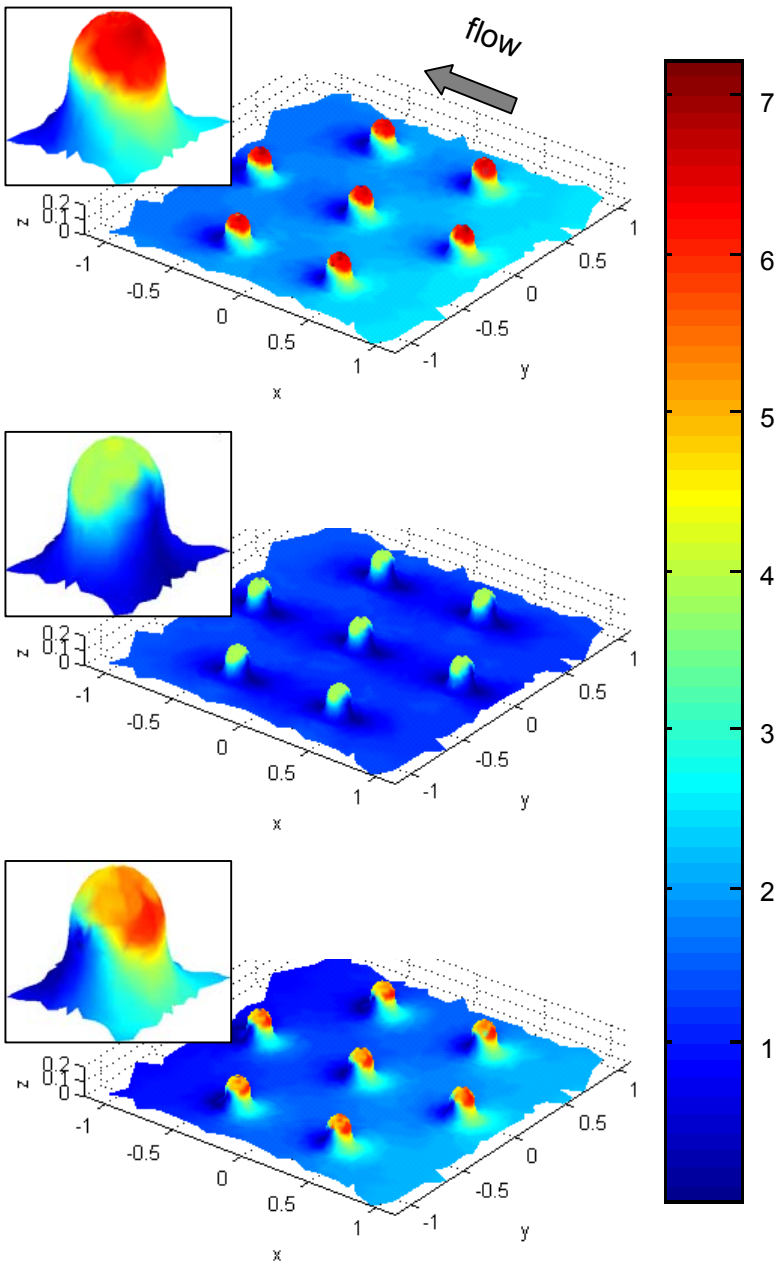


**Figure 26 Normalized surface stress distributions on sparsely spaced membrane folds.**

The tips of membrane folds experience higher shear stresses (middle). The upstream region of each fold is exposed to the highest normal stresses (bottom). The top shows the resultant stress distribution. Insets show a magnified view of the stress distributions on the fold in the center of the group shown. The surface stresses are normalized with respect to applied wall shear (2.2dyn/cm$^2$) and are therefore unitless. The axes are are in units of μm.

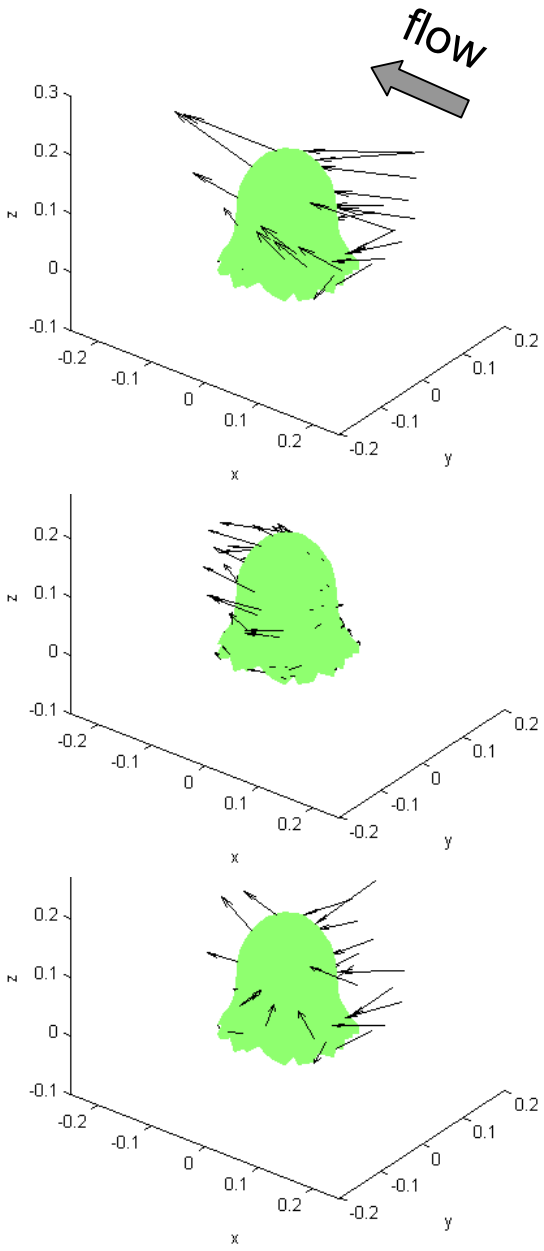


**Figure 27 Directions of normalized fluid stresses on the surface of the middle protrusion in a group of sparsely spaced membrane folds.**

Top: Resultant stresses act predominantly in the same direction as flow. Middle: Shear stresses always act tangential to the cell surface. Bottom: Normal stresses always act perpendicular to the cell surface. Similar to individual cell geometries but different from closely clustered membrane folds, these stresses are compressive in the upstream region but tensile in the downstream region due to lack of recirculation zones in the flow. Arrow size is proportional to the magnitude of the stress.

on the back side of each membrane fold, contrary to the case in which when the folds are clustered together.

Regardless of the spacing between each membrane fold, the computational results from these two examples showed an enhancement of the fluid stresses at the tips. However, when the folds are closer together, they also serve to reduce the stresses in the troughs formed between neighboring protrusions and change the direction of normal stresses on the backside of protrusions that have downstream neighbors.

## FPR ANALYSIS

## Background

Leukocyte activation in the normal circulation can be mediated by membrane receptors stimulated by various chemotactic factors. However, in the absence of such inflammatory mediators, leukocyte activation and deactivation may be regulated by fluid shear stress (Moazzam, DeLano et al. 1997; Coughlin and Schmid-Schonbein 2004).

*In vitro* experiments demonstrated that cleaving the glycocalyx (a matrix of polysaccharides that cover the extracellular surface of the plasma membrane of a cell) enhances the shear response of human neutrophils (Coughlin and Schmid-Schonbein 2004), possibly due to exposure of local receptors on the cell surface to direct shear. CD18 was shown to relocate to the posterior edges of the cell during shear (Fukuda and Schmid-Schonbein 2003). It is still unknown if such translocation is a result of another receptor-initiated signaling cascade that instructs CD18 to be displaced, or if CD18 is the shear-sensing element that causes the eventual shape changes in the cell. Blockage of voltage-dependent calcium channels can also attenuate abnormal shear stress response in glucocorticoid-treated cells (Fukuda, Yasu et al. 2000; Fukuda and Schmid-Schonbein 2002; Fukuda, Mitsuoka et al. 2004), suggesting that ion channels may also serve as membrane mechanosensors.

Makino *et al* showed that fluid shear would change the activities of the Rho family small GTPases during pseudopod retraction (Makino, Glogauer et al. 2005). Since neutrophils form constitutively activated pseudopods in the absence of fluid

shear stress and the activities of the small GTPases are regulated by GPCRs, Makino *et al* hypothesized that formyl peptide receptor (FPR), a large family of GPCR members which have a high constitutive activity, is a membrane mechanosensor that transmits the mechanical fluid stress into intracellular signaling cascades (Makino, Prossnitz et al. 2005). In the experiments that followed, Makino *et al* showed that inhibiting FPR with inverse agonists completely abolishes pseudopod retraction response to fluid shear in neutrophil-like differentiated HL60 cells.

The aforementioned evidence suggests that multiple receptors act in accordance with shear in modulating the individual fluid shear response observed in leukocytes. The specific location of these receptors may be the reason that different shear responses had been observed. Published findings showed that FPR concentrate in motile regions of the polarized neutrophils but are distributed uniformly on the membrane in unstimulated cells (Loitto, Rasmusson et al. 2001), suggesting that these receptors are free to move around the plasma membrane of the cell. In addition, the investigators observed that upon stimulation by formylated agonists, the receptors aggregate to the tail-end quickly and become internalized. This may be a mechanism by which the cells regulate the location and extent to which extracellular chemical and mechanical signals will be transmitted. Along with the findings by Makino *et al* mentioned above, it is of interest to observe the distribution of these surface receptors before and after fluid shear application. This may provide the link for understanding the distinct leukocyte behaviors recorded in various published records.

In the following experiments a GFP-transfected monocytic cell line is used to visualize the FPR distribution on the cell before, during and after fluid shear. GFP provides a much brighter fluorescent image compared to phycoerythrin-tagged FPR antibodies and undergoes little photobleaching. It is a useful tool for repeated fluorescent imaging and therefore suitable for the purposes of this experiment in tracking the overall distribution of the tagged receptors over the course of flow application.

## Materials and Methods

### Cell Culture

Human leukemic monocyte lymphoma cells stably transfected with FPR-GFP (U937 FPR-GFP, generous gift from Dr. Eric Prossnitz, University of New Mexico Health Sciences Center, Albuquerque, NM) are cultured in RPMI40 media supplemented with 10% fetal bovine serum (FBS), 1% penicillin/streptomycin, and 1% G418 (Invivogen, San Diego, CA). They exhibit many monocytic characteristics (Sundstrom and Nilsson 1976). GFP allows for real-time observations of the location of FPR molecules in the cell.

### *In vitro* Flow Chamber Experiments

The glass coverslips used in the experiments were soaked in 1N sodium hydroxide overnight to allow better adherence of cells. All parts used in the set-up were autoclaved or soaked in 70% isopropyl to minimize environmental contamination. The parallel-plate flow chamber was first assembled by placing the coverslip and the gasket between two stainless chamber plates (Figure 3). The thickness of the gasket, approximately 250μm, was the thickness of the

chamber. The width of the cut-out in the gasket determined the width of the flow chamber and the distance between the cut-outs in one of the chamber plates indicated the length of the flow chamber. The chamber was then filled with the shearing fluid, pH-adjusted and calcium-fortified PlasmaLyte, and air bubbles were removed from all ports of the flow chamber. Subsequently, U937 FPR-GFP cells, suspended in culturing medium, were injected into the flow chamber and allowed to settle and migrate freely on the glass coverslip (Fisherbrand, Fisher Scientific) for ~10min. A laminar flow at ~5dyn/cm$^2$ was applied by a syringe pump (Harvard Apparatus Compact Infusion Pump, model 975) for 10 minutes.

Three control experiments were performed. In the first control, cells were observed for the same amount of time without applying a flow. It was done to observe whether FPR distribution undergoes similar changes in the absence of flow. In the second control, the cells were allowed to settle onto coverslip for 10 minutes and then fixed in 0.4% paraformaldehyde for 1 hour. The flow chamber was assembled with the cells already attached to the coverslip. The rest of the conditions and procedures were exactly the same as the experimental group. This was done to confirm that any observed changes in GFP location resulted from cellular responses rather than a disengagement of GFP from the FPR or an imaging error. In the third control, the chamber was first filled with culture medium before cells were injected and then the cells were subjected to fluid shear with culture medium of the same wall shear stress for the same length of time. The purpose was to observe if depletion of serum and proteins by shearing fluid for the duration of the experiment enabled the observed response of the cell under shear.

## GFP and FPR-Ab Colocalization Experiment

To show that GFP was tagged to FPR throughout the experiment and served as a valid indicator of the location of FPR, I labeled the cells with a mouse anti-human antibody for FPR that was conjugated with R-phycoerythrin (BDPharmingen, San Jose, CA). FPR-GFP U937 cells were allowed to adhere onto the coverslip for ~10min. No-shear control cells were then fixed on the coverslip with 1% paraformaldehyde for 1 hour. They were permeabilized with 0.1% Triton-X for 3-5 minutes and then incubated in 1% BSA for 1 hour. A final concentration of 1:250 PE-conjugated FPR antibody (4μL bottled concentration in 1mL of 1% BSA solution, manufacturer suggested starting concentration was 20μL for 1mL of $10^7$ cells in suspension) was added to the cells and incubated at $4^oC$ overnight. Cells were washed very gently in PBS and then imaged immediately under epifluorescence. For the sheared group, cells were allowed to adhere onto the coverslip for ~10min. The coverslip was then assembled into the flow chamber and cells were sheared for 10min at ~5dyn/$cm^2$. The flow chamber was quickly dissembled immediately following flow cessation and cells were fixed on the glass coverslip with 1% paraformaldehyde for 1hr. Cells were then permeabilized, incubated in BSA solution, labeled with antibodies, washed, and imaged (same way as no-shear group).

## Image Acquisition

### In-Vitro Flow Chamber Experiments

Bright field images in grayscale (Olympus IX70-S1F2 inverted microscope, tungsten-halogen bulb, 60× 1.25NA or 100× 1.30NA Olympus UPlanFl objectives)

of the cells are captured with the Olympus U-CMAD3 camera coupled to a computer. Images were taken at 30-second or 1-min intervals for a total of 21 minutes (1 minute of observation before starting flow, 10 minutes of flow at ~5dyn/cm$^2$, 10 minutes of observation after flow has stopped).

Detection of GFP signals were accomplished using the same microscope and lenses with an external Olympus BH2-RFL-T3 epifluorescence source. Epifluorescent images were recorded, using the same setup as the bright field image capture, at five time points during the experiment: 1 minute before the onset of flow, right at the onset of flow, 5 minutes into flow application, immediately after flow had been stopped, and 10 minutes after the flow has been stopped. The focal plane was adjusted to allow for the clearest image of the mid-section of the cell of interest at each time point, with particular attention given to obtaining an image showing the GFP aggregate in the cell at its highest fluorescent intensity.

### GFP and FPR-Ab Colocalization Experiment

Cells on the glass coverslip were identified in bright field. Green epifluorescence (GFP) was detected with the same set-up as previously mentioned. Red epifluorescence from the PE-tagged FPR antibodies were detected using the same microscope but through a rhodamine filter.

## Data Analysis

To understand the morphological cell response to laminar fluid flow the roundness ratio (see below) was computed for the three different cases of control and the normal experimental conditions described before (a minimum of n=3 in

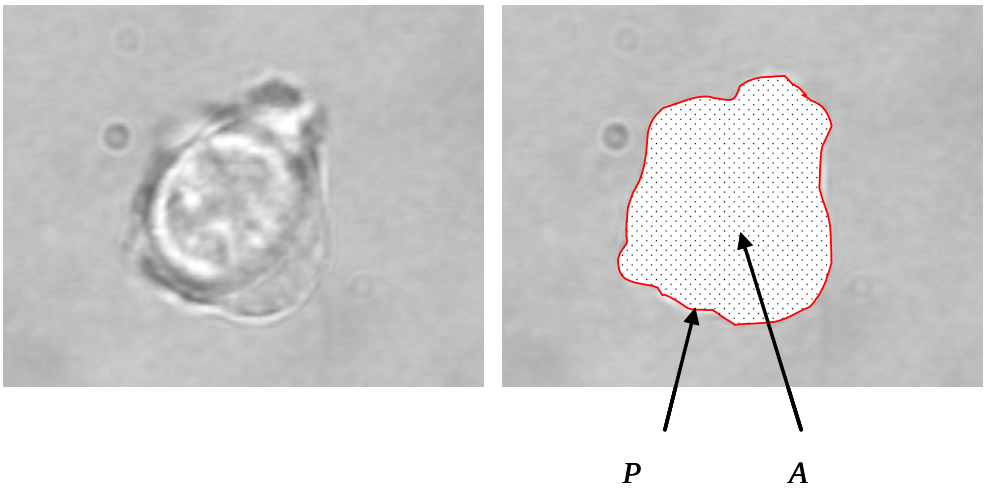


**Figure 28 Roundness measurement for cell under fluid shear.**

The projected area of the cell is traced by hand on a computer. The roundness ratio is defined as the square of the perimeter divided by $4\pi A$.

each case from images taken from a minimum of 2 different days). Using bright field images for each 1-min interval, the projected area of the cell was traced by hand on a computer. The roundness ratio was defined as $\frac{P^2}{4\pi A}$ where $P$ was the perimeter of the projected area of the cell and $A$ was the enclosed area. The roundness ratio was calculated using Image-Pro Plus (version 4.5, Media Cybernetics, Inc) for each time point and presented as a function of time.

Fluorescence intensity of various parts of the cell was measured to in order to get a quantitative measure of possible FPR translocation during laminar fluid flow. The following measurements were based on the assumptions that there was one GFP molecule for each FPR in the cell, the intensity of the fluorescence was directly proportional to the number of GFP molecules in the cell, GFP did not disengage from the FPR at anytime during the experiment, and that no GFP was degraded by the cell without FPR and vice versa. The outline of the cell under fluorescence at each of the 5 aforementioned time points was traced by hand on a computer. The area of the cell, in terms of number of pixels (each pixel was equivalent to a length of 0.28μm), was therefore obtained. A histogram, which showed a frequency distribution of the intensities in the area of interest, was used to find the number of pixels that were at each level of brightness on a scale of 0 to 255 where 0 represented black and 255 represented white. It yielded the dynamic range of the cell fluorescence. The total fluorescence intensity was obtained by adding up all of the pixels at all of the intensity levels. The average fluorescence intensity was obtained by dividing the total fluorescence intensity by the area of the cell. Using a line profile measurement of Image-Pro Plus, which

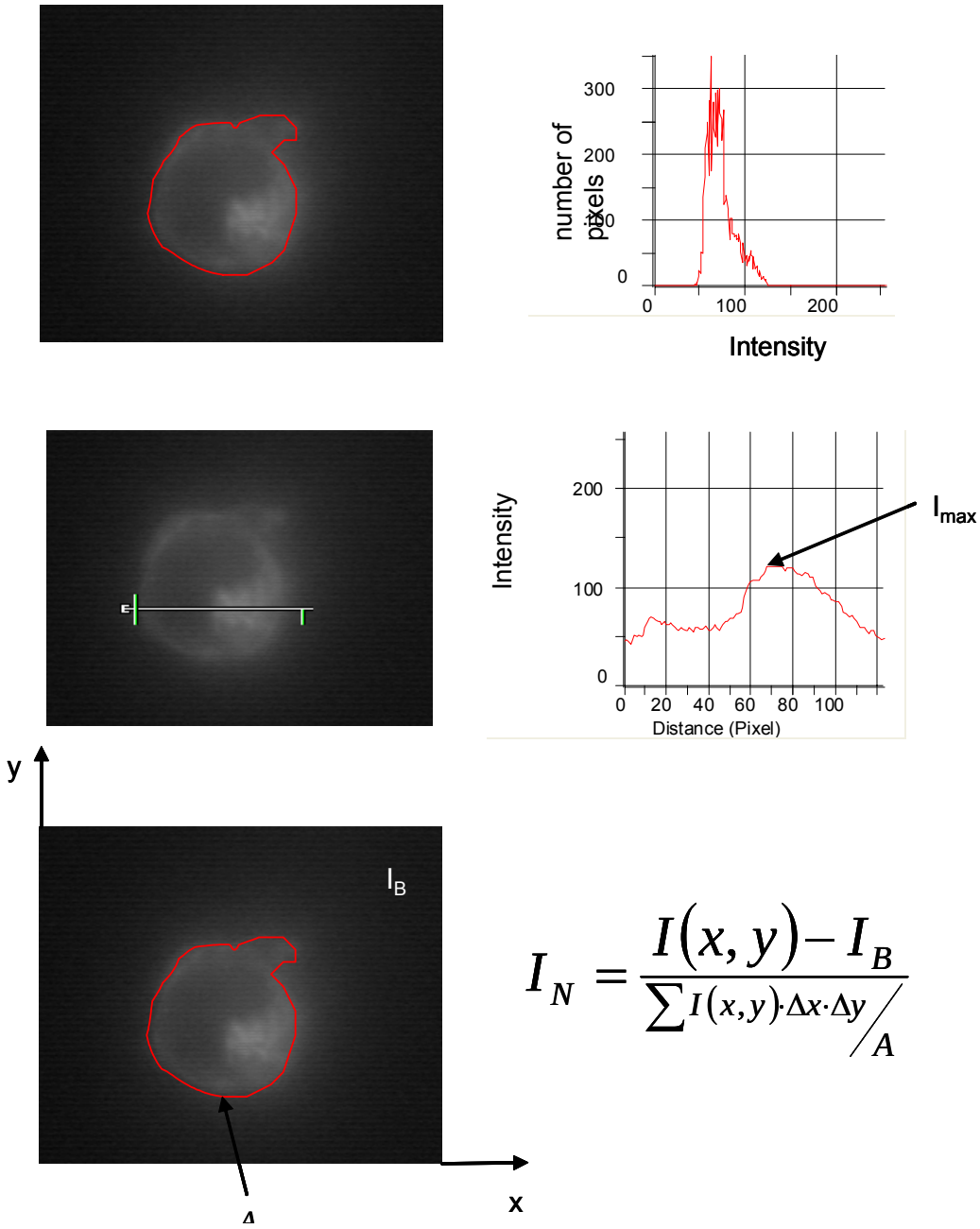


**Figure 29 Image analysis for FPR distribution.**

Top: Cell outline (shown in red) is traced by auto-detection and by hand. The histogram shows the range of intensities for the pixels within the perimeter. The area under the curve in the histogram gives the total fluorescent intensity of the cell at that given time point. Middle: A line intensity profile, and subsequently, the maximum intensity ($I_{max}$), is obtained for the aggregate of GFP shown in the image. Bottom: The normalized intensity value is obtained by first subtracting the background intensity and then divided by the average intensity of the cell (as outlined by the red perimeter).

plotted the intensity values along a user-specified line, the maximum intensity of the GFP aggregate inside the cell was obtained. The line intensity profile was normalized by the average intensity of the cell after subtracting the background fluorescence. The photobleaching effects and relatively small intensity differences in the background were eliminated by this process. The normalized maximum intensity within the cell was compared over the 5 time points. However, application of flow (pH balanced Plasma-Lyte) removed the auto-fluorescent media from the chamber, despite background subtraction and normalization with the average intensity of the cell at the same time point, an accurate comparison between the first time point and the other four could not be made. In the analysis presented below, comparison of fluorescence intensity over time was made for the second through fourth time points only: at the onset of flow, 5 minutes into shear, and seconds after flow was stopped.

Fluorescence intensity measurements for the upstream (with the highest normal fluid stress) and downstream (with the lowest normal stress) regions of the cell membrane in the focal plane were made by first manually outlining the membrane regions in the image (Figure 30). The boundaries of the membrane regions were determined by visual inspection and auto-detection by the image processing software (Image-Pro Plus). The combined upstream and downstream average intensity (after background subtraction and normalization to the cell intensity) within the area of interest was obtained from images at the aforementioned 3 time points. To detect changes in fluorescence of the cytoplasm, measurements were made within a small area (see Figure 30) of the cell for the same time points.

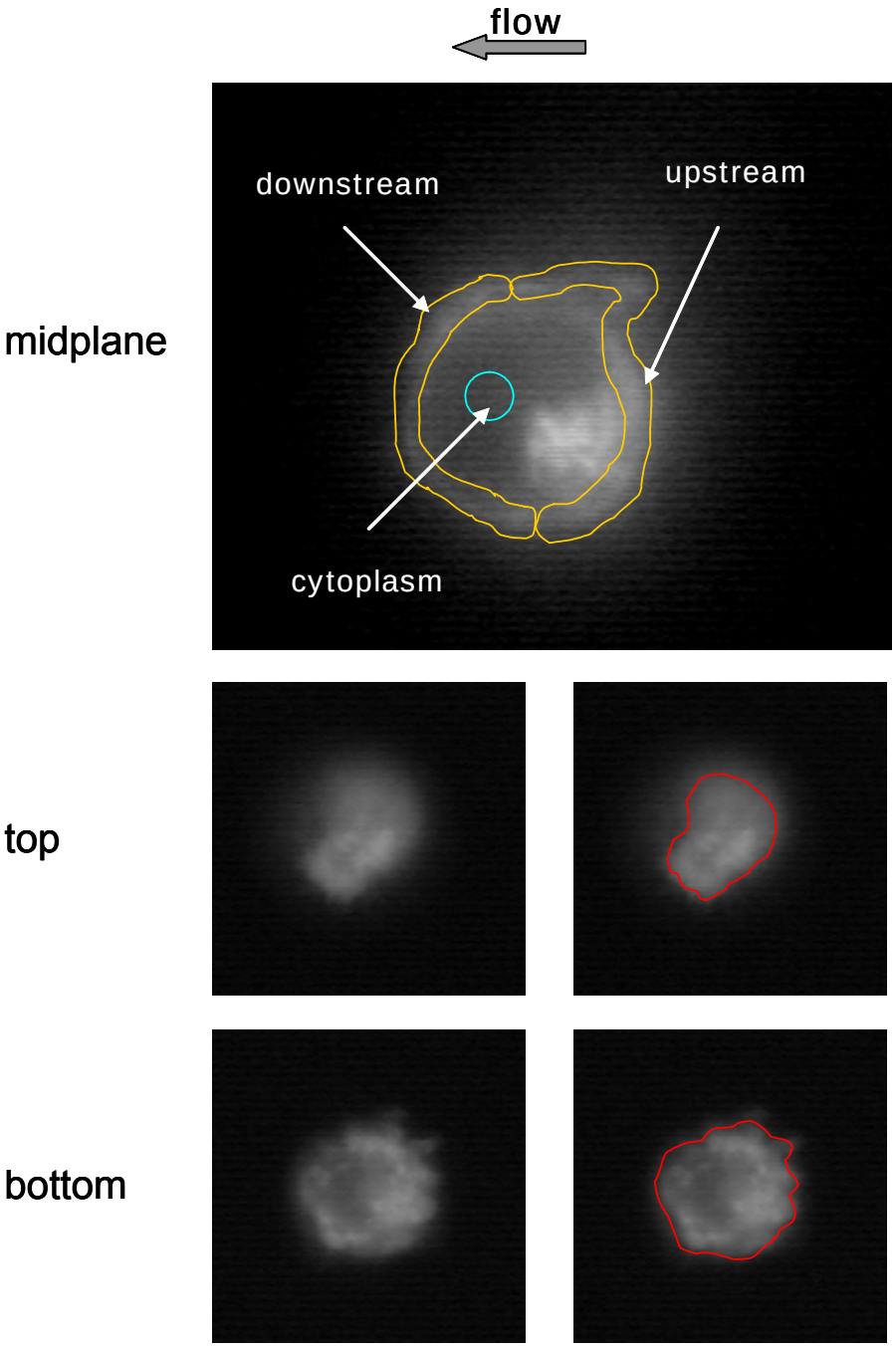


**Figure 30 GFP intensity analysis on the cell membrane and in the cytoplasm.**

Top: The entire membrane region is outlined manually on the computer to obtain the total and average membrane intensity. The fluorescence intensity of the cytoplasmic domain is obtained for only the region within the blue circle. Middle and bottom: Using auto-detection and hand-tracing, the top and bottom regions, respectively, are defined and total intensity measurements are taken.

Fluorescence intensity measurements were also obtained on a top and bottom focal plane of the cell to explore a possible FPR redistribution under different stress magnitudes. Each focal plane was adjusted to obtain a focused membrane domain of the top and at the bottom substrate-contact regions of the cell (Figure 30). The outlines of these planes were manually traced on a computer (with the help of auto-detection) and the average intensity (after background subtraction) within the area of interest was obtained. Comparisons of these and the upstream/downstream region intensities were determined to identify possible shear-induced changes in GFP levels.

## Results

### U937 Cell Pseudopod Retraction during Fluid Shear

In the experimental group (10 minute shear with pH-balanced and calcium-enriched Plasma-Lyte), all of the cells retracted their pseudopods during fluid shear. However, the extent of retraction differed among individual cells. Out of 40 cells used in the shear response experiments, about 25% of the cells showed limited reduction in projected area. It was also noted that 2 cells retracted the main cell body while maintaining one or more long finger-like membrane projections on the substrate (filipodia). These filipodia were not present when flow started but remained on the substrate throughout fluid shear and even for the 10 minutes of observation afterwards. The projected area for the majority of the cells that showed quick retraction response was traced by hand for the entire duration of the experiment at 1-min intervals (1 minute before starting shear, 10min shear by Plasma-Lyte, 10 more minutes after flow stopped). Due to the

diverse cell responses to fluid shear, the following analysis was based on the group of cells that showed clear and quick retraction under flow.

The first control experiment (no shear) was performed in one day using the same group of cells. Placement of U937 cells into the flow chamber followed by the same duration of observation (as the sheared group) without flow application yielded a random pattern of pseudopod extension and retraction over the course of the experiment. Three cells were selected from 3 separate experiments. Their outlines were traced in order to determine the roundness ratio. The cells showed great variations in their projected areas throughout, as seen by the relatively large error bars in Figure 31. Throughout the experiment, there were no observable changes in cell behavior. This suggested that, for the duration of this experiment, the amount of time that a cell was adhered to the glass coverslip was not a factor that influenced the cell behavior.

In the second control experiment, adherent cells were fixed on the coverslip and then subjected to shear. The experiment was performed on two different days and the images of three cells from separate experiments were analyzed. In this case, since the cells were already fixed, the projected area stayed constant and shear stress did not dislodge any cells from their original position on the coverslip.

In the third control experiment, cells were injected into a flow chamber after filling with culture medium that contained 10% FBS. The serum proteins had already coated the coverslip and we observed that the cells become less adhered to the glass coverslip. However, the adherent cells were still able to retract their

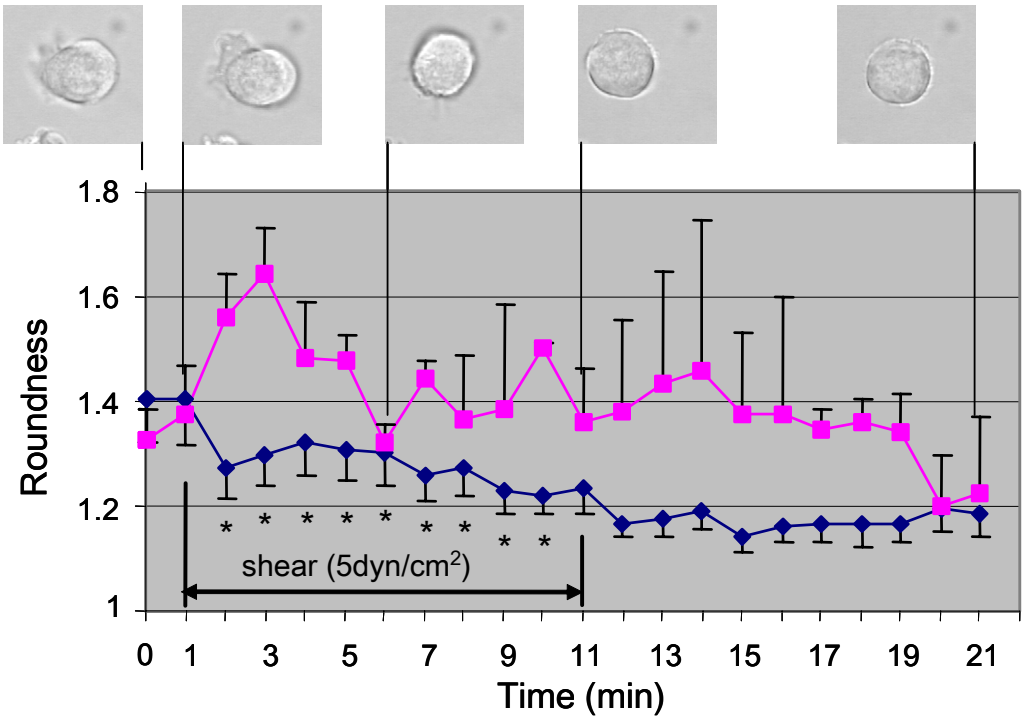


**Figure 31 Measurement of U937 cell response under fluid shear.**

The roundness ratio for U937 cells is computed and plotted with respect to time. The cells exposed to 10 minutes of shear (blue diamonds) exhibit a retraction in the projected area (as shown by images above the plot) under fluid shear and stay retracted after shear removal (n=19). No-shear control cells (pink squares) were observed for the same duration of time. They exhibit a random pseudopod extension and retraction (n=3). Error bars: SE.

pseudopods under fluid shear stress and continue to round up even after flow cessation. This response was different from the experimental group in that 11 out of the 15 cells rounded quickly and followed by a deformation of the membrane which was derived from the resultant force of the fluid flow. Such cells deformed into a teardrop shape because they were attached to the coverslip by one single point on the upstream region of the membrane. As flow continued and the rest of the cell lost firm adhesion with the coverslip, the drag force on the surface of the cell pulled on a single attachment point, a process that led to elongation of the cell even at these relatively low shear stresses. Under bright field it could be easily seen in some of these cells that the membrane in the upstream region had detached from the cell cytoskeleton, leading to the teardrop shape seen eventually during flow application.

Some cells also slid along the coverslip (the distances varied) before stopping and become deformed. When the flow was stopped, few cells recoiled immediately and stayed round through the remaining 10 minutes of imaging. Most cells recovered from the membrane detachment in a slow and steady fashion over a few minutes instead of a few seconds. Of the remaining 4 cells that did not exhibit teardrop shape during flow, 2 of them retracted the projected area without being deformed or pushed along the coverslip by the flow. The two remaining cells from this control experiment extended small filipodia and pseudopods into the flow during the first few minutes and finally retracted during the last 2 minutes of flow. These membrane extensions were different from the filipodia seen in the Plasma-Lyte-sheared group of cells because these were not

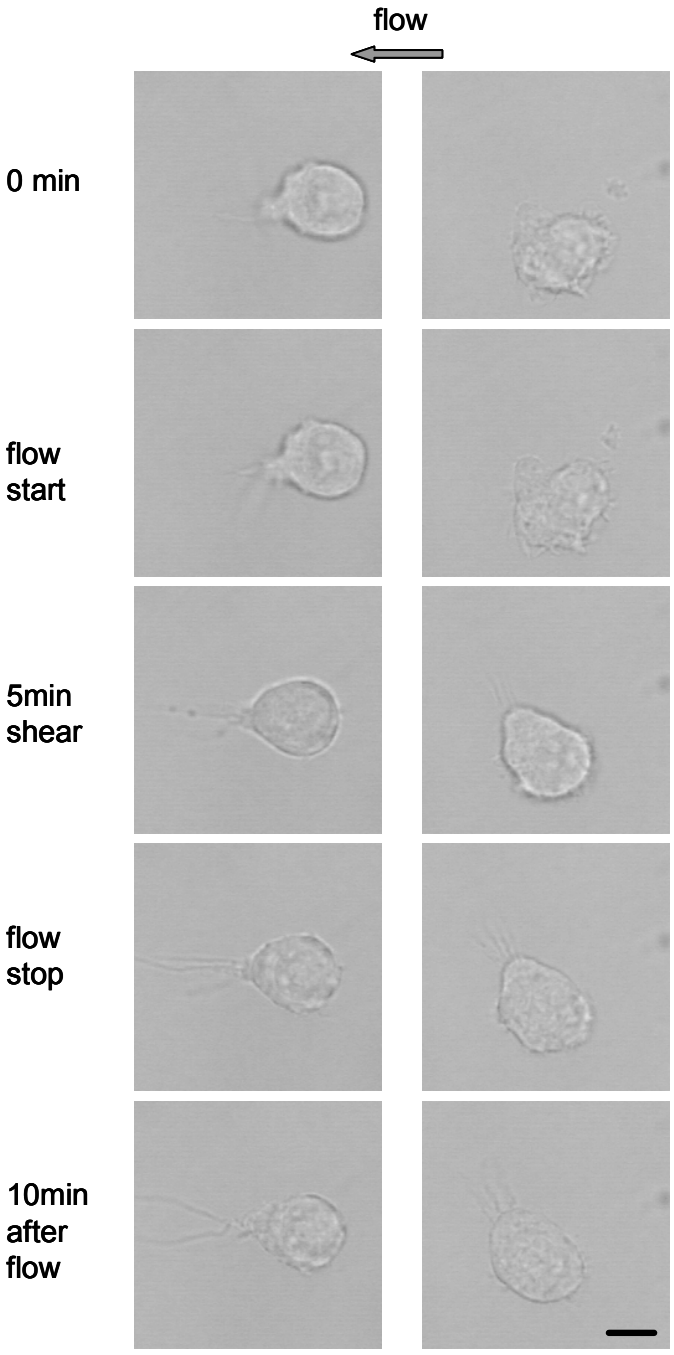


**Figure 32 Uncharacteristic shear response of cells under flow by pH-balanced Plasma-Lyte.**

In rare cases cells sheared by pH-balanced Plasma-Lyte for 10 minutes show extension of filipodia in different regions of the cell along the glass coverslip. These finger-like extensions increase the roundness ratio even though the cell body exhibited mild retraction under flow. Bar denotes 10μm.

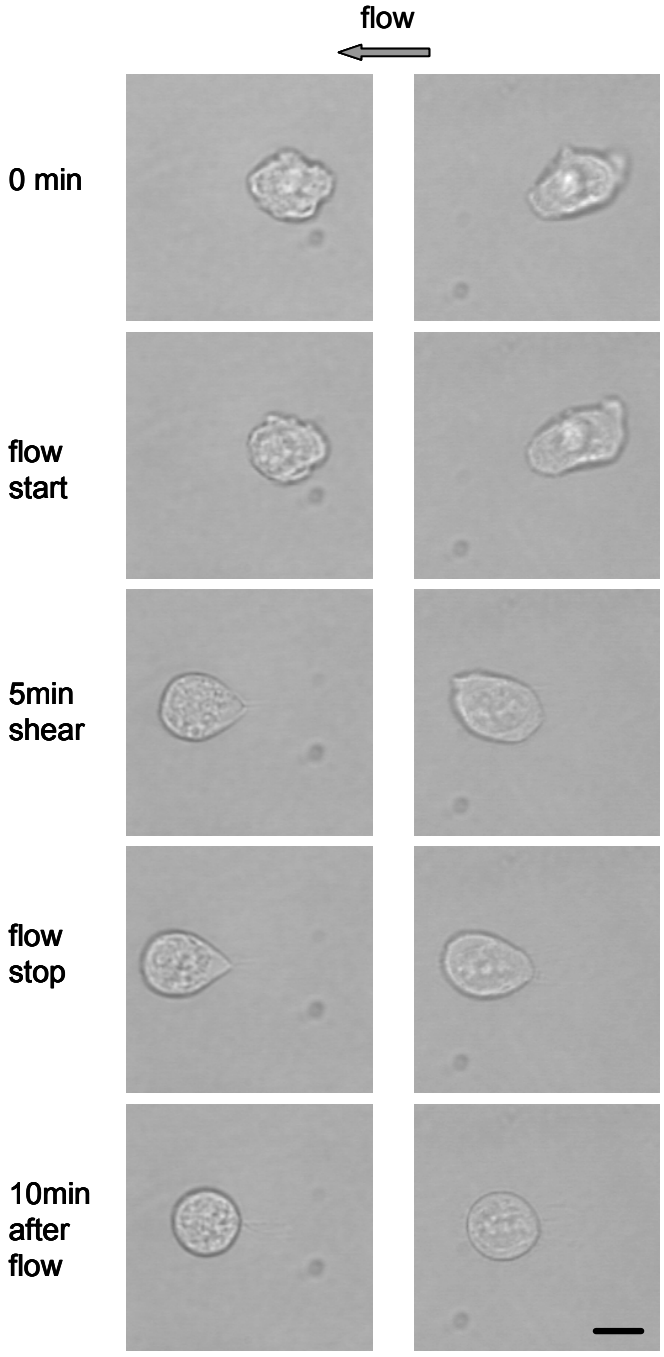


**Figure 33 Representative shear response of cells under flow by culturing medium.**

Cells sheared by culturing medium for 10 minutes typically slide in the direction of flow and become stretched out. In the 2 cases shown here, it can be seen that the cell retracts early on in the flow, followed by stretch in the membrane in the region proximal to source of flow. The cell interior appears to have separated from the membrane. After flow stops, the cell recoils and become round. Bar denotes 10μm.

projected along the substrate and both cells extended them downstream of flow. After shear cessation, both cells stayed round.

## GFP Intensities within the Cell and on the Cell Membrane

Based on the fluorescence distribution of GFP in images taken before, during, and after flow application, the FPR distribution was obtained. As seen from Figure 34, GFP fluorescence colocalized with fluorescence from PE-tagged FPR-antibody, indicating that GFP did not get separated from FPR during the experiment. This observation was also in line with results reported in the literature where extensive colocalization occurred between FPR-mRFP1 (FPR plasmid and method of transfection were the same as those for the FPR-GFP cells that I used in my experiments) and fluorescent ligand in U937 cells (Vines, Revankar et al. 2003). In addition, Dr. E. Prossnitz of University of New Mexico had confirmed, through personal communication, that there was no detachment of the GFP molecule from FPR in his FPR-GFP U937 cells, though it was in a non-shear experimental setting.

It had been noted that one compartment within the cell increased in fluorescence intensity when the cell had been subjected to shear. This compartment appeared to be immediately outside the nucleus, as could be seen from comparing bright field images with fluorescence images of the cells taken a few seconds apart. Searching through the literature, it was found that this compartment was most likely a perinuclear recycling endosome that would be identified by labeling of Rab11, a small GTPase that was known to be recycled in such vesicular structures (Ernst, Zobiack et al. 2004; Key, Vines et al. 2005).

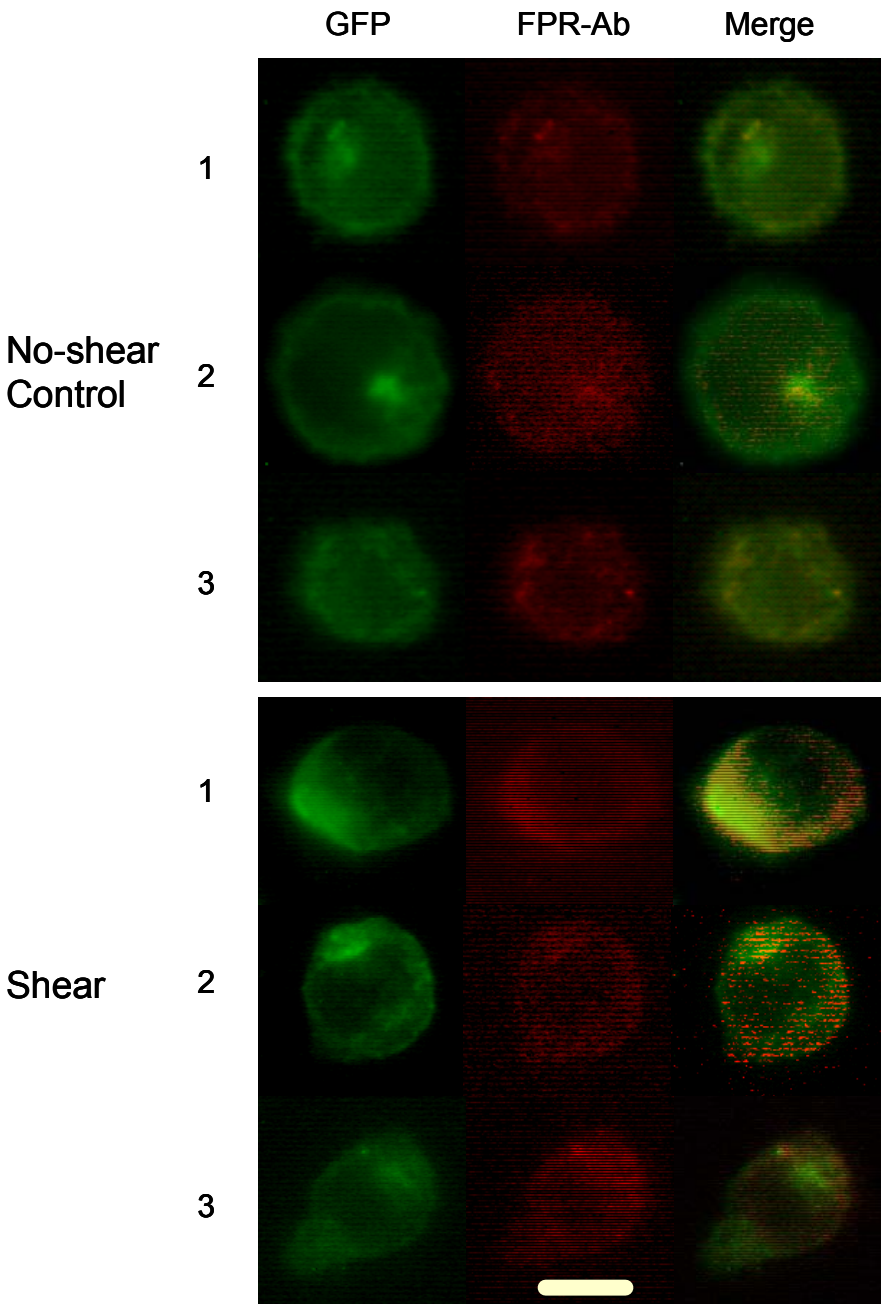


**Figure 34 GFP and PE-conjugated FPR-Ab colocalization in FPR-GFP transfected U937 cells.**

Top: Three separate examples of no-shear control FPR-GFP transfected U937 cells. GFP colocalizes with PE-conjugated FPR-specific antibody. Bottom: Three separate examples of sheared FPR-GFP transfected U937 cells. GFP continues to colocalize with PE-conjugated FPR-specific antibody. All images have been enhanced to show the fluorescence. Bar: 10μm.

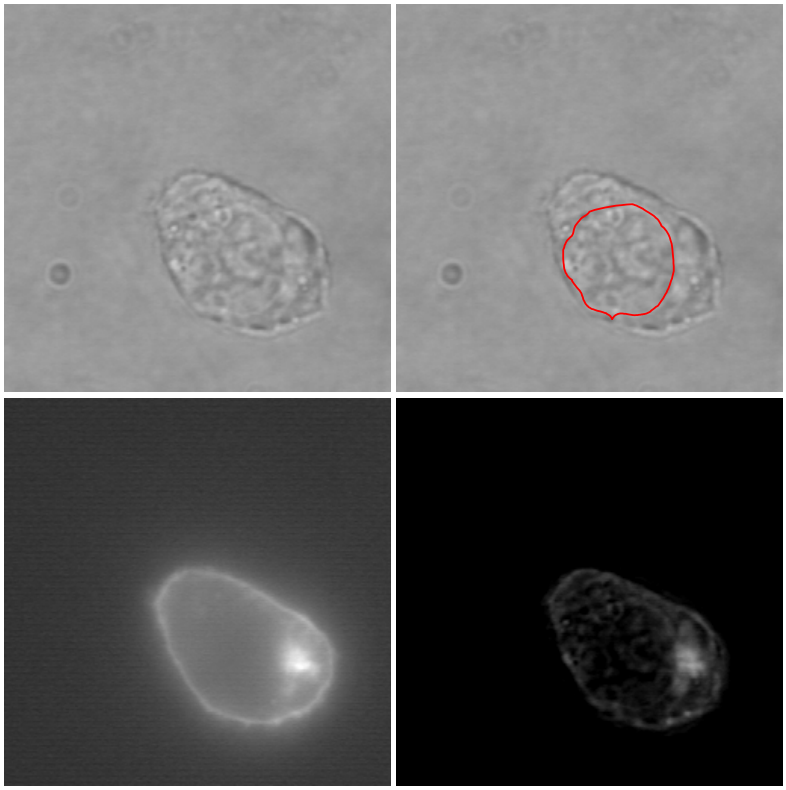

**Figure 35 FPR-GFP aggregate in the perinuclear compartment of U937 cells.**

Top left: A bright field image of a single adherent U937 cell. Top right: Red line indicates the location of the nucleus. Bottom left: A fluorescent image of the same cell at the same time point (the focal plane is slightly different for the two images to obtain the brightest fluorescence within the cell). Bottom right: By subtracting the bright field image from the inverted fluorescent image, a new image is obtained where the outline of the nucleus is evident and the GFP aggregate is located immediately outside of the nucleus.

However, this recycling has currently only been shown to occur after the activation of FPR by chemotactic factors. It is not yet known if and how mechanical stimulus causes internalization and recycling of the receptor.

The fluorescence intensities of different parts of the cell were measured at the 3 pre-determined time points (flow onset, 5 minutes into shear, end of 10min shear). The cells subjected to shear by Plasma-Lyte showed an increase in normalized GFP intensity in the perinuclear compartment, but not in the membrane regions. The normalized intensity value was obtained by subtracting the background and then divided by the average intensity of the cell (at that focal plane and at that time point). Cells from the first control group (no shear) did not exhibit changes in GFP intensities in both the perinuclear region and the membranes. No fluorescence intensity changes were observed from U937 cells of the second control group (fixed in paraformaldehyde and then sheared), indicating that the action of applying fluid flow over the cell did not cause intensity increases in the experimental group. To confirm that cell retraction and subsequent fluorescence changes in live cells were not the result of activation or deactivation by molecules in Plasma-Lyte, culturing medium was used for the third control experiment. The results showed a similar enhancement of GFP intensity within the cell but no significant changes in the membrane regions.

The same method was used to measure the fluorescence intensities of the intracellular compartment and of the upstream and downstream membrane regions. Cells that were exposed to shear exhibited a significant decrease in GFP intensities in the cytoplasm as early as the 5min time point (Figure 37 bottom

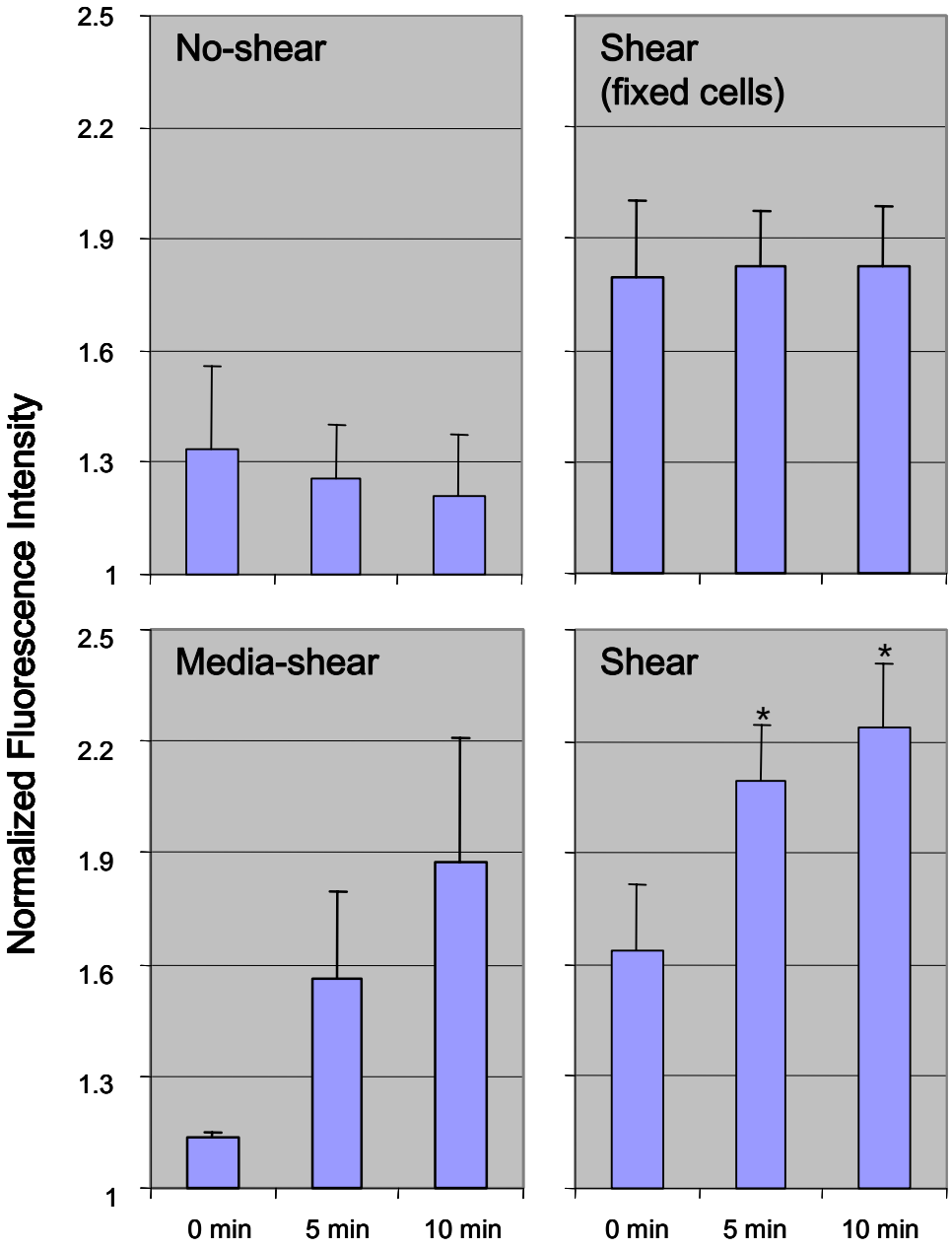


**Figure 36 Normalized GFP intensity in perinuclear compartment.**

The fluorescent intensities are normalized with respect to the average cell intensity at the same time point after background subtraction. Top left: U937 cells not exposed to fluid shear do not show significant changes in GFP intensity level in the perinuclear compartment (n=3). Top right: Fixed U937 cells exposed to shear by pH-balanced Plasma-Lyte exhibit a constant GFP intensity in the perinuclear compartment for the duration of the experiment (n=3). Bottom left: U937 cells exposed to shear by culturing medium showed marked increase (but not statistically significant) of GFP intensity (n=3). Bottom right: Live U937 cells subjected to shear of pH-balanced Plasma-Lyte shows statistically significant (*P<0.05) increase in GFP fluorescenc (n=8) compared to the 0min time point. Error bars denote standard error.

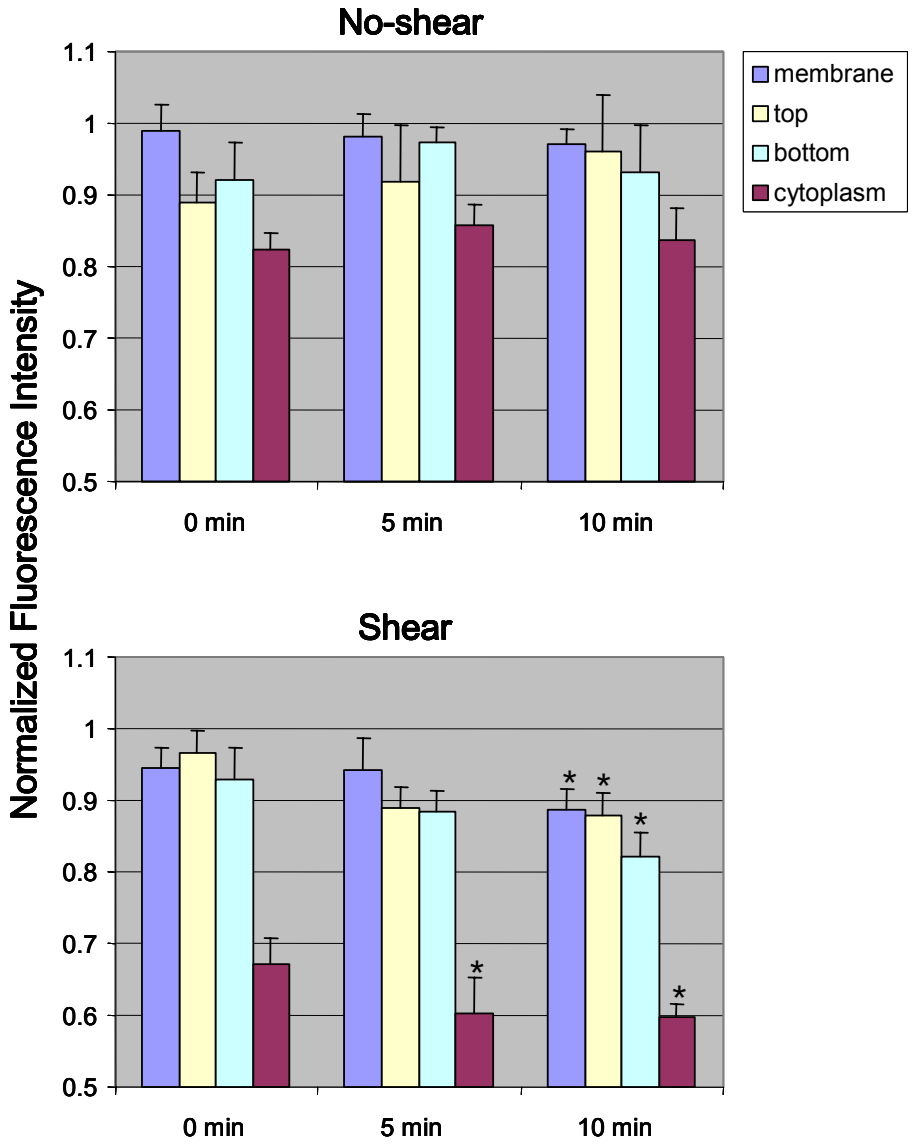


**Figure 37 Normalized GFP intensity on the cell membrane and in the cytoplasmic region.**

The fluorescent intensities are normalized with respect to the average cell intensity at that given time point after background subtraction. Top: No-shear control U937 cells show no significant changes in GFP intensities for the membrane region, the top region, the bottom region, and the cytoplasmic region. Bottom: U937 cells exposed to 10min shear in pH-balanced Plasma-Lyte exhibit a significant decrease (*P<0.05 compared to 0 min) in GFP intensities in all of the regions (membrane: -6%, n=7; cytoplasm: -11%, n=8; top: -9%, n=6; bottom: -11%, n=4). The cytoplasmic region showed a significant change as early as the 5min timepoint (-10%, n=8).

panel). The membrane region (obtained by combining the measurements for upstream and downstream regions) also showed a significant decreased of intensity after 10 minutes of shearing. As a method to verify if receptor internalization occurred at the surface where there was highest shear, we obtained average intensities from fluorescence images of the top surface and the bottom (substrate-contact) region. The changes were small between the different time points. Six cells were used in the evaluation of top region fluorescence and another four cells were used for bottom region fluorescence measurements. The top region fluorescence intensity for one cell showed an increase after shearing. The focal plane may not be exactly the same through the experiment because it was constantly adjusted to obtain the plane of highest GFP intensity in the center of the cell. The cell retraction also caused the top plane to move, making it difficult to track intensity fluctuations on the cell surface. We believe that the small changes as indicated by the graphs were due to fluorescence reduction on the cell membrane, and this is confirmed by the statistical significance obtained between subsequent time points and the initial time point.

# DISCUSSION AND CONCLUSIONS

The objectives of this work were to draw a clear connection between the fluid stresses and cell morphological changes. It was necessary to first identify the local stresses and then the key players in transducing these mechanical signals into biological events in the cell. Hence this study had been divided into two major parts in which the first section was devoted to finding the surface stresses from fluid flow in better details than before whereas the focus of the second section was on FPR spatial location through the duration of shear.

## Membrane Fluid Stress Analysis

The finite element modeling presented in this work is to-date the best computation of fluid stresses on the surface of a leukocyte. It provides the details in understanding the stress distributions and a tool for seeking how these stresses correlate with the cell's morphological changes under shear. Interestingly, the highest fluid stresses are found at the top of the cell and their magnitudes are determined almost exclusively by the height of the cell regardless of other surface features. There are surface undulations that lead to more localized variations in stress values. However, since the current method of analysis does not provide tracking of the exact changes in the surface radius, in this work we are only focusing on larger domains of the membrane that are defined by the two extremes (maximum and minimum) in stress magnitudes.

It is observed that the morphological changes in cells are individualistic. The cell shown in the figures in the second chapter of this dissertation exhibited an immediate retraction upon shear and remained retracted through the end of

the flow application. However, the four cells shown in the Appendix did not all respond with retraction. Two have continued with the cycles of pseudopod extension and retraction observed in human neutrophils that adhered to glass coverslips (Fukuda, Yasu et al. 2000). The exact mechanisms for such varied behavior have not been resolved and it is the goal of this work to present evidence in support of one possible mechanism.

From studies done on confluent endothelial layer and a fluid mechanics point of view, it is thought that leukocytes actively change their shape in order to minimize shear (drag force and torque). Yet this work and previous publications from this lab have shown that there is a different underlying mechanism for their shape change. The computations showed that overall shear stress levels have not reduced, and instead increased, on the cell surface. In fact, in agreement with my computational results, the retraction of pseudopods observed by many (Moazzam, DeLano et al. 1997; Marschel and Schmid-Schonbein 2002; Makino, Glogauer et al. 2005) would lead to increased drag force because the cell goes from a thin pancake-like shape to round that extends further into the flow field. This drag force sometimes leads to detachment of the cell (Fukuda, Yasu et al. 2000). Only one set of studies, which shows that leukocytes spread along the substrate under flow (Coughlin and Schmid-Schonbein 2004), supports the line of thought that cellular morphological changes serve to reduce shear stresses (Barbee, Mundel et al. 1995). The disparity in these observations from leukocyte shear experiments may be due to the individual cell's receptor distribution.

In the finite element computations of fluid stress over the entire cell, the surface of the cell was assumed to be smooth for the purposes of the model but in reality there were smaller membrane ripples much less than 1μm in height that cannot be distinguished in bright field images of leukocytes. Based on scanning electron micrographs, neutrophil surfaces are fully covered by folds that may be finger-like or ridge-like (Figure 10) but are all about 0.2μm in height (Schmid-Schonbein, Shih et al. 1980). Another study used transmission electron micrographs to show that neutrophils, monocytes, and lymphocytes all exhibited 20-30 membrane microvilli at the tips of which L-selectins and P-selectin glycoprotein ligand 1 (PSGL-1) localized (Bruehl, Springer et al. 1996). From observations of neutrophil rolling and tethering on substrate, blocking CD18 has no effect on this initial cell-capturing process, suggesting that CD18 is hiding away from the microvilli tips (Schmidtke and Diamond 2000). It is not yet known if FPR localize on the tips of microvilli in a fashion similar to L-selectin. Modeling of fluid drag force (applied shear of 5-30dyn/cm$^2$) on a stereocilia shows that 75% of the drag is experienced at the tip (Weinbaum, Guo et al. 2001). This shows that membrane molecules at the tip or the base of a microvillus experience varying levels of fluid shear stress and such localized differentials elicit different biological responses of the cell.

From my own computations on a model that represents a small section of membrane with micro-protrusions (Figures 24-27) that are the same size as leukocyte membrane folds, I showed that the protrusions indeed enhance fluid stresses at the tip and reduce stresses in the trough. When the protrusions are closely clustered (Figures 24 & 25), the shear stress at the tip of the middle

protrusion is several times of the membrane stress, indicating that any receptors at the tips on the top surface of the cell may experience ~30 times the applied wall shear stress receptors in the troughs are completely shielded from any fluid stresses. When the protrusions are much further apart (Figures 26 & 27), the maximum shear stresses at the tips of the protrusions are enhanced further though at the same order of magnitude as the cluster. The troughs between the protrusions in this case do not serve to shield any fluid stresses and therefore any receptors here will experience the same stresses as presented in the case of a smooth membrane (Figures 14-17).

The flow field has been disturbed slightly by the closely spaced membrane folds, leading to compressive normal stresses on the backside (near the base) of the middle protrusion. Since the focus of fluid shear studies has always been on only the shear component of stresses caused by flow, there is no concrete evidence to suggest the role of normal stresses in mechanotransduction of cells in a flow field. It is unclear at this point if a compressive normal stress in only a very small fraction of the total cell surface area would cause the cell to behave differently.

## FPR Analysis

There is small variation in fluid shear response within a population of U937 cells, but almost all cells retract to some extent. Such individualistic responses are further support of observations made previously by myself and other colleagues. However, for the purposes of this study, the focus is on the FPR spatial distribution in a cell that exhibits retraction upon flow.

It is evident that when the glass coverslip comes in contact with serum proteins, the ability for cells to firmly adhere is greatly decreased. Due to the reduced adhesion, cells sheared by culture medium have a higher tendency to roll and slide off the coverslip upon shear. Of the cells that stayed adherent on the coverslip, they are attached by only one point upstream and therefore the cells were stretched into a teardrop shape. When the flow was stopped, these cells exhibited a recoiling behavior indicative of a passive displacement of the cell due to flow.

From published molecular biology experiments, it has been known that upon agonist binding, FPRs cluster into lipid rafts on the cell membrane and then get internalized (Loitto, Rasmusson et al. 2001; Xue, Vines et al. 2004). We hypothesized that FPR's role in mechanotransduction will be carried out in a similar fashion, that is, we may see a redistribution of FPR on the cell surface that is followed by internalization of the receptor. The first images from pilot experiments showed that shearing the U937 cells led to an unexpected aggregation of GFP in a compartment next to the nucleus. More experiments were performed to focus on just observing the compartment and its intensity had consistently increased over the course of flow. The experimental time was too short for any new GFP to be synthesized, suggesting that this increase came from some other parts of the cell. Based on previously published data (Makino, Prossnitz et al. 2005), we put forward the idea that membrane FPR has been internalized and the aggregation of GFP fluorescence simply reflects that process.

As a first step in evaluating FPR internalization, it was hypothesized that the receptors exposed to highest magnitudes of fluid stress will respond differently from those exposed to lowest magnitudes of stress. Therefore it would be interesting to look at the receptor distribution between surface regions that experience very different stresses. From the computations it could be seen that the largest differentials in fluid stress values on the surface of the cell were between the upstream and downstream regions and also between the top and the substrate-contact region. We chose to focus on these regions for the analysis on FPR redistribution under flow.

The upstream and downstream domains experience similar shear stresses but vary greatly in normal stresses. By taking a simple measurement for average membrane intensity, we found significant changes of the entire membrane domain over time only after 10 minutes of shearing. We initially hypothesized that receptors were activated by shear and therefore get internalized, and these measurements supported that hypothesis. The small changes observed (6% decrease), in contrast to the ~30% increase of the perinuclear compartment fluorescence intensity, might be due to the fact receptor internalization was occurring all over the cell membrane or more in areas on the surface where the shear stresses were highest.

The top and bottom membrane domains are analyzed for GFP intensities because the disparity of stresses between these two regions was the largest. The top experienced surface stresses about 6 times that of the applied wall shear whereas the bottom saw zero stress. Evaluation of the intensities from

fluorescence images showed that there was a minor reduction with respect to time, suggesting that FPR was being removed from those regions. Both the top and bottom regions experienced similar reductions of fluorescence, at 9% and 11%, respectively. The decrease in the bottom region was more consistent from cell to cell, possibly due to the fact that it was easier to determine the plane where the bottom lied. One challenge with the analysis of intensity from the top surface was that there was a great halo-effect from fluorescence from the rest of the cell that complicated the determination of where exactly the top region was. Since these images were taken with epifluorescence instead of confocal microscopy, adjusting the focus to the top of the cell was not sufficient in eliminating intracellular fluorescence.

As presented in the results section in the previous chapter, the intracellular compartment where FPR aggregated was likely a Rab11-positive perinuclear recycling endosome (Ernst, Zobiack et al. 2004; Key, Vines et al. 2005). Shear stresses might have initially activated the receptors even in the absence of chemoattractant and led to their internalization. However, in contrast to internalization caused by fMLP, shear appeared to have kept the receptors in the perinuclear compartment instead of allowing the receptor to be recycled. This prolonged internalization of FPR supported the previous finding that G-protein activity was significantly decreased after fluid shear (Makino, Prossnitz et al. 2005). Shear stress might have prevented FPR from returning to the membrane and therefore the constitutive activity that regulated pseudopod retraction and extension was downregulated. This might be accomplished through an arrestin-regulated pathway as Key *et al* showed that stable ternary binding of FPR to

active arrestins inhibited recycling of the receptor (Key, Vines et al. 2005). These observations did not offer an explanation for the pseudopod extension behaviors observed by Coughlin (Coughlin and Schmid-Schonbein 2004). We hypothesize that in those experiments, majority of the FPR is in the substrate-contact region and shielded from the effects of shear and continue with the constitutive activities while FPR on the rest of the cell is internalized. However, the reasons for such variations in FPR distribution on individual unstimulated cells remain unknown.

The results of this work have shown that the fluid stress distributions on the cell do not have the initially hypothesized linear correlation to cell behavior exhibited through the changes in its morphology. That has led to the idea that there is at least one other player involved in this regulation of leukocyte fluid shear response. The analysis indirectly supports the argument that FPR activity is reduced during flow application by showing that there is a significant increase in intracellular FPR concentration accompanied by significant membrane and cytoplasmic FPR decrease, suggesting that fewer receptors are on the membrane to constitutively regulate leukocyte pseudopod projection. It is unexpected that the membrane distribution of FPR before, during, and after fluid shear application is quite uniform. This may be explained by the fact that even though the top of the cell experiences the highest shear stresses, most of the cell surface is exposed to at least 0.5dyn/cm$^2$ of shear. In addition to that, the micro-protrusions that cover the entire cell surface serve to magnify the shear and normal stresses several-fold. It is possible that only FPR on the tips of these membrane folds had been internalized by fluid shear while FPR in the troughs between folds are safely shielded from all fluid stresses and continue with their constitutive activities.

Therefore even though we observed a global reduction of FPR from both low and high shear surface regions of the cell, this decrease may have resulted from only the portion of FPRs that are at the tips of membrane folds.

Much work yet has to be done to connect all the dots in leukocyte functional behavior, but the observations put forth in this dissertation have put us one small step closer to elucidating that path.

# APPENDIX

The figures presented in the following pages are fluid stress plots and graphs mapping the changes in stress magnitudes for four HL60 cells at the same time points during the experiment as the one shown in the second chapter. Contrary to the cell shown previously, these cells did not all show an overall retraction response to fluid shear. However, the individual membrane domains on these cells did not show significant changes in average surface stress magnitudes. It is suggested from the stress distributions of these 5 cells that retraction or extension of pseudopods are not linearly correlated to the stress magnitudes (resultant, shear, or normal components).

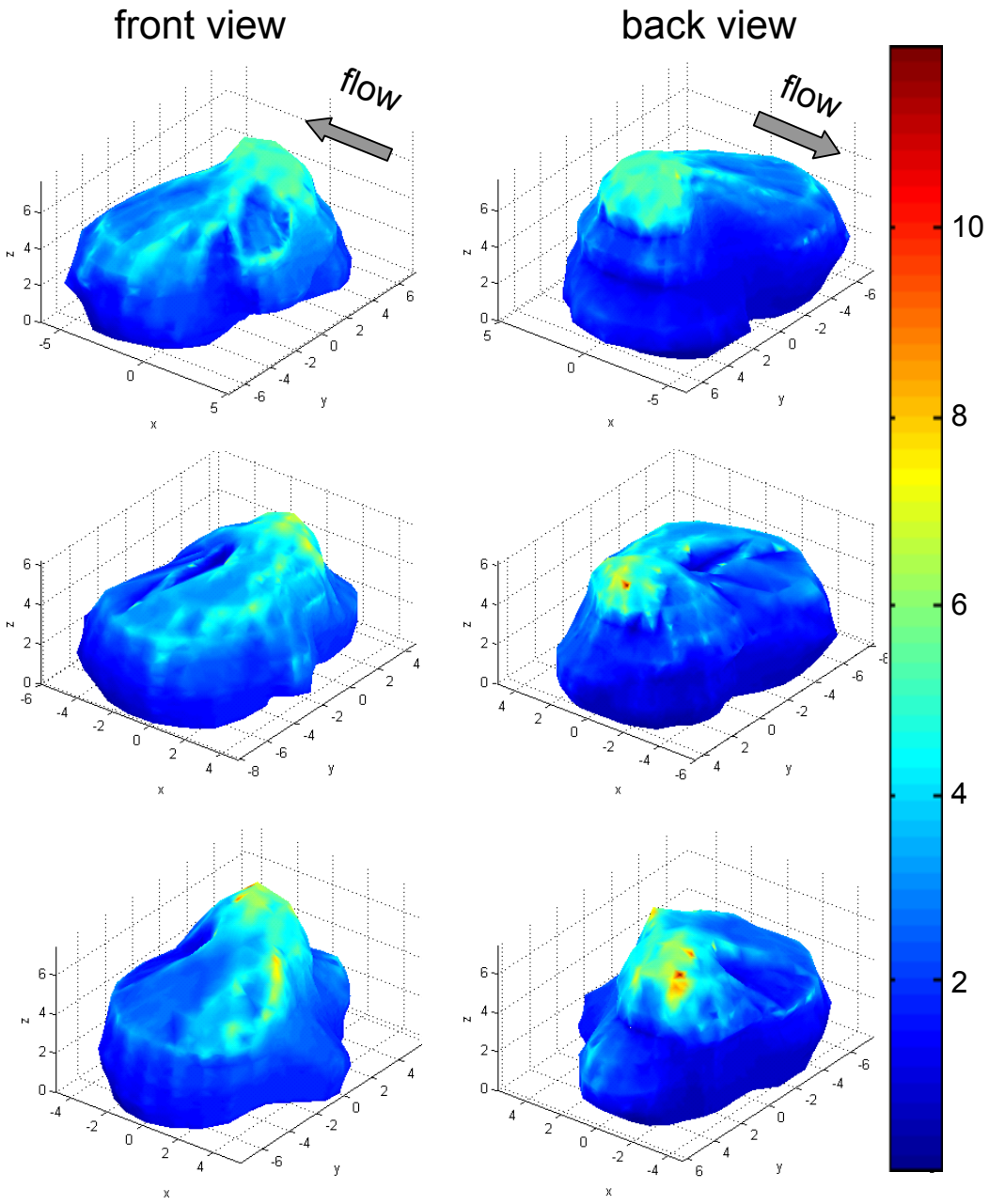


**Figure 38 Normalized resultant stress distributions on the surface of an adherent leukocyte (2).**

Resultant stress distributions (left: front view; right: back view) on the surface of one neutrophil are normalized with respect to the applied wall shear stress of 2.2dyn/cm$^2$ in the negative x-direction at the onset of flow (top), 1 minute into the flow (middle), and the end of a 3-min laminar flow application (bottom). The color bar is unitless and the axes are in μm.

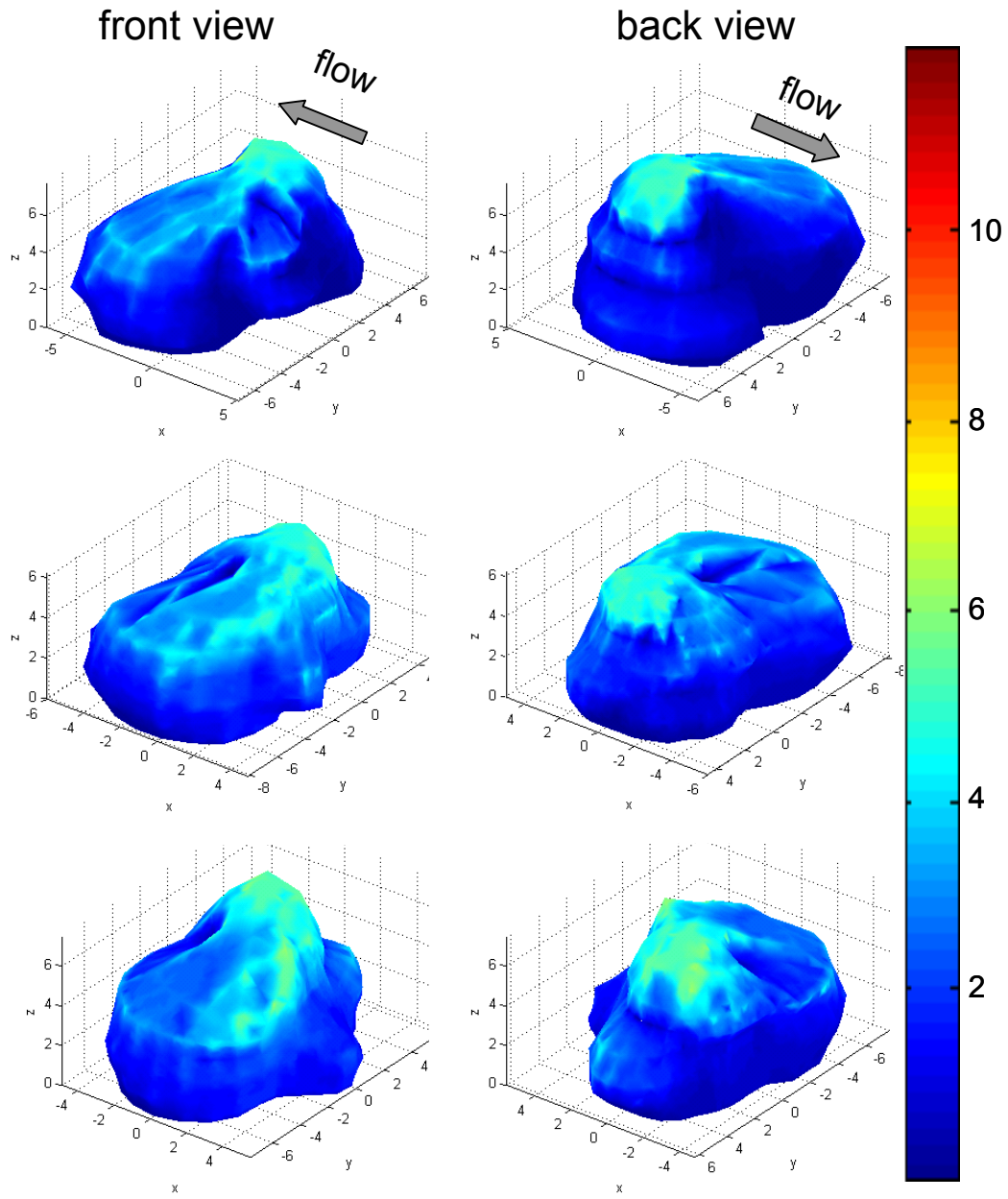


**Figure 39 Normalized shear stress distributions on the surface of an adherent leukocyte (2).**

Shear stress distributions (left: front view; right: back view) on the surface of one neutrophil are normalized with respect to the applied wall shear stress of 2.2dyn/cm$^2$ in the negative x-direction at the onset of flow (top), 1 minute into the flow (middle), and the end of a 3-min laminar flow application (bottom). The color bar is unitless and the axes are in μm.

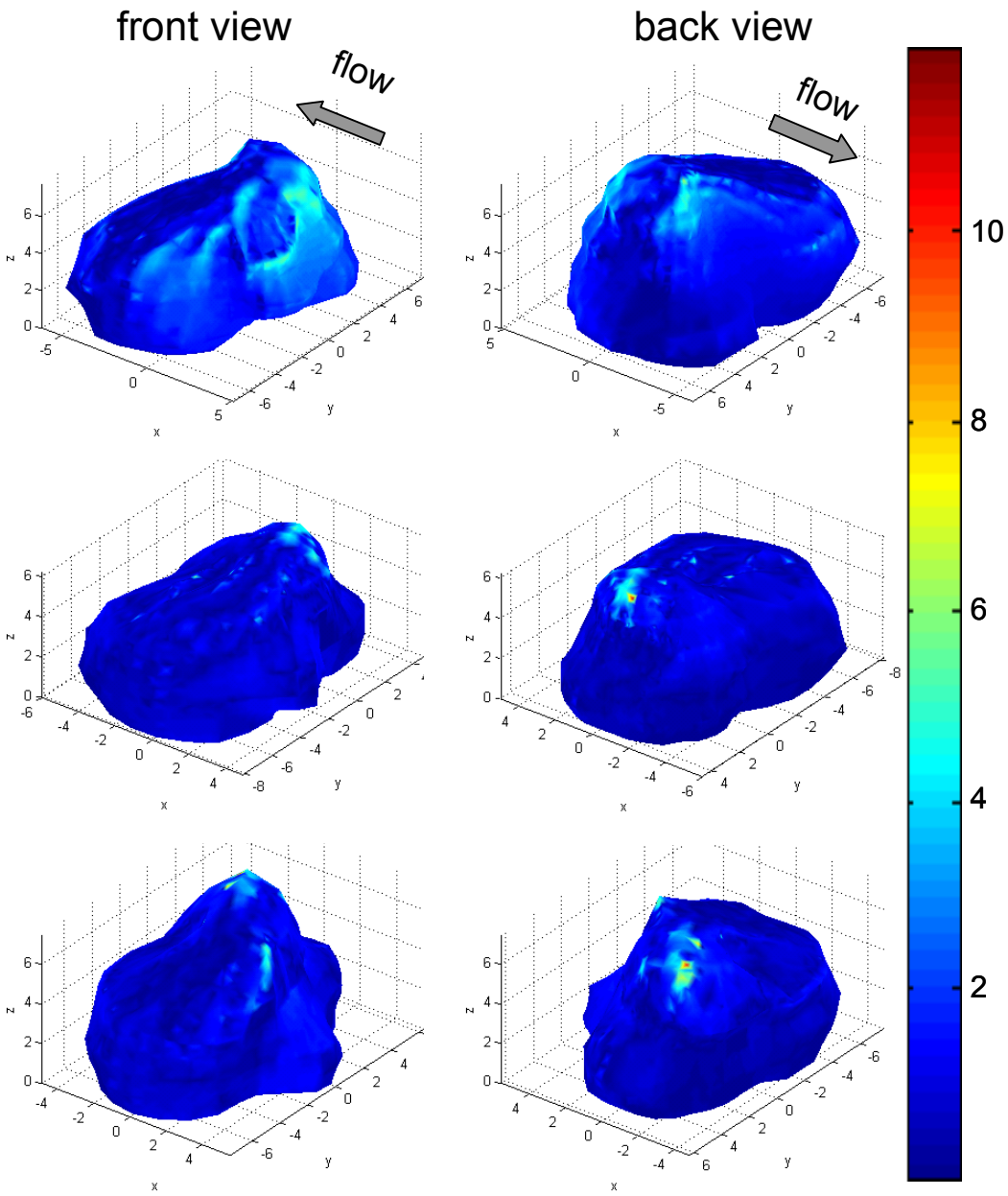


**Figure 40 Normalized normal stress distributions on the surface of an adherent leukocyte (2).**

Normal stress distributions (left: front view; right: back view) on the surface of one neutrophil are normalized with respect to the applied wall shear stress of 2.2dyn/cm$^2$ in the negative x-direction at the onset of flow (top), 1 minute into the flow (middle), and the end of a 3-min laminar flow application (bottom). The color bar is unitless and the axes are in μm.

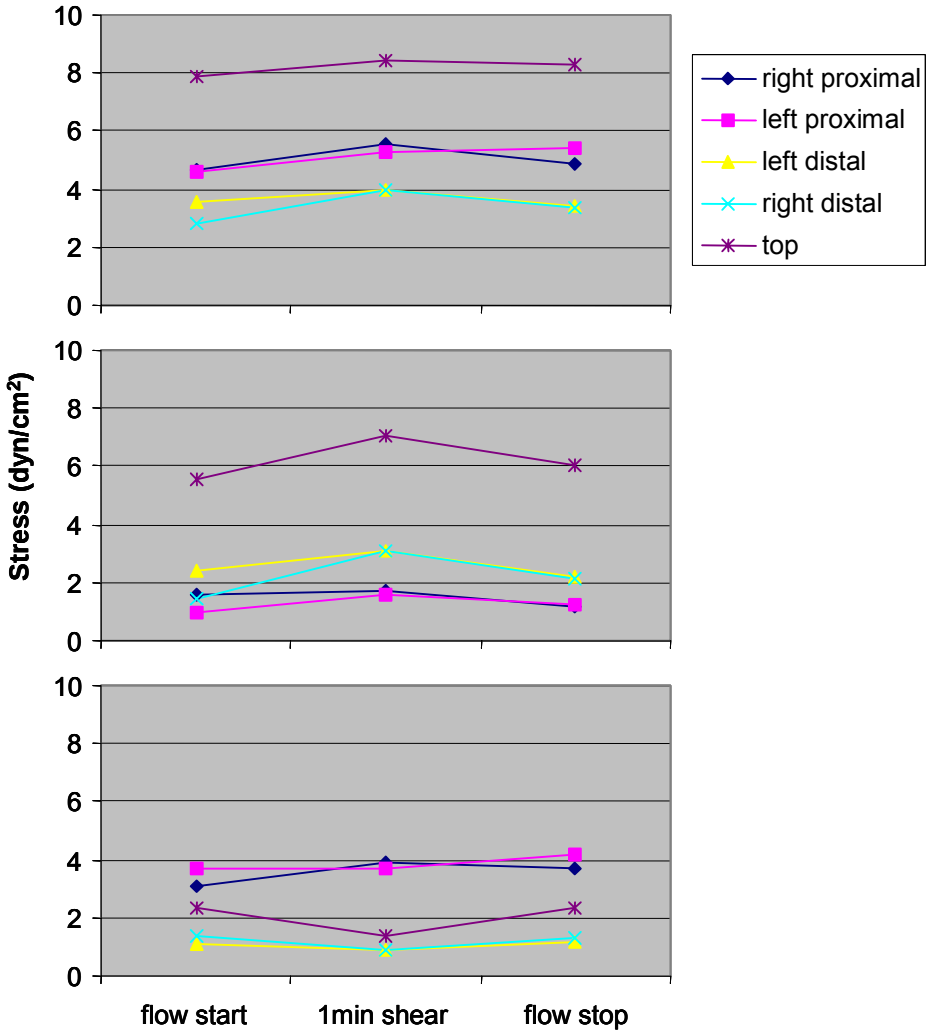


**Figure 41 Average regional cell surface fluid stress over time (2).**

The average resultant stress (top), shear stress (middle), normal stress (bottom) are computed for each region and plotted for the 3 time points (onset of flow, 1 minute into flow, and at the end of a 3-min flow). The change in average stress within each surface domain is very small compared to the magnitude of the stress.

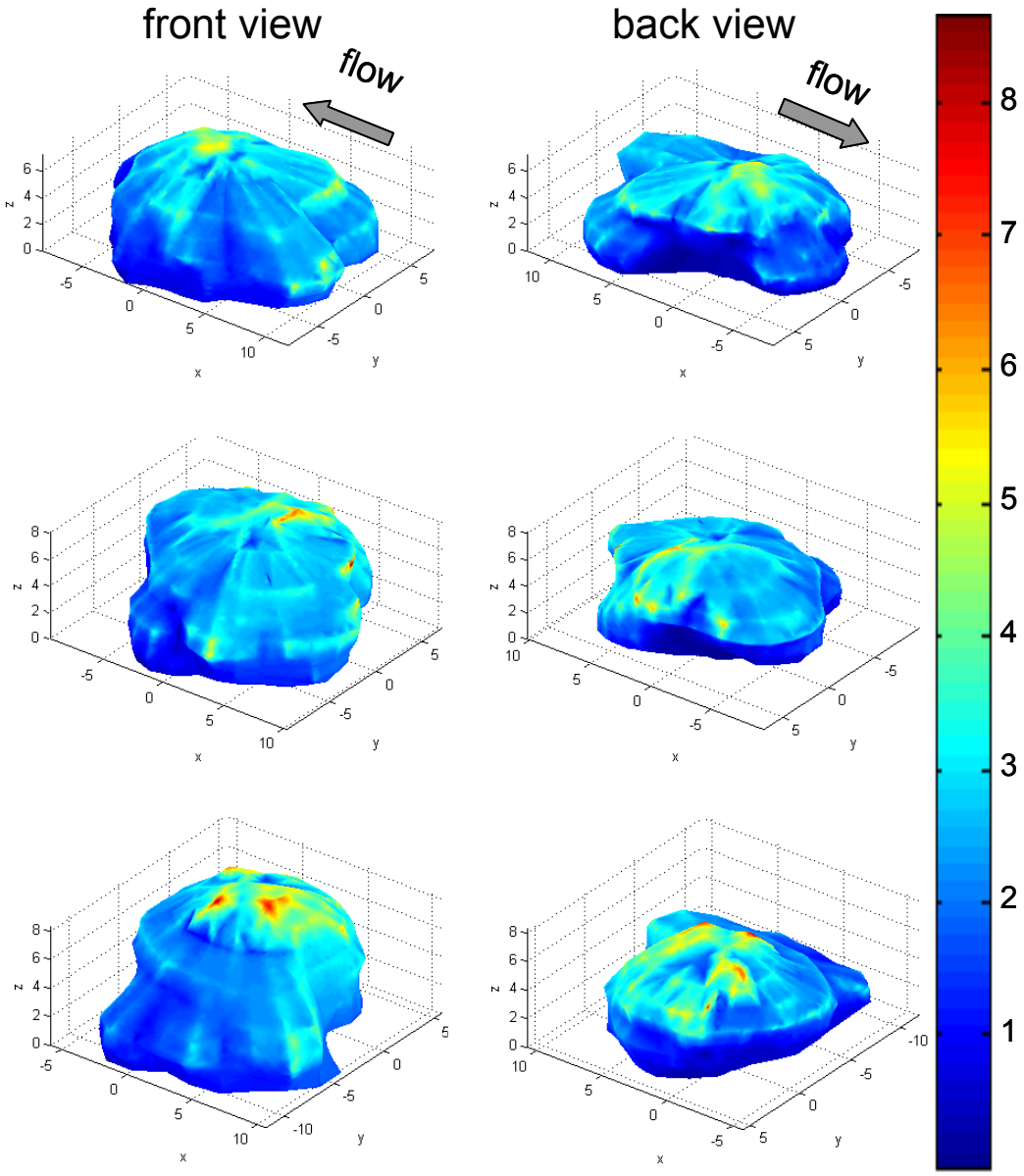


**Figure 42 Normalized resultant stress distributions on the surface of an adherent leukocyte (3).**

Resultant stress distributions (left: front view; right: back view) on the surface of one neutrophil are normalized with respect to the applied wall shear stress of 2.2dyn/cm$^2$ in the negative x-direction at the onset of flow (top), 1 minute into the flow (middle), and the end of a 3-min laminar flow application (bottom). The color bar is unitless and the axes are in μm.

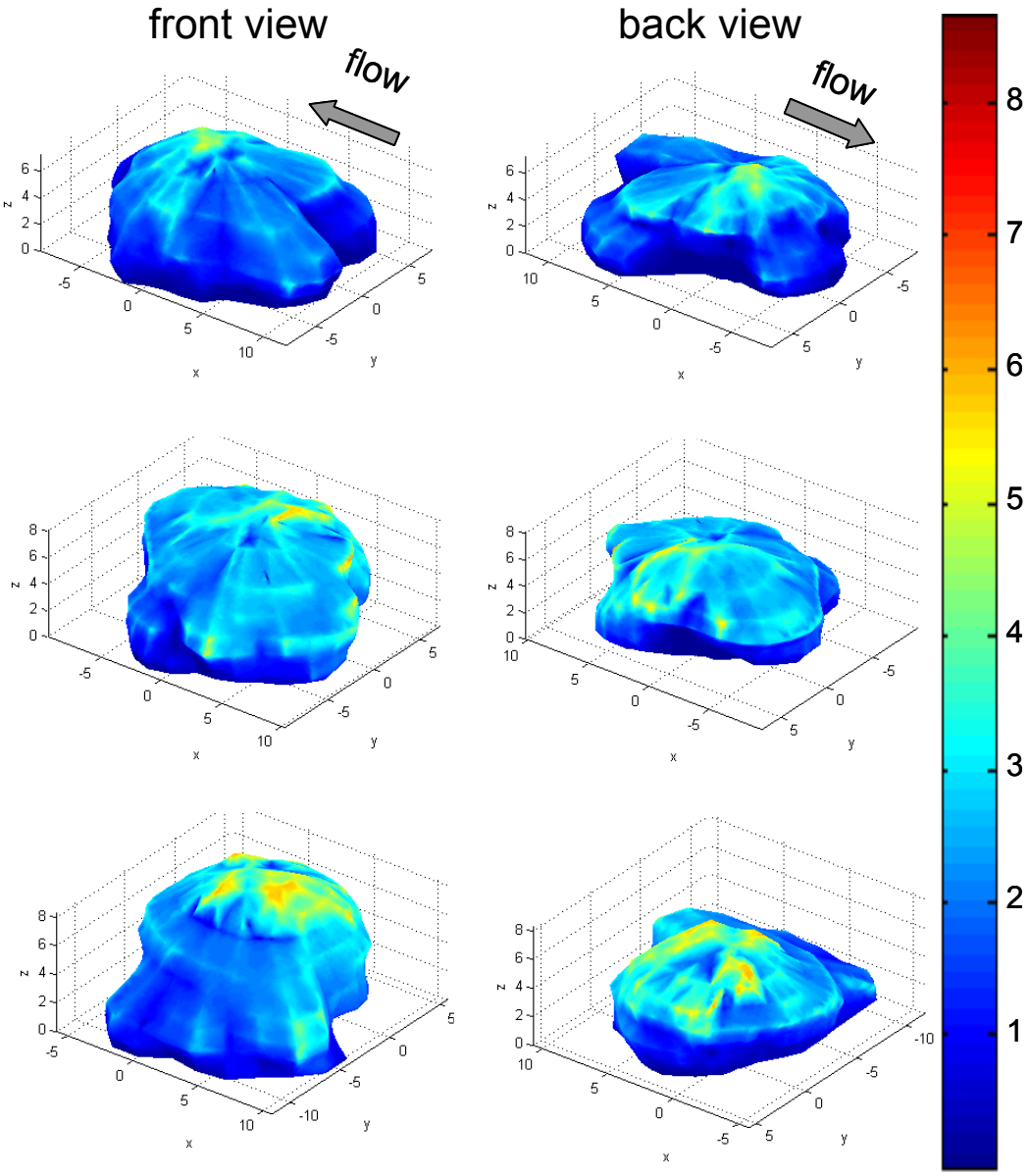


**Figure 43 Normalized shear stress distributions on the surface of an adherent leukocyte (3).**

Shear stress distributions (left: front view; right: back view) on the surface of one neutrophil are normalized with respect to the applied wall shear stress of 2.2dyn/cm$^2$ in the negative x-direction at the onset of flow (top), 1 minute into the flow (middle), and the end of a 3-min laminar flow application (bottom). The color bar is unitless and the axes are in μm.

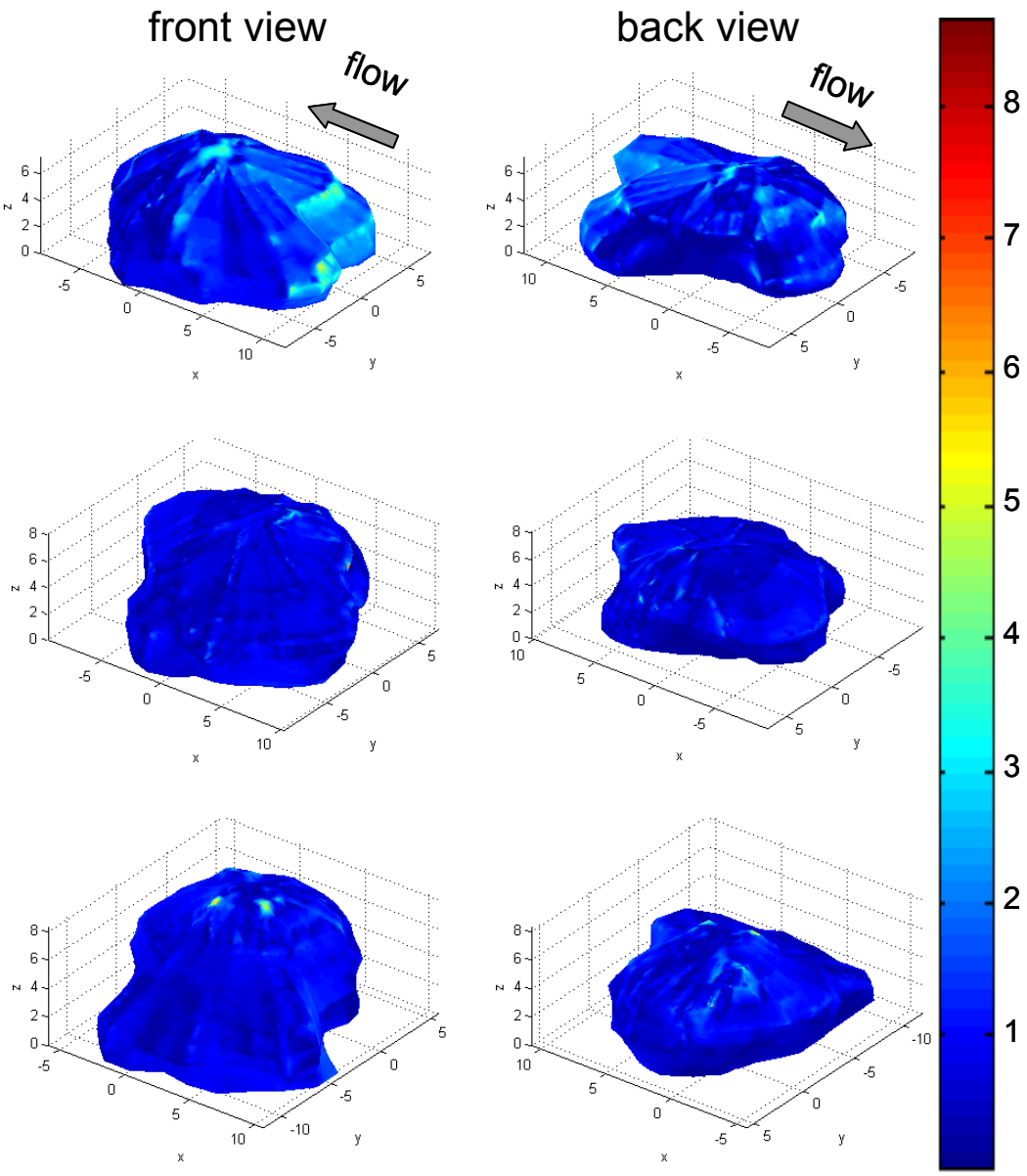


**Figure 44 Normalized normal stress distributions on the surface of an adherent leukocyte (3).**

Normal stress distributions (left: front view; right: back view) on the surface of one neutrophil are normalized with respect to the applied wall shear stress of 2.2dyn/cm$^2$ in the negative x-direction at the onset of flow (top), 1 minute into the flow (middle), and the end of a 3-min laminar flow application (bottom). The color bar is unitless and the axes are in μm.

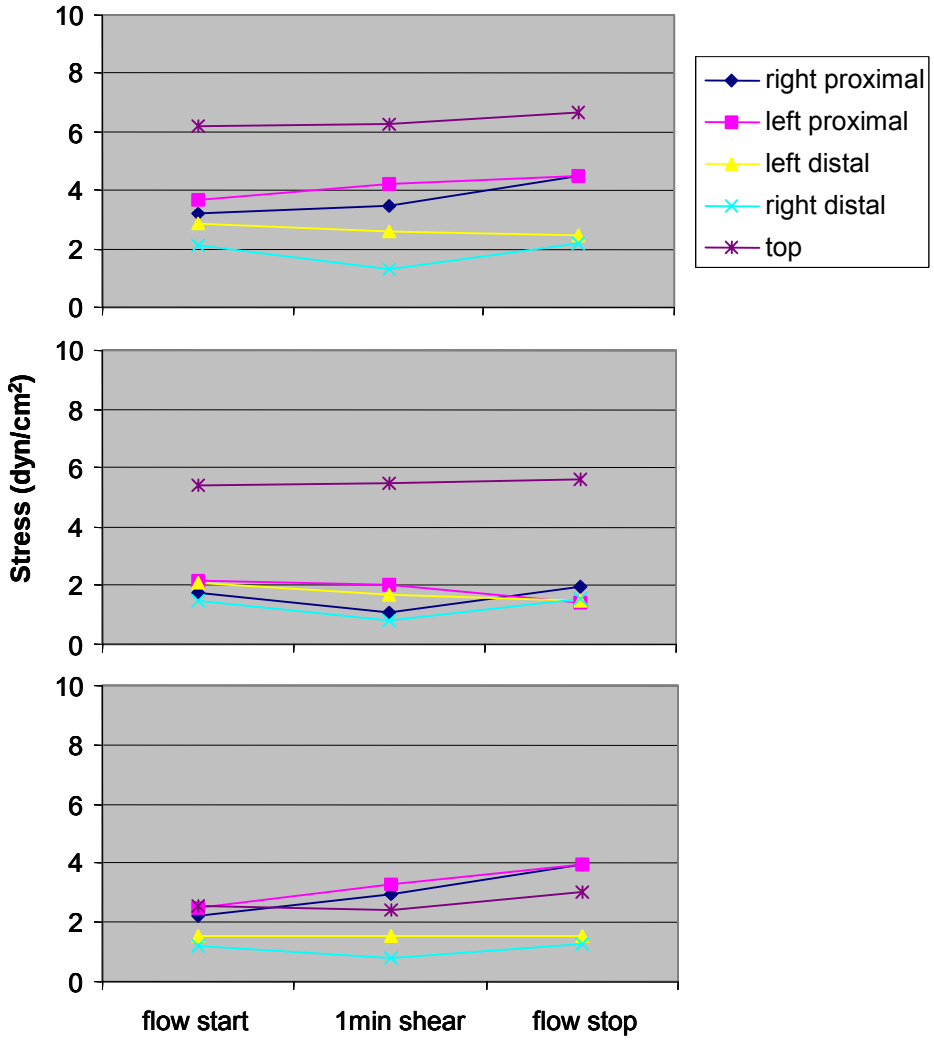


**Figure 45 Average regional cell surface fluid stress over time (3).**

The average resultant stress (top), shear stress (middle), normal stress (bottom) are computed for each region and plotted for the 3 time points (onset of flow, 1 minute into flow, and at the end of a 3-min flow). The change in average stress within each surface domain is very small compared to the magnitude of the stress.

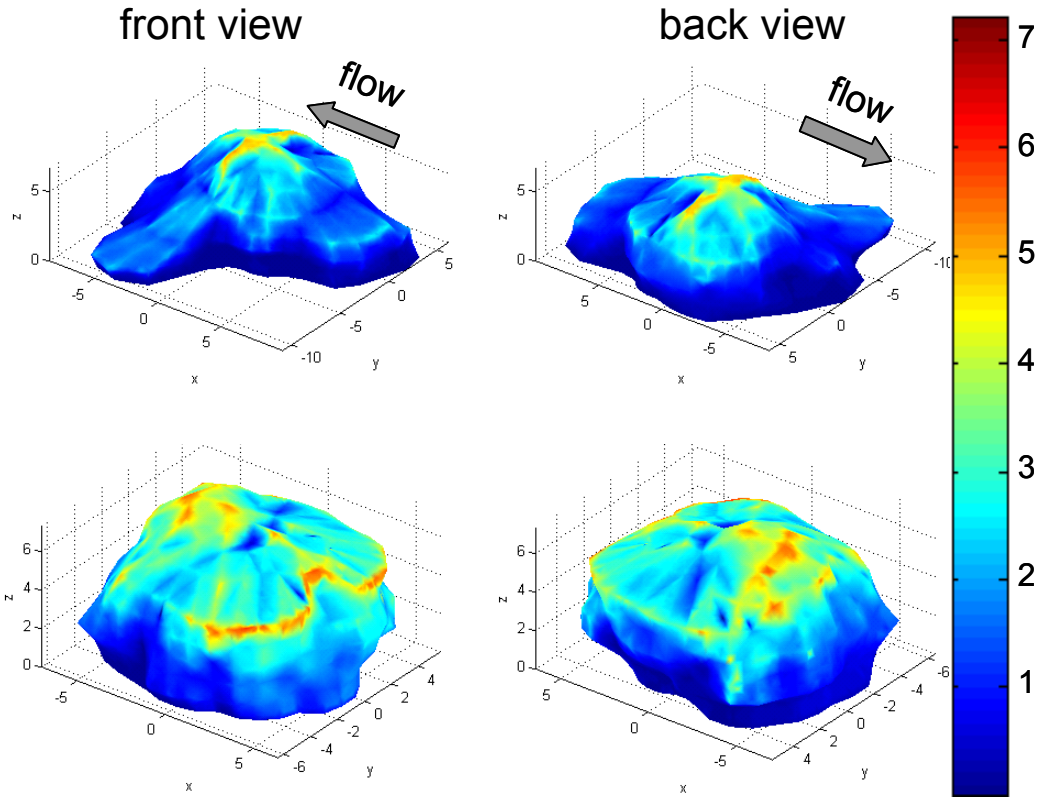


**Figure 47 Normalized shear stress distributions on the surface of an adherent leukocyte (4).**

Shear stress distributions (left: front view; right: back view) on the surface of one neutrophil are normalized with respect to the applied wall shear stress of 2.2dyn/cm$^2$ in the negative x-direction at the onset of flow (top) and the end of a 3-min laminar flow application (bottom). The color bar is unitless and the axes are in μm.

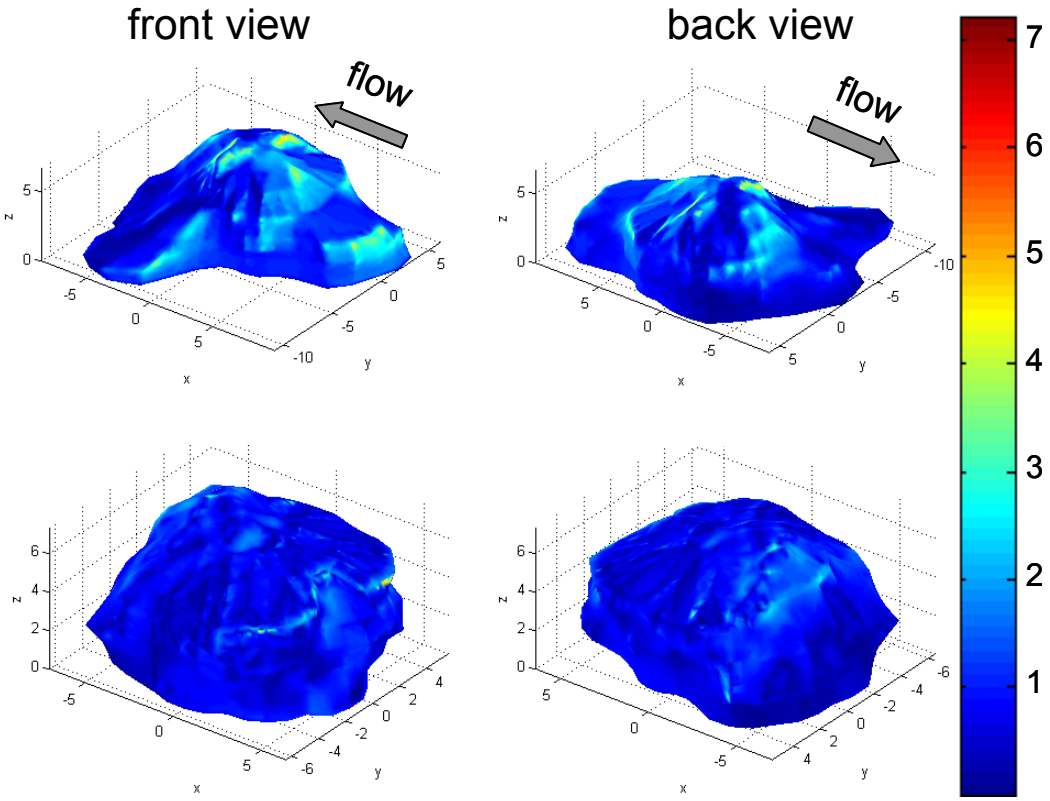


**Figure 48 Normalized normal stress distributions on the surface of an adherent leukocyte (4).**

Normal stress distributions (left: front view; right: back view) on the surface of one neutrophil are normalized with respect to the applied wall shear stress of 2.2dyn/cm$^2$ in the negative x-direction at the onset of flow (top) and the end of a 3-min laminar flow application (bottom). The color bar is unitless and the axes are in μm.

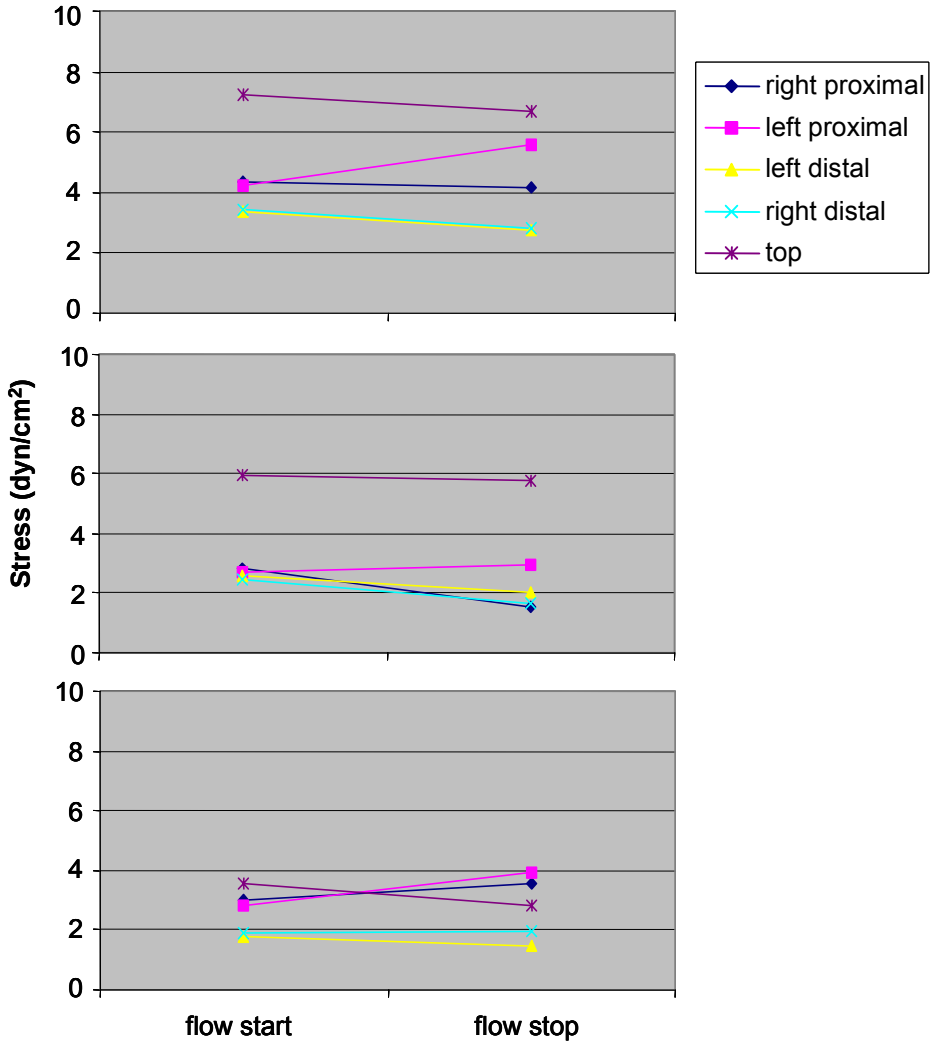


**Figure 49 Average regional cell surface fluid stress over time (4).**

The average resultant stress (top), shear stress (middle), normal stress (bottom) are computed for each region and plotted for the 2 time points (onset of flow and at the end of a 3-min flow). The change in average stress within each surface domain is very small compared to the magnitude of the stress.

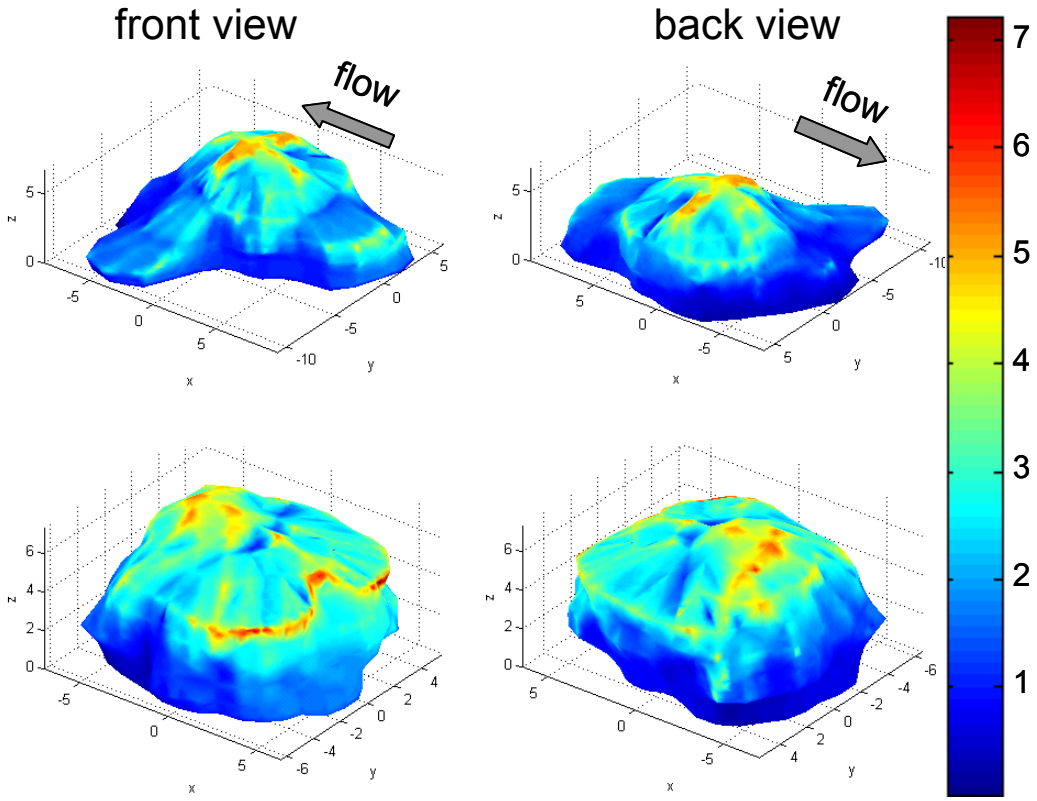


**Figure 46 Normalized resultant stress distributions on the surface of an adherent leukocyte (4).**

Resultant stress distributions (left: front view; right: back view) on the surface of one neutrophil are normalized with respect to the applied wall shear stress of 2.2dyn/cm$^2$ in the negative x-direction at the onset of flow (top) and the end of a 3-min laminar flow application (bottom). The color bar is unitless and the axes are in μm.

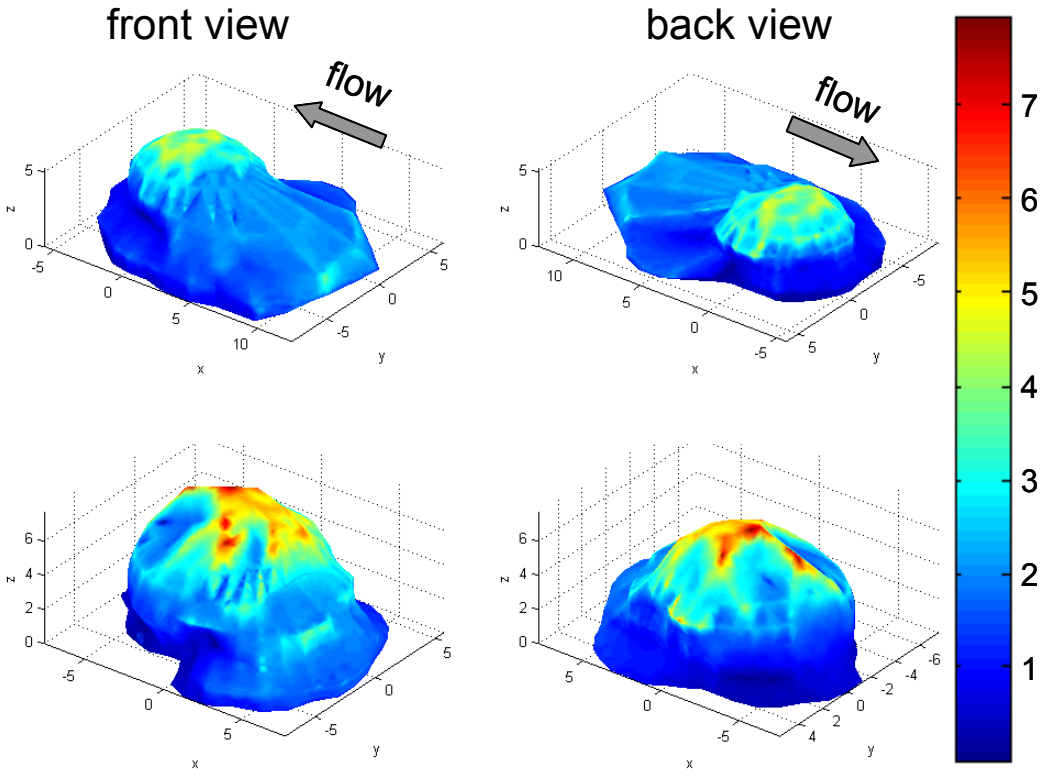


**Figure 50 Normalized resultant stress distributions on the surface of an adherent leukocyte (5).**

Resultant stress distributions (left: front view; right: back view) on the surface of one neutrophil are normalized with respect to the applied wall shear stress of 2.2dyn/cm$^2$ in the negative x-direction at the onset of flow (top) and the end of a 3-min laminar flow application (bottom). The color bar is unitless and the axes are in μm.

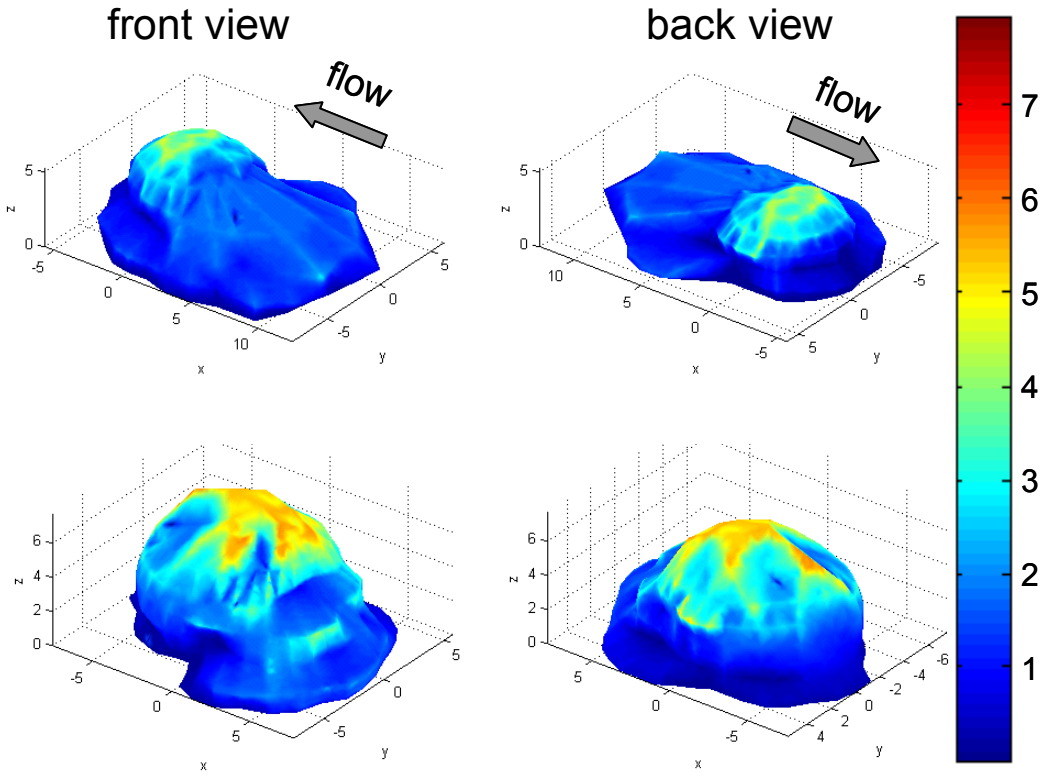


**Figure 51 Normalized shear stress distributions on the surface of an adherent leukocyte (5).**

Shear stress distributions (left: front view; right: back view) on the surface of one neutrophil are normalized with respect to the applied wall shear stress of 2.2dyn/cm$^2$ in the negative x-direction at the onset of flow (top) and the end of a 3-min laminar flow application (bottom). The color bar is unitless and the axes are in μm.

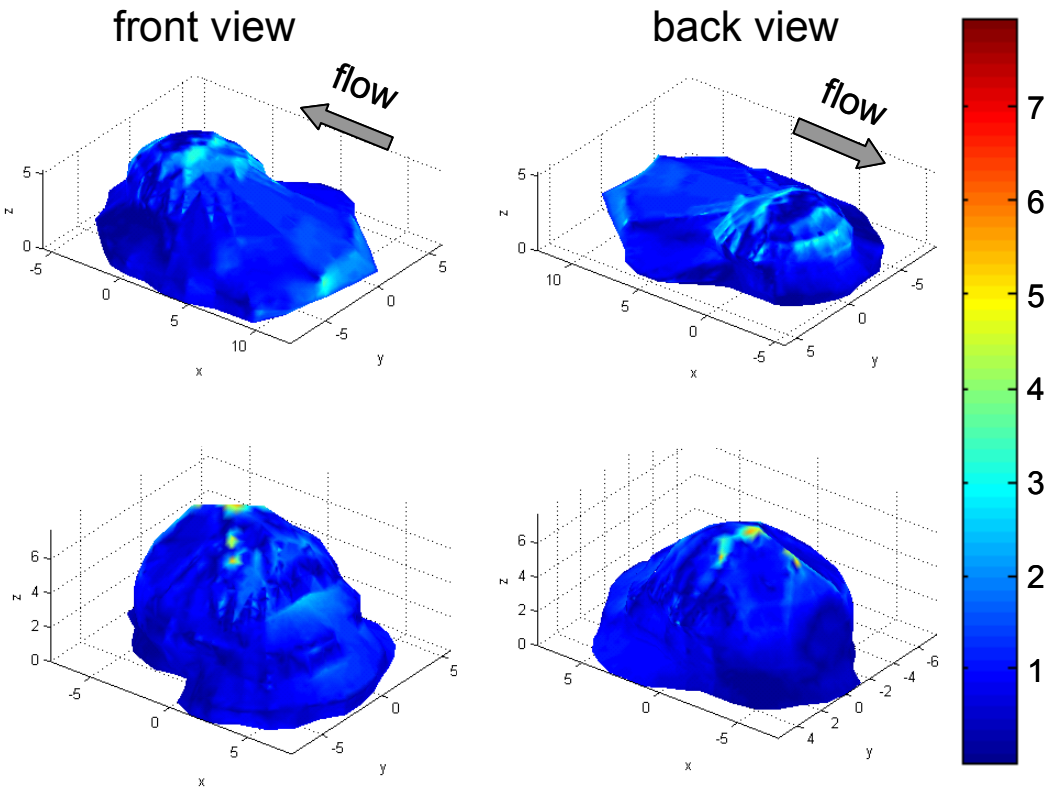


**Figure 52 Normalized normal stress distributions on the surface of an adherent leukocyte (5).**

Normal stress distributions (left: front view; right: back view) on the surface of one neutrophil are normalized with respect to the applied wall shear stress of 2.2dyn/cm$^2$ in the negative x-direction at the onset of flow (top) and the end of a 3-min laminar flow application (bottom). The color bar is unitless and the axes are in μm.

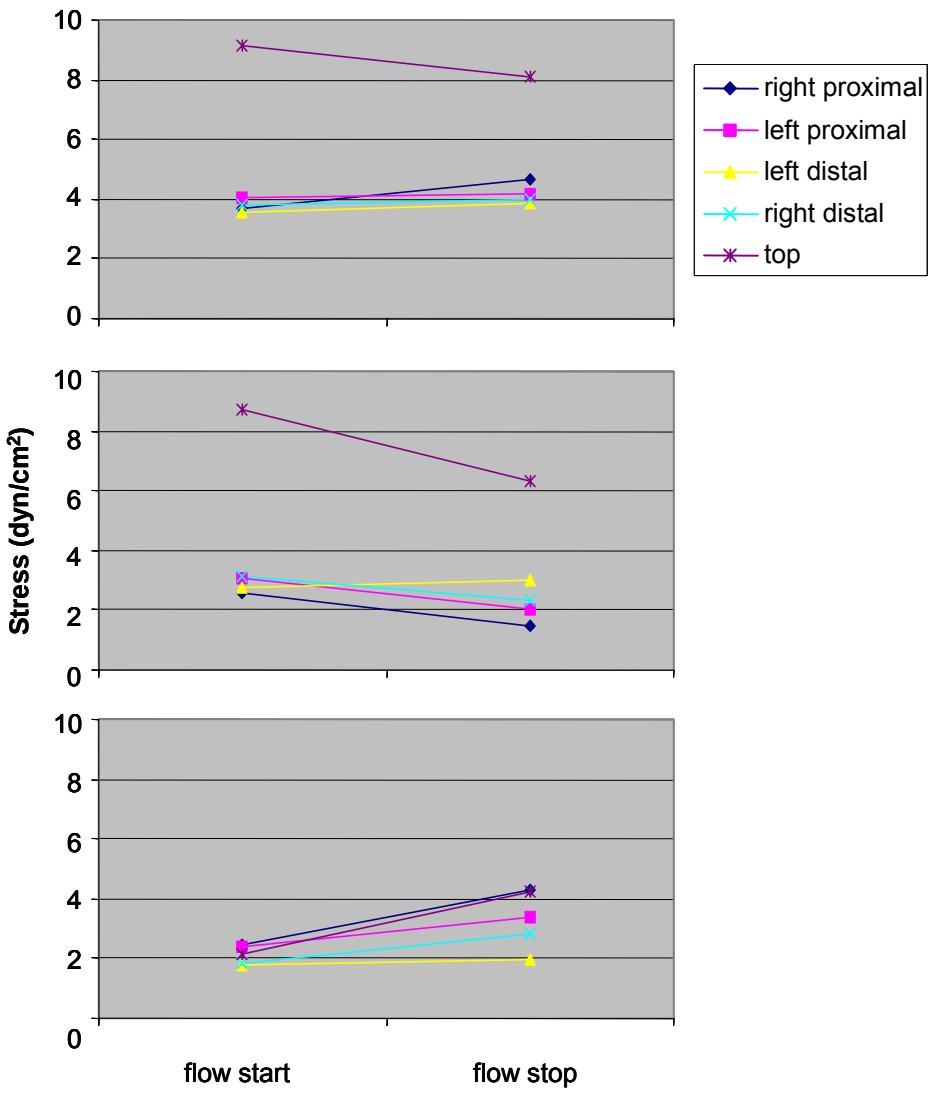


**Figure 53 Average regional cell surface fluid stress over time (5).**

The average resultant stress (top), shear stress (middle), normal stress (bottom) are computed for each region and plotted for the 2 time points (onset of flow and at the end of a 3-min flow). The change in average stress within each surface domain is very small compared to the magnitude of the stress.

## REFERENCES


Ahn, K. C., A. J. Jun, et al. (2005). "Preferential binding of platelets to monocytes over neutrophils under flow." Biochem Biophys Res Commun **329**(1): 345-55.

Akimoto, S., M. Mitsumata, et al. (2000). "Laminar shear stress inhibits vascular endothelial cell proliferation by inducing cyclin-dependent kinase inhibitor p21(Sdi1/Cip1/Waf1)." Circ Res **86**(2): 185-90.

Alevriadou, B. R., J. L. Moake, et al. (1993). "Real-time analysis of shear-dependent thrombus formation and its blockade by inhibitors of von Willebrand factor binding to platelets." Blood **81**(5): 1263-76.

Alvarez, A., M. Cerda-Nicolas, et al. (2004). "Direct evidence of leukocyte adhesion in arterioles by angiotensin II." Blood **104**(2): 402-8.

Andrews, R. K. and M. C. Berndt (2004). "Platelet physiology and thrombosis." Thromb Res **114**(5-6): 447-53.

Andrews, R. K., Y. Shen, et al. (2001). "Platelet adhesion receptors and (patho)physiological thrombus formation." Histol Histopathol **16**(3): 969-80.

Avogaro, A. and S. V. de Kreutzenberg (2005). "Mechanisms of endothelial dysfunction in obesity." Clin Chim Acta.

Bagge, U. and P. I. Branemark (1981). "Red cell shapes in capillaries." Scand J Clin Lab Invest Suppl **156**: 59-61.

Barbee, K. A., T. Mundel, et al. (1995). "Subcellular distribution of shear stress at the surface of flow-aligned and nonaligned endothelial monolayers." Am J Physiol **268**(4 Pt 2): H1765-72.

Baskurt, O. K. and H. J. Meiselman (2003). "Blood rheology and hemodynamics." Semin Thromb Hemost **29**(5): 435-50.

Boulay, F. and M. J. Rabiet (2005). "The chemoattractant receptors FPR and C5aR: same functions--different fates." Traffic **6**(2): 83-6.

Boulay, F., M. Tardif, et al. (1990). "Synthesis and use of a novel N-formyl peptide derivative to isolate a human N-formyl peptide receptor cDNA." Biochem Biophys Res Commun **168**(3): 1103-9.

Bruehl, R. E., T. A. Springer, et al. (1996). "Quantitation of L-selectin distribution on human leukocyte microvilli by immunogold labeling and electron microscopy." J Histochem Cytochem **44**(8): 835-44.

Carlos, T. M. and J. M. Harlan (1994). "Leukocyte-endothelial adhesion molecules." Blood **84**(7): 2068-101.

Carman, C. V. and T. A. Springer (2004). "A transmigratory cup in leukocyte diapedesis both through individual vascular endothelial cells and between them." J Cell Biol **167**(2): 377-88.

Cavicchioni, G., M. Turchetti, et al. (2003). "Properties of a novel chemotactic esapeptide, an analogue of the prototypical N-formylmethionyl peptide." Bioorg Chem **31**(4): 322-30.

Ciarkowski, J., M. Witt, et al. (2005). "A hypothesis for GPCR activation." J Mol Model (Online).

Coates, T. D., R. G. Watts, et al. (1992). "Relationship of F-actin distribution to development of polar shape in human polymorphonuclear neutrophils." J Cell Biol **117**(4): 765-74.

Coughlin, M. F. and G. W. Schmid-Schonbein (2004). "Pseudopod projection and cell spreading of passive leukocytes in response to fluid shear stress." Biophys J **87**(3): 2035-42.

Coussens, L. M. and Z. Werb (2002). "Inflammation and cancer." Nature **420**(6917): 860-7.

Curat, C. A., A. Miranville, et al. (2004). "From blood monocytes to adipose tissue-resident macrophages: induction of diapedesis by human mature adipocytes." Diabetes **53**(5): 1285-92.

Dalpiaz, A., M. E. Ferretti, et al. (1999). "Phe-D-Leu-Phe-D-Leu-Phe derivatives as formylpeptide receptor antagonists in human neutrophils: cellular and conformational aspects." Biochim Biophys Acta **1432**(1): 27-39.

Davies, P. F. (1995). "Flow-mediated endothelial mechanotransduction." Physiol Rev **75**(3): 519-60.

Davies, P. F., T. Mundel, et al. (1995). "A mechanism for heterogeneous endothelial responses to flow in vivo and in vitro." J Biomech **28**(12): 1553-60.

Davies, P. F., A. Robotewskyj, et al. (1994). "Quantitative studies of endothelial cell adhesion. Directional remodeling of focal adhesion sites in response to flow forces." J Clin Invest **93**(5): 2031-8.

Del Maschio, A., A. Zanetti, et al. (1996). "Polymorphonuclear leukocyte adhesion triggers the disorganization of endothelial cell-to-cell adherens junctions." J Cell Biol **135**(2): 497-510.

Doerschuk, C. M. (2001). "Mechanisms of leukocyte sequestration in inflamed lungs." Microcirculation **8**(2): 71-88.

Doerschuk, C. M., N. Beyers, et al. (1993). "Comparison of neutrophil and capillary diameters and their relation to neutrophil sequestration in the lung." J Appl Physiol **74**(6): 3040-5.

Edwards, A. O., R. Ritter, 3rd, et al. (2005). "Complement factor H polymorphism and age-related macular degeneration." Science **308**(5720): 421-4.

Engelhardt, B. and H. Wolburg (2004). "Mini-review: Transendothelial migration of leukocytes: through the front door or around the side of the house?" Eur J Immunol **34**(11): 2955-63.

Ernst, S., C. Lange, et al. (2004). "An annexin 1 N-terminal peptide activates leukocytes by triggering different members of the formyl peptide receptor family." J Immunol **172**(12): 7669-76.

Ernst, S., N. Zobiack, et al. (2004). "Agonist-induced trafficking of the low-affinity formyl peptide receptor FPRL1." Cell Mol Life Sci **61**(13): 1684-92.

Esmon, C. T. (2004). "Crosstalk between inflammation and thrombosis." Maturitas **47**(4): 305-14.

Evans, E. A. (1989). "Structure and deformation properties of red blood cells: concepts and quantitative methods." Methods Enzymol **173**: 3-35.

Fabbri, E., S. Spisani, et al. (2000). "Studies on fMLP-receptor interaction and signal transduction pathway by means of fMLP-OMe selective analogues." Cell Signal **12**(6): 391-8.

Feng, D., J. A. Nagy, et al. (1998). "Neutrophils emigrate from venules by a transendothelial cell pathway in response to FMLP." J Exp Med **187**(6): 903-15.

Fox, R. W. and A. T. McDonald (1998). Introduction to Fluid Mechanics, John Wiley & Sons, Inc.

Frostegard, J. (2005). "Atherosclerosis in Patients With Autoimmune Disorders." Arterioscler Thromb Vasc Biol **25**.

Fujiwara, N. and K. Kobayashi (2005). "Macrophages in inflammation." Curr Drug Targets Inflamm Allergy **4**(3): 281-6.

Fukuda, S., H. Mitsuoka, et al. (2004). "Leukocyte fluid shear response in the presence of glucocorticoid." J Leukoc Biol **75**(4): 664-70.

Fukuda, S. and G. W. Schmid-Schonbein (2002). "Centrifugation attenuates the fluid shear response of circulating leukocytes." J Leukoc Biol **72**(1): 133-9.

Fukuda, S. and G. W. Schmid-Schonbein (2003). "Regulation of CD18 expression on neutrophils in response to fluid shear stress." Proc Natl Acad Sci U S A **100**(23): 13152-7.

Fukuda, S., T. Yasu, et al. (2004). "Contribution of fluid shear response in leukocytes to hemodynamic resistance in the spontaneously hypertensive rat." Circ Res **95**(1): 100-8.

Fukuda, S., T. Yasu, et al. (2000). "Mechanisms for regulation of fluid shear stress response in circulating leukocytes." Circ Res **86**(1): E13-8.

Galbraith, C. G., R. Skalak, et al. (1998). "Shear stress induces spatial reorganization of the endothelial cell cytoskeleton." Cell Motil Cytoskeleton **40**(4): 317-30.

Gallagher, R., S. Collins, et al. (1979). "Characterization of the continuous, differentiating myeloid cell line (HL-60) from a patient with acute promyelocytic leukemia." Blood **54**(3): 713-33.

Gallin, J. I. (1984). "Human neutrophil heterogeneity exists, but is it meaningful?" Blood **63**: 977-983.

Green, C. E., D. N. Pearson, et al. (2004). "Shear-dependent capping of L-selectin and P-selectin glycoprotein ligand 1 by E-selectin signals activation of high-avidity beta2-integrin on neutrophils." J Immunol **172**(12): 7780-90.

Haines, J. L., M. A. Hauser, et al. (2005). "Complement factor H variant increases the risk of age-related macular degeneration." Science **308**(5720): 419-21.

Harlan, J. M. and R. K. Winn (2002). "Leukocyte-endothelial interactions: clinical trials of anti-adhesion therapy." Crit Care Med **30**(5 Suppl): S214-9.

Hauert, A. B., S. Martinelli, et al. (2002). "Differentiated HL-60 cells are a valid model system for the analysis of human neutrophil migration and chemotaxis." Int J Biochem Cell Biol **34**(7): 838-54.

Helmke, B. P. (2005). "Molecular control of cytoskeletal mechanics by hemodynamic forces." Physiology (Bethesda) **20**: 43-53.

Helmke, B. P. and P. F. Davies (2002). "The cytoskeleton under external fluid mechanical forces: hemodynamic forces acting on the endothelium." Ann Biomed Eng **30**(3): 284-96.

Jesaitis, A. J., J. R. Naemura, et al. (1984). "Rapid modulation of N-formyl chemotactic peptide receptors on the surface of human granulocytes: formation of high-affinity ligand-receptor complexes in transient association with cytoskeleton." J Cell Biol **98**: 1378-1387.

Johnson, R. M. (1994). "Membrane stress increases cation permeability in red cells." Biophys J **67**(5): 1876-81.

Key, T. A., C. M. Vines, et al. (2005). "Inhibition of chemoattractant N-formyl peptide receptor trafficking by active arrestins." Traffic **6**(2): 87-99.

Klein, R. J., C. Zeiss, et al. (2005). "Complement factor H polymorphism in age-related macular degeneration." Science **308**(5720): 385-9.

Komai, Y. and G. W. Schmid-Schonbein (2005). "De-activation of neutrophils in suspension by fluid shear stress: a requirement for erythrocytes." Ann Biomed Eng **33**(10): 1375-86.

Kon, K., N. Maeda, et al. (1987). "Erythrocyte deformation in shear flow: influences of internal viscosity, membrane stiffness, and hematocrit." Blood **69**(3): 727-34.

Konstantopoulos, K., K. K. Wu, et al. (1995). "Flow cytometric studies of platelet responses to shear stress in whole blood." Biorheology **32**(1): 73-93.

Kopaniak, M. M., A. C. Issekutz, et al. (1980). "Kinetics of acute inflammation induced by *E. Coli* in rabbits: quantitation of blood flow, enhanced vascular permeability, hemorrhage and leukocytes accumulation." Am J Pathol **98**: 485-498.

Kroll, M. H., J. D. Hellums, et al. (1996). "Platelets and shear stress." Blood **88**(5): 1525-41.

Kuchan, M. J. and J. A. Frangos (1994). "Role of calcium and calmodulin in flow-induced nitric oxide production in endothelial cells." Am J Physiol **266**(3 Pt 1): C628-36.

Kuper, H., H. O. Adami, et al. (2000). "Infections as a major preventable cause of human cancer." J Intern Med **248**(3): 171-83.

Lacy, M., J. Jones, et al. (1995). "Expression of the receptors for the C5a anaphylatoxin, interleukin-8 and FMLP by human astrocytes and microglia." J Neuroimmunol **61**(1): 71-8.

Langille, B. L. and S. L. Adamson (1981). "Relationship between blood flow direction and endothelial cell orientation at arterial branch sites in rabbits and mice." Circ Res **48**(4): 481-8.

Lansman, J. B., T. J. Hallam, et al. (1987). "Single stretch-activated ion channels in vascular endothelial cells as mechanotransducers?" Nature **325**(6107): 811-3.

Lard, L. R., F. P. Mul, et al. (1999). "Neutrophil activation in sickle cell disease." J Leukoc Biol **66**(3): 411-5.

Laudanna, C. and R. Alon (2006). "Right on the spot. Chemokine triggering of integrin-mediated arrest of rolling leukocytes." Thromb Haemost **95**(1): 5-11.

Le, Y., W. Gong, et al. (1999). "Utilization of two seven-transmembrane, G protein-coupled receptors, formyl peptide receptor-like 1 and formyl peptide receptor, by the synthetic hexapeptide WKYMVm for human phagocyte activation." J Immunol **163**(12): 6777-84.

Levesque, M. J. and R. M. Nerem (1985). "The elongation and orientation of cultured endothelial cells in response to shear stress." J Biomech Eng **107**(4): 341-7.

Li, J. J. and J. L. Chen (2005). "Inflammation may be a bridge connecting hypertension and atherosclerosis." Med Hypotheses **64**(5): 925-9.

Li, S., P. Butler, et al. (2002). "The role of the dynamics of focal adhesion kinase in the mechanotaxis of endothelial cells." Proc Natl Acad Sci U S A **99**(6): 3546-51.

Li, Y. S., J. H. Haga, et al. (2005). "Molecular basis of the effects of shear stress on vascular endothelial cells." J Biomech **38**(10): 1949-71.

Loitto, V. M., B. Rasmusson, et al. (2001). "Assessment of neutrophil N-formyl peptide receptors by using antibodies and fluorescent peptides." J Leukoc Biol **69**(5): 762-71.

Lum, A. F., T. Wun, et al. (2004). "Inflammatory potential of neutrophils detected in sickle cell disease." Am J Hematol **76**(2): 126-33.

Macconi, D., M. Foppolo, et al. (1995). "PAF mediates neutrophil adhesion to thrombin or TNF-stimulated endothelial cells under shear stress." Am J Physiol **269**(1 Pt 1): C42-7.

Mach, F., U. Schonbeck, et al. (1998). "Reduction of atherosclerosis in mice by inhibition of CD40 signalling." Nature **394**(6689): 200-3.

Makino, A., M. Glogauer, et al. (2005). "Control of neutrophil pseudopods by fluid shear: role of Rho family GTPases." Am J Physiol Cell Physiol **288**(4): C863-71.

Makino, A., E. R. Prossnitz, et al. (2005). "Control of neutrophil pseudopods by fluid shear: role of GPCR constitutive activity." Proceedings of 2005 BMES Annual Fall Meeting: 13.

Marschel, P. and G. W. Schmid-Schonbein (2002). "Control of fluid shear response in circulating leukocytes by integrins." Ann Biomed Eng **30**(3): 333-43.

Milligan, G. (2001). "Oligomerisation of G-protein-coupled receptors." J Cell Sci **114**(Pt 7): 1265-71.

Mizuno, T., T. Tsukiya, et al. (2002). "Ultrastructural alterations in red blood cell membranes exposed to shear stress." Asaio J **48**(6): 668-70.

Moazzam, F. (1996). The response of human neutrophils to fluid stress. Bioengineering. La Jolla, University of California, San Diego**:** 141.

Moazzam, F., F. A. DeLano, et al. (1997). "The leukocyte response to fluid stress." Proc Natl Acad Sci U S A **94**(10): 5338-43.

Movat, H. Z. (1985). The Inflammatory Reaction. New York, Elsevier.

Nagel, T., N. Resnick, et al. (1999). "Vascular endothelial cells respond to spatial gradients in fluid shear stress by enhanced activation of transcription factors." Arterioscler Thromb Vasc Biol **19**(8): 1825-34.

Nakajima, T., K. Kon, et al. (1990). "Deformation response of red blood cells in oscillatory shear flow." Am J Physiol **259**(4 Pt 2): H1071-8.

Nesbitt, W. S., P. Mangin, et al. (2006). "The impact of blood rheology on the molecular and cellular events underlying arterial thrombosis." J Mol Med.

Ney, P. A., M. M. Christopher, et al. (1990). "Synergistic effects of oxidation and deformation on erythrocyte monovalent cation leak." Blood **75**(5): 1192-8.

Niggli, V. (2003). "Signaling to migration in neutrophils: importance of localized pathways." Int J Biochem Cell Biol **35**(12): 1619-38.

Noria, S., F. Xu, et al. (2004). "Assembly and reorientation of stress fibers drives morphological changes to endothelial cells exposed to shear stress." Am J Pathol **164**(4): 1211-23.

Ohshima, H. and H. Bartsch (1994). "Chronic infections and inflammatory processes as cancer risk factors: possible role of nitric oxide in carcinogenesis." Mutat Res **305**(2): 253-64.

Okuyama, M., J. Kambayashi, et al. (1996). "LFA-1/ICAM-3 mediates neutrophil homotypic aggregation under fluid shear stress." J Cell Biochem **60**(4): 550-9.

Okuyama, M., Y. Ohta, et al. (1996). "Fluid shear stress induces actin polymerization in human neutrophils." J Cell Biochem **63**(4): 432-41.

Olesen, S. P., D. E. Clapham, et al. (1988). "Haemodynamic shear stress activates a K+ current in vascular endothelial cells." Nature **331**(6152): 168-70.

Olivier, L. A. and G. A. Truskey (1993). "A numerical analysis of forces exerted by laminar flow on spreading cells in a parallel plate flow chamber assay." Biotechnology and Bioengineering **42**: 963-973.

Panaro, M. A., A. Acquafredda, et al. (2006). "Biological role of the N-formyl peptide receptors." Immunopharmacol Immunotoxicol **28**(1): 103-27.

Park, P. S., S. Filipek, et al. (2004). "Oligomerization of G protein-coupled receptors: past, present, and future." Biochemistry **43**(50): 15643-56.

Passerini, A. G., A. Milsted, et al. (2003). "Shear stress magnitude and directionality modulate growth factor gene expression in preconditioned vascular endothelial cells." J Vasc Surg **37**(1): 182-90.

Pfaff, M., S. Liu, et al. (1998). "Integrin beta cytoplasmic domains differentially bind to cytoskeletal proteins." J Biol Chem **273**(11): 6104-9.

Piqueras, L., P. Kubes, et al. (2000). "Angiotensin II induces leukocyte-endothelial cell interactions in vivo via AT(1) and AT(2) receptor-mediated P-selectin upregulation." Circulation **102**(17): 2118-23.

Pozrikidis, C. (1997). "Shear flow over a protuberance on a plane wall." Journal of Engineering Mathematics **31**(1): 29-42.

Pradhan, A. D., J. E. Manson, et al. (2001). "C-reactive protein, interleukin 6, and risk of developing type 2 diabetes mellitus." Jama **286**(3): 327-34.

Robker, R. L., R. G. Collins, et al. (2004). "Leukocyte migration in adipose tissue of mice null for ICAM-1 and Mac-1 adhesion receptors." Obes Res **12**(6): 936-40.

Ross, R. (1999). "Atherosclerosis--an inflammatory disease." N Engl J Med **340**(2): 115-26.

Sampath, R., P. J. Gallagher, et al. (1998). "Cytoskeletal interactions with the leukocyte integrin beta2 cytoplasmic tail. Activation-dependent regulation of associations with talin and alpha-actinin." J Biol Chem **273**(50): 33588-94.

Schmid-Schonbein, G. W. (2006). "Analysis of inflammation." Annu Rev Biomed Eng **8**: 93-131.

Schmid-Schonbein, G. W., Y. Y. Shih, et al. (1980). "Morphometry of human leukocytes." Blood **56**(5): 866-75.

Schmid-Schonbein, G. W., K. L. Sung, et al. (1981). "Passive mechanical properties of human leukocytes." Biophys J **36**(1): 243-56.

Schmidtke, D. W. and S. L. Diamond (2000). "Direct observation of membrane tethers formed during neutrophil attachment to platelets or P-selectin under physiological flow." J Cell Biol **149**(3): 719-30.

Schwarz, G., G. Callewaert, et al. (1992). "Shear stress-induced calcium transients in endothelial cells from human umbilical cord veins." J Physiol **458**: 527-38.

Seifert, R. and K. Wenzel-Seifert (2003). "The human formyl peptide receptor as model system for constitutively active G-protein-coupled receptors." Life Sci **73**(18): 2263-80.

Sfikakis, P. P. and G. C. Tsokos (1995). "Lymphocyte adhesion molecules in autoimmune rheumatic diseases: basic issues and clinical expectations." Clin Exp Rheumatol **13**(6): 763-77.

Simon, S. I. and C. E. Green (2005). "Molecular mechanics and dynamics of leukocyte recruitment during inflammation." Annu Rev Biomed Eng **7**: 151-85.

Springer, T. A. (1994). "Traffic signals for lymphocyte recirculation and leukocyte emigration: the multistep paradigm." Cell **76**(2): 301-14.

Su, S. B., W. H. Gong, et al. (1999). "T20/DP178, an ectodomain peptide of human immunodeficiency virus type 1 gp41, is an activator of human phagocyte N-formyl peptide receptor." Blood **93**(11): 3885-92.

Sugimoto, M., S. Tsuji, et al. (1999). "Shear-dependent functions of the interaction between soluble von Willebrand factor and platelet glycoprotein Ib in mural thrombus formation on a collagen surface." Int J Hematol **69**(1): 48-53.

Sun, R., P. Iribarren, et al. (2004). "Identification of neutrophil granule protein cathepsin G as a novel chemotactic agonist for the G protein-coupled formyl peptide receptor." J Immunol **173**(1): 428-36.

Sundstrom, C. and K. Nilsson (1976). "Establishment and characterization of a human histiocytic lymphoma cell line (U-937)." Int J Cancer **17**(5): 565-77.

Tardy, Y., N. Resnick, et al. (1997). "Shear stress gradients remodel endothelial monolayers in vitro via a cell proliferation-migration-loss cycle." Arterioscler Thromb Vasc Biol **17**(11): 3102-6.

Thiagarajan, R. R., R. K. Winn, et al. (1997). "The role of leukocyte and endothelial adhesion molecules in ischemia-reperfusion injury." Thromb Haemost **78**(1): 310-4.

Thurston, G. B. (1972). "Viscoelasticity of human blood." Biophys J **12**(9): 1205-17.

Tricot, O., Z. Mallat, et al. (2000). "Relation between endothelial cell apoptosis and blood flow direction in human atherosclerotic plaques." Circulation **101**(21): 2450-3.

Tschoepe, D., U. Rauch, et al. (1997). "Platelet-leukocyte-cross-talk in diabetes mellitus." Horm Metab Res **29**(12): 631-5.

Tzima, E., M. A. del Pozo, et al. (2001). "Activation of integrins in endothelial cells by fluid shear stress mediates Rho-dependent cytoskeletal alignment." Embo J **20**(17): 4639-47.

VanCompernolle, S. E., K. L. Clark, et al. (2003). "Expression and function of formyl peptide receptors on human fibroblast cells." J Immunol **171**(4): 2050-6.

Vines, C. M., C. M. Revankar, et al. (2003). "N-formyl peptide receptors internalize but do not recycle in the absence of arrestins." J Biol Chem **278**(43): 41581-4.

von Andrian, U. H., S. R. Hasslen, et al. (1995). "A central role for microvillous receptor presentation in leukocyte adhesion under flow." Cell **82**(6): 989-99.

Wang, N., J. P. Butler, et al. (1993). "Mechanotransduction across the cell surface and through the cytoskeleton." Science **260**(5111): 1124-7.

Weinbaum, S., P. Guo, et al. (2001). "A new view of mechanotransduction and strain amplification in cells with microvilli and cell processes." Biorheology **38**(2-3): 119-42.

Werr, J., X. Xie, et al. (1998). "beta1 integrins are critically involved in neutrophil locomotion in extravascular tissue In vivo." J Exp Med **187**(12): 2091-6.

White, C. R., M. Haidekker, et al. (2001). "Temporal gradients in shear, but not spatial gradients, stimulate endothelial cell proliferation." Circulation **103**(20): 2508-13.

Wick, G., M. Knoflach, et al. (2004). "Autoimmune and inflammatory mechanisms in atherosclerosis." Annu Rev Immunol **22**: 361-403.

Wiesner, S., A. Lange, et al. (2006). "Local call: from integrins to actin assembly." Trends Cell Biol **16**(7): 327-9.

Witko-Sarsat, V., P. Rieu, et al. (2000). "Neutrophils: molecules, functions and pathophysiological aspects." Lab Invest **80**(5): 617-53.

Wong, T. Y., W. Rosamond, et al. (2005). "Retinopathy and risk of congestive heart failure." Jama **293**(1): 63-9.

Wymann, M. P., P. Kernen, et al. (1990). "Corresponding oscillations in neutrophil shape and filamentous actin content." J Biol Chem **265**(2): 619-22.

Xue, M., C. M. Vines, et al. (2004). "N-formyl peptide receptors cluster in an active raft-associated state prior to phosphorylation." J Biol Chem **279**(43): 45175-84.

Yasu, T., N. Ikeda, et al. (2002). "Nicorandil and leukocyte activation." J Cardiovasc Pharmacol **40**(5): 684-92.

Yonekawa, K. and J. M. Harlan (2005). "Targeting leukocyte integrins in human diseases." J Leukoc Biol **77**(2): 129-40.

Zhelev, D. V. and A. Alteraifi (2002). "Signaling in the motility responses of the human neutrophil." Ann Biomed Eng **30**(3): 356-70.